

## Revised Flow and Solute Transport Modelling for ASTR Operations, South Australia

Sarah Kremer, Konrad Miotlinski, Karen Barry, Peter Dillon and Kerry Levett

January 2010

Australia is founding its future on science and innovation. Its national science agency, CSIRO, is a powerhouse of ideas, technologies and skills.

CSIRO initiated the National Research Flagships to address Australia's major research challenges and opportunities. They apply large scale, long term, multidisciplinary science and aim for widespread adoption of solutions. The Flagship Collaboration Fund supports the best and brightest researchers to address these complex challenges through partnerships between CSIRO, universities, research agencies and industry.

The Water for a Healthy Country Flagship aims to achieve a tenfold increase in the economic, social and environmental benefits from water by 2025. The work contained in this report is collaboration between CSIRO and City of Salisbury, United Water, SA Water Corporation and the SA Department of Water, Land and Biodiversity Conservation.

For more information about Water for a Healthy Country Flagship or the National Research Flagship Initiative visit [www.csiro.au/org/HealthyCountry.html](http://www.csiro.au/org/HealthyCountry.html)

Citation: Kremer *et al.* 2010. Revised Flow and Solute Transport Modelling for ASTR Operations. CSIRO: Water for a Healthy Country National Research Flagship

#### **Copyright and Disclaimer**

© 2010 CSIRO To the extent permitted by law, all rights are reserved and no part of this publication covered by copyright may be reproduced or copied in any form or by any means except with the written permission of CSIRO.

#### **Important Disclaimer:**

CSIRO advises that the information contained in this publication comprises general statements based on scientific research. The reader is advised and needs to be aware that such information may be incomplete or unable to be used in any specific situation. No reliance or actions must therefore be made on that information without seeking prior expert professional, scientific and technical advice. To the extent permitted by law, CSIRO (including its employees and consultants) excludes all liability to any person for any consequences, including but not limited to all losses, damages, costs, expenses and any other compensation, arising directly or indirectly from using this publication (in part or in whole) and any information or material contained in it.

#### **Cover Photograph:**

Description: Horizontal distribution of mixing fraction at the end of an injection phase (left) and a recovery phase (right) at the ASTR site (model D, simulation "normal", numerical layer five) showing the extent of the fresh injected plume within the aquifer.

© 2010 CSIRO

# CONTENTS

Contents .....	iii
Acronyms .....	iv
List of Figures .....	iv
List of Tables.....	vi
Acknowledgments .....	viii
Executive Summary.....	ix
<b>1. Introduction .....</b>	<b>1</b>
<b>2. Site characterisation .....</b>	<b>1</b>
2.1. Location and configuration.....	1
2.2. Hydrogeological setting .....	2
2.3. Operational schedule .....	4
2.3.1. ASTR well field .....	4
2.3.2. Water balance .....	5
<b>3. Source water and groundwater monitoring .....</b>	<b>9</b>
3.1. Methods .....	9
3.2. Comparison of sampled versus <i>in situ</i> EC.....	9
3.3. Source water salinity.....	10
3.4. Groundwater level and salinity.....	11
3.4.1. Hydraulic head observations .....	11
3.4.2. Solute observations .....	13
<b>4. Groundwater modelling .....</b>	<b>18</b>
4.1. Simulation package.....	18
4.2. Methods of analysis .....	19
4.2.1. Mixing fraction .....	19
4.2.2. Residence time.....	19
4.3. Previous groundwater modelling at the ASTR site .....	20
4.4. Revised conceptual model.....	23
4.5. Revised numerical model and input data .....	23
4.5.1. Spatial discretisation.....	23
4.5.2. Input parameters .....	24
4.6. Revised model calibration and verification .....	25
4.6.1. Calibration strategy.....	25
4.6.2. Calibration results.....	26
4.6.3. Calibration sensitivity analysis .....	30
4.6.4. Model Verification .....	30
4.7. Numerical modelling predictions.....	33
4.7.1. Prediction of mixing fraction.....	33
4.7.2. Prediction of residence time .....	38
4.7.3. Limitations of the model.....	40
4.8. Analytical modelling predictions.....	41
<b>5. Conclusions and recommendations.....</b>	<b>44</b>
References .....	46
Appendix A: Lithological and Geophysical log .....	48

<b>Appendix B: Profiled EC and temperature data.....</b>	<b>50</b>
<b>Appendix C: Operational Input data for numerical simulations.....</b>	<b>59</b>
C.1 Calibration simulations.....	59
C.2 Verification simulations.....	60
C.3 Predictive modelling of mixing fraction.....	60
C.4 Predictive modelling of residence time.....	66
<b>Appendix D: Parafield ASR operations .....</b>	<b>67</b>

## ACRONYMS

AHD	Australian height datum
ASR	Aquifer Storage and Recovery
ASTR	Aquifer Storage Transfer and Recovery
bgs	below ground surface
CTD	conductivity temperature and depth
DO	dissolved oxygen
DWLBC	SA Department of Water, Land and Biodiversity Conservation
EC	electrical conductivity of water
FA	flux-averaged
FEFLOW	Finite Element Subsurface Flow & Transport Simulation System
GRS	Greenfields Railway Station
IW	injection well
ME	mean error
P1,2,3	Piezometer 1,2,3
RMSE	root-mean-square error
RW	recovery well
TDS	total dissolved solids
VA	volume-averaged

## LIST OF FIGURES

Figure 1 Diagram of City of Salisbury water harvesting facilities in the Parafield area, identifying the location of wells at the ASTR, Parafield ASR and Greenfields Railway Station (GRS) sites (after Kremer <i>et al.</i> 2008).....	2
Figure 2 Hydrogeological cross-section through Quaternary and Neogene aquifers in the ASTR site area. Groundwater flow directions and pressures are relevant for the natural conditions (when the ASTR system is not operating). Line of the cross section is shown in Figure 1. ....	3
Figure 3 Close up of the ASTR well-field showing four outer injection wells (IW1-IW4), two inner recovery wells (RW1-RW2) and three piezometers (P1-P3) (from Kremer <i>et al.</i> 2008).....	5
Figure 4 Cumulative volume injected and recovered from the start of ASTR operation in September 2006 up to April 2009. This includes flushing phase (injection into RW - September 2006–June 2008), injection into IW (September - December 2008), and recovery (February-April 2009).....	6
Figure 5 Volume-averaged versus flux-averaged EC, measured at IWs, P1, P2 and P3 between July 2007 and April 2009.....	10
Figure 6 Salinity of the source water versus time measured from logger and laboratory and field measurements from the wetland. Periods of injection at the RWs (flushing) and IWs (injection) are also presented, as well as periods when Parafield ASR water was used as source water for injection at ASTR. ....	11

Figure 7 Water level versus time in IW1 (10.4 m AHD), IW2 (10.1 m AHD), IW3 (10.0 m AHD) and IW4 (10.3 m AHD). Operations periods at ASTR are also shown for information. ....	12
Figure 8 Water level versus time in P1 (10.2 m AHD), P2 (11.1 m AHD) and P3 (11.2 m AHD), and manual SWL measurements between August 2008 and June 2009. Operations at ASTR and at nearby Parafield ASR are also presented for information. ....	13
Figure 9 Depth-averaged EC data versus time obtained from down-hole profiles over the open intervals, and EC data collected during sampling, at the 4 IW during the flushing phase. Flushing periods are presented as grey areas. ....	14
Figure 10 Mixing fraction $f$ measured in the IW wells as a function of volume injected .....	15
Figure 11 EC over time observed at P1 from a down-hole CTD diver; and EC data collected at P1 and P3 from sampling and profiling measurement, between August 08 and March 2009. ....	16
Figure 12 EC versus volume measured at RW1, P3, P1 and IW1 showing the evolution of salinity on the transect RW1-IW1 during recovery of 104.7 ML via RWs between February and April 2009 (date of data collection is also presented). ....	17
Figure 13 EC versus time observed at P2 from a down-hole CTD diver; and EC data collected at P2 from sampling and profiling measurement, between August 08 and June 09. Average EC values of ambient groundwater and source water are also presented. ....	18
Figure 14 Schematic 3D view of conceptual models CM1 & CM2 (from Kremer <i>et al.</i> 2008)	21
Figure 15 Schematic 3D view of conceptual model CM3 .....	23
Figure 16 Comparison of simulated and observed drawdown at IW1, IW3, IW4, RW1 and RW2 during pumping test at IW2 for simulations 3 (a) and 9 (b). ....	27
Figure 17 Comparison of observed (dot) and simulated (lines) $f$ at IWs during injection at RWs for calibration simulations 3f (a) and 9 (b) which presented the best overall fit during the calibration process. ....	29
Figure 18 Observed and simulated $f$ at P2 during injection at the ASTR site for calibration simulation 3f and 9 (day 0 to day 886), and extraction via RWs for verification simulations 3f (model C) and 9 (model D), (day 886 to 964) .....	29
Figure 19 Observed and simulated mixing fraction at RWs (a) and IWs (b), during extraction via RWs over 72 days, using models C (grey line) and D (black line) .....	31
Figure 20 Cross-sectional distribution of mixing fraction at the end of the injection period simulated with models C (a) and D (b). Horizontal scale: 300 m, vertical scale: 60 m. ....	32
Figure 21 Cross-sectional distribution of mixing fraction at the end of the recovery period simulated with models C (a) and D (b). Horizontal scale: 300 m, vertical scale: 60 m. ....	32
Figure 22 Mixing fraction at RWs versus time during 3 injection/recovery cycles with (dot lines) and without (plain lines) influence of Parafield ASR scheme simulated on model C and D. Periods of injection and recovery at ASTR are also presented. ....	34
Figure 23 Minimum mixing fraction predicted at RWs in function of the cycle, over 6 cycles, simulated on models C (a) and D (b), under normal, dry and wet conditions for recovery efficiency of 80%. Thresholds of 300 and 500 mg/L TDS are also presented. ....	35
Figure 24 Minimum mixing fraction predicted at RWs in function of the cycle, over 6 cycles simulated on models C and D involving injection of 200 ML per cycle and a recovery efficiency of 60, 80, 100 and 120%. Thresholds of 300 and 500 mg/L TDS are also presented. ....	36
Figure 25 Distribution of mixing fraction at the end of the 6 <sup>th</sup> injection period (a) and of the 6 <sup>th</sup> recovery period (b) for scenario normal on model D (numerical layer 5; scale: 1,000 m). ....	37
Figure 26 Change in minimum simulated mixing fraction at RWs after 3 years of ASTR operations in function of porosity (a) and dispersivity (b) for models C and D. ....	38

Figure 27 Distribution of residence time within the aquifer of the recovered water as a function of the volume extracted at RW1 and RW2, without a storage period between the end of injection at IW and recovery via RW .....	39
Figure 28 Change in minimum residence time of the injected water before recovery in function of porosity (a) and dispersivity (b) values, using model C.....	40
Figure 29 Amount of injected and recovered water in three predictive scenarios .....	42
Figure 30 Volume recovered versus volume injected in the each cycle. a) direct comparison, b) recovery efficiency in function of amount of injected water. Solid line in fig. b indicates min achievable recovery .....	43
Figure 31 Comparison of the operational approaches of the ASTR system. The new approach allows one to generate a “dry weather buffer” which would increase the effectiveness of the system in dry years.....	44
Figure 32 Geophysical logs as a function of depth (only for 160 to 225 m interval) collected at P2 in July 2008 prior to casing.....	49
Figure 33 EC and temperature versus depth at RW1 between March and October 2007 ...	50
Figure 34 EC and temperature versus depth at RW2 between March and October 2007 ...	51
Figure 35 EC and temperature versus depth at IW1 between March 2007 and April 2009. Peak in the profile sampled 17/02/2009 reflects start of recovery on 1/02/2009. ....	52
Figure 36 EC and temperature versus depth at IW2 between March 2007 and April 2009. Sharp increase in the temperature profile sampled 17/02/2009 reflects start of recovery on 1/02/2009.....	53
Figure 37 EC and temperature versus depth at IW3 between March 2007 and April 2009. Sharp increase in the temperature profile sampled 17/02/2009 reflects start of recovery on 1/02/2009.....	54
Figure 38 EC and temperature versus depth at IW4 between March 2007 and April 2009. Sharp increase in the temperature profile sampled 17/02/2009 reflects start of recovery on 1/02/2009.....	55
Figure 39 EC and temperature versus depth at P1 between August 2008 and June 2009... ..	56
Figure 40 EC and temperature versus depth at P3 between August 2008 and June 2009... ..	57
Figure 41 EC and temperature versus depth at P2 between November 2008 and June 2009 .....	58
Figure 42 Monthly cumulative volume at the Parafield ASR scheme between June 2003 and June 2009 .....	67

## LIST OF TABLES

Table 1 Generalised hydrogeological setting at the ASTR site (modified from AGT 2007).....	4
Table 2 Quantities of water injected and extracted in the ASTR system, from September 2006 to March 2009 (from Page <i>et al.</i> 2009).....	7
Table 3 Summary of modelling works undertaken at the ASTR site between 2004 and 2009 and field data used for each study.....	22
Table 4 Summary of adjusted parameters and changes in errors of mixing fraction and hydraulic head during the calibration simulation constrained by hydraulic head and EC data observed at the ASTR site. Simulations 1, 2 and 4 to 8 simulate only flow while simulations 3 (a to f) and 9 simulate flow and solute transport.....	28
Table 5 Qualitative review of a sensitivity analysis of input data adjusted in CM3 during the calibration process.....	30
Table 6 Summary of recovery efficiency and volume and length of injection and extraction periods of each cycle for scenarios normal, wet and drought.....	33
Table 7 Lithological and stratigraphical units intersected at P2 at the ASTR site (adapted from Well Construction Report and AGT 2007).....	48
Table 8 Injection flow rates (Q) and periods of injection at RW1 and RW2 used as input data for the calibration simulation .....	59

Table 9 Injection flow rates (Q) and periods of injection at IW1, IW2, IW3 and IW4 used as input data for the calibration simulation .....	59
Table 10 Injection and extraction flow rates (Q) and periods of injection at ASR well used as input data for the calibration simulation .....	60
Table 11 Extraction flow rates (Q) and periods of recovery at RW1 and RW2 used as input data for the verification simulation .....	60
Table 12 Summary of input data for the simulations of mixing fraction, showing flow rates (Q), total volume injected and extracted per period, and the storage period between two operations at the ASTR site. ....	61
Table 13 Summary of input data for the ASTR wells for the simulation of residence time for the “normal” scenario (Q = flow rate).....	66
Table 14 Summary of input data for the ASTR wells for the simulation of residence time for the “wet” scenario (Q = flow rate) .....	66

## **ACKNOWLEDGMENTS**

The Salisbury Aquifer Storage Transfer and Recovery (ASTR) Project is supported by the Australian Government Department of Innovation, Industry, Science and Research through its International Science Linkages Programme, enabling participation within the European Union Project 'Reclaim Water', which is supported in the 6<sup>th</sup> Framework Programme (Contract 018309). The ASTR project is also supported by the South Australian Premier's Science and Research Foundation and the Australian Government National Water Commission through the Water Smart Australia Programme commitment to Water Proofing Northern Adelaide Project. Project partners include CSIRO Land and Water, City of Salisbury, United Water, SA Water Corporation and the SA Department of Water, Land and Biodiversity Conservation (DWLBC).

We wish to thank the following people for making a significant contribution to this study:

- Paul Pavelic (International Water Management Institute) for his initial contribution to the ASTR modelling
- Rudi Regel (United Water) for project management and field assistance
- Mark Purdie (City of Salisbury) for operational support
- Groundwater and Geophysical Technical Services of Department of Water, Land Biodiversity and Conservation (DWLBC) for field assistance and geophysical investigation
- Chris Burgess and Paul Carter (City of Salisbury) for data provision
- Nabil Gerges of AGT Consultants for supervision of construction of piezometers P1-P3
- Kylie Hyde (United Water) for review of the final draft of the report

## EXECUTIVE SUMMARY

The Aquifer Storage Transfer and Recovery (ASTR) project has been undertaken to establish if reedbed-treated urban stormwater can be injected into a brackish aquifer and later recovered using separate recovery wells at a standard which meets Australian Drinking Water Guidelines. The ASTR scheme involves six wells partially penetrating a brackish limestone aquifer at a site situated in the City of Salisbury, north of Adelaide in South Australia. This report provides an assessment of the performance of the ASTR scheme based upon field investigations undertaken at the ASTR site between 2006 and 2009, and presents a revised 3D flow groundwater and solute transport model. The outcomes are expected to assist in the development of strategies to manage the operations at the site in the future.

The operation of the ASTR site began in September 2006 with a flushing phase to flush brackish groundwater out of the storage area, with 377 ML of fresh water injected by June 2008. After the flushing phase an additional injection of 30 ML occurred in operational mode and was followed by a first recovery period involving the extraction of 106 ML between February and April 2009.

Field investigations at the ASTR site include hydraulic and salinity monitoring, using sampling and *in situ* measurements to describe the migration of injected water within the aquifer. During the flushing phase, electrical conductivity (EC) data collected at ASTR wells showed a clear breakthrough of the injected water across the study zone with concentrations dropping from 3620  $\mu\text{S}/\text{cm}$  in June 2006 to 591  $\mu\text{S}/\text{cm}$  in August 2008. Additional data collected from a new piezometer open in the lower part of aquifer not intersected by the ASTR wells showed a clear breakthrough of fresh water. EC values recorded during sampling decreased from 2700  $\mu\text{S}/\text{cm}$  in September 2008 to 1380  $\mu\text{S}/\text{cm}$  in January 2009, suggesting a flow exchange occurring between the storage area and the lower part of the aquifer. The salinity of the recovered water was measured below the threshold of salinity for drinking water of 500 mg/L TDS (approximately 890  $\mu\text{S}/\text{cm}$ ) with an average conductivity of 532  $\mu\text{S}/\text{cm}$ .

Groundwater flow and solute transport modelling at the ASTR site for this study involved the revision of existing 2D (Pavelic *et al.* 2004) and 3D (Kremer *et al.* 2008) models that used a layered structure to describe the heterogeneity within the aquifer. The first modelling study by Pavelic *et al.* (2004) explored the tradeoffs between injection volume, size of well spacing and full and partial penetrating wells with the salinity of recovered water and its residence time in the aquifer. The work undertaken by Pavelic *et al.* (2004) was based on data from nearby Parafield wells and wells drilled near Greenfields Railway Station. The adopted well configuration and site selection was made at Greenfields Oval based on the outcomes of the Pavelic *et al.* (2004) report.

The second Kremer *et al.* (2008) modelling study utilised data derived from the drilling of the injection and recovery wells at the ASTR site in 2006-2007 and the initial flushing of the aquifer by injection of stormwater into the central recovery wells executed between September 2006 and October 2007. This work revealed that quite contrasting models could be fitted equally well to the data but provided divergent predictions for recovered water salinity for future operations. The modelling identified locations for piezometers, which were subsequently constructed, to give a clearer picture of the aquifer behaviour.

This third modelling report draws on new field data on hydrogeological conditions and water salinity collected since October 2007, the date of last data acquisition in the previous study; and notably data from three new piezometers drilled in July 2008, which allows access to the previously unstudied lower part of the aquifer not intersected by the ASTR wells. The revised conceptual model (CM3) appeared to fit well with both observed flow and solute transport data, and two alternative sets of parameters of CM3 were found to fit equally well the observed head and EC data during the calibration process.

Since the results generated by numerical model were ambiguous, the two alternative models were then used to simulate salinity and aquifer residence time of the recovered water under actual and proposed ASTR operations. Results from the simulations of the mixing fraction of brackish ambient water with fresh injected water for six years of ASTR operations after the flushing phase implied that salinity of the recovered water should remain below 500 mg/L TDS provided that the site is properly operated. When data from the longer operational period are acquired and verification of the models is performed, one of those models will be adopted for further simulations.

To ensure that the recovered water is maintained at an acceptable salinity level over a long period, it is recommended to keep recovery efficiency up to 80%. In all cases tested, residence time of the injected water within the aquifer before recovery exceeds 150 days (without taking into account any storage period between injection and extraction). The mean residence times calculated for two models were in the range of 255-306 days.

The results from this study support the expected viability of ASTR operations even under stressed (i.e. low rainfall) conditions and reinforce that a brackish aquifer may be transformed into a storage that has potential to provide supplies which meet Australian Drinking Water Guidelines.

In addition, the revised and validated modelling provides a powerful field-based predictive tool which is able to simulate the fate of injected water within the aquifer to assess the viability of the ASTR scheme under various operational scenarios.

# 1. INTRODUCTION

Aquifer Storage Transfer and Recovery (ASTR) describes a concept that is being trialled at Salisbury on the Northern Adelaide Plains in South Australia. The research project at the ASTR site aims to establish if reedbed-treated urban stormwater can be injected into a brackish aquifer and later recovered using separate injection and recovery wells at a standard which meets Australian Drinking Water Guidelines (Rinck-Pfeiffer *et al.* 2005; Swierc *et al.* 2005; Dillon *et al.* 2008; Page *et al.* 2009).

Similar to Aquifer Storage and Recovery (ASR) systems that operate throughout the world, ASTR is a method of utilising subsurface storage to provide a buffer against seasonal variation in water demands and supplies, and allows natural treatment to take place within the aquifer. ASR uses the same well for both injection and recovery. ASTR differs from ASR as it uses separate injection and recovery wells with a view of providing a longer and more uniform residence time within the aquifer to ensure more reliable inactivation of pathogens and biodegradation of trace organics.

This report provides an assessment of the performance of the ASTR scheme based upon field investigations undertaken at the ASTR site between 2006 and 2009, and a revised 3D flow and solute transport model, including:

- details of the configuration of the ASTR site, hydrogeological setting and operational framework (Section 2);
- the monitoring of the site and analysis of hydraulic and salinity data collected during the ASTR operations that took place between September 2006 and April 2009 (Section 3);
- summary of the results of previous modelling work undertaken on the ASTR site and extension and revision of the previous modelling using new data collected in the previously unstudied lower part of the target aquifer (Section 4);
- results from simulations of actual and proposed ASTR operations using the revised field-based calibrated model (Section 4); and
- recommendations regarding site monitoring and management (section 5).

## 2. SITE CHARACTERISATION

### 2.1. Location and configuration

The ASTR site is located in the City of Salisbury, which is part of the Adelaide Metropolitan Area in South Australia. This site was chosen ahead of two nearby sites at Parafield and Greenfields North with existing wells based on considerations such as land use and availability, the number of existing monitoring wells, distance from the stormwater harvesting scheme and the potential for interactions with the existing well fields.

The ASTR system consists of four outer injection wells and two inner recovery wells that are all equi-spaced (50 metres apart) and contained within a rhombic domain (Figure 1).

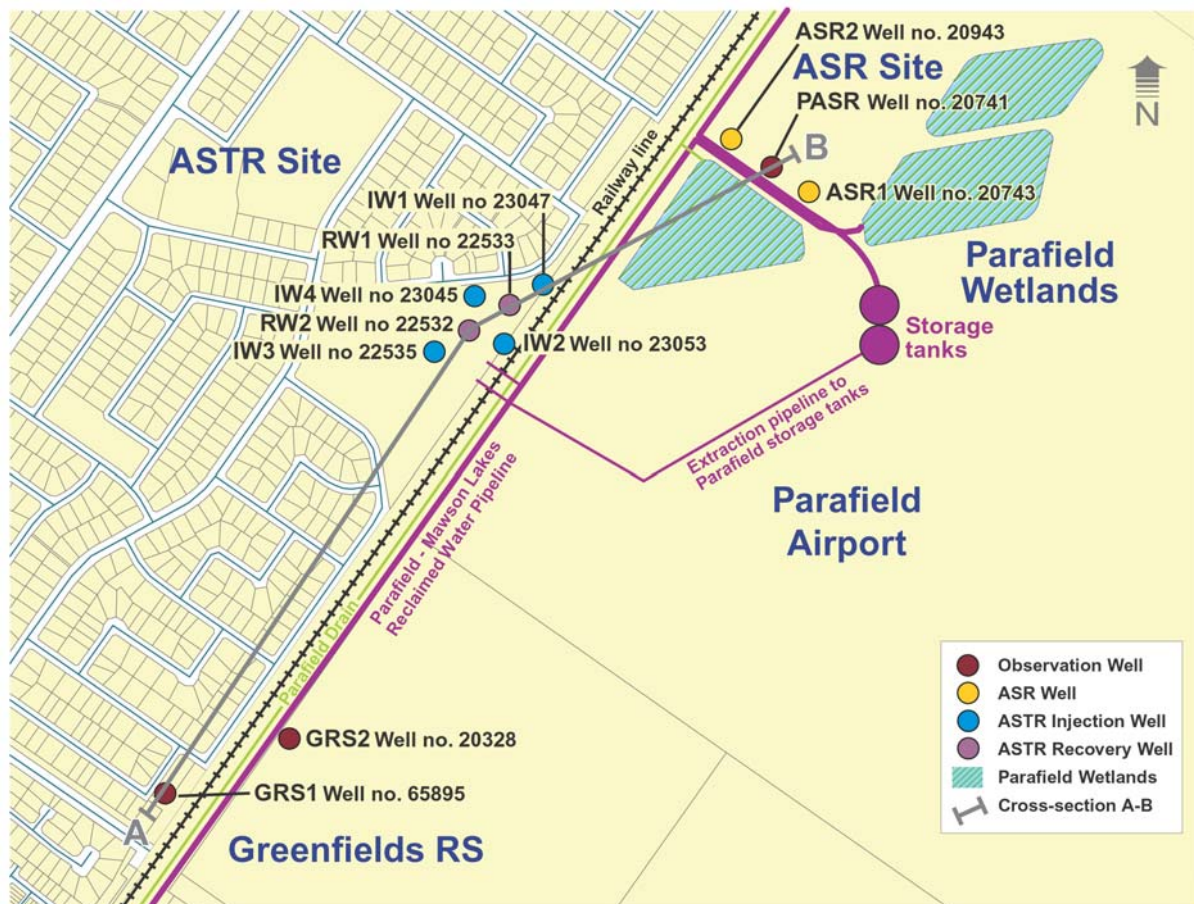


**Figure 1** Diagram of City of Salisbury water harvesting facilities in the Parafield area, identifying the location of wells at the ASTR, Parafield ASR and Greenfields Railway Station (GRS) sites (after Kremer *et al.* 2008)

## 2.2. Hydrogeological setting

From a geological point of view, the ASTR site is located within the Adelaide Embayment which is a section of the St Vincent Basin. The area is underlain by a thick sequence of sedimentary deposits of Quaternary and Neogene age overlying the Precambrian basement.

One can distinguish four Quaternary (Q1, Q2, Q3, Q4) and two Neogene (“Tertiary” – T1, T2) aquifers in the profile (Figure 2; Table 1). Differing from the Quaternary aquifers, the underlying Neogene ones feature high extent and transmissivity. The ASTR project targets the T2 aquifer which is also known as the Port Willunga Formation. The T2 aquifer consists of limestone series with sandy and silty admixtures. At the ASTR site, the T2 aquifer is located from -150 to -210 m AHD which corresponds to the depth of 160-220 m below ground surface (Figure 2; Table 1). On the basis of lithological data (Gerges 2005; 2006a; 2006b) the aquifer was subdivided into three units called T2a, T2b and T2c (Figure 2).

The pumping tests performed in the area revealed that the average values of transmissivity and storativity of the T2 aquifer are 200 m<sup>2</sup>/day and 2.7x10<sup>-4</sup>, respectively (AGT 2007). The aquifer is quite heterogeneous over depth and this is directly related to its layered structure. The transmissivity of the T2a and T2b units is 50 m<sup>2</sup>/day (AGT, 2007), which indicates that the lower part of the profile (T2c) largely contributes to the total value of aquifer’s transmissivity. One would anticipate that this is due to the existence of the layer of high permeability which was encountered within the T2c aquifer at the ASR Parafield site (176-181.5 m AHD) and Greenfields Railway Station (175-181 m AHD) (Gerges 2005; Figure 2). Nevertheless, the occurrence of this layer was not definitely confirmed at the ASR site while

drilling the P2 piezometer to a depth of 225 m bgs (214 m AHD) in July 2008 (Appendix A) or during subsequent flowmeter analysis. Overall, the T2 aquifer is believed to be relatively homogeneous in the lateral direction (Gerges 2005; AGT 2007).

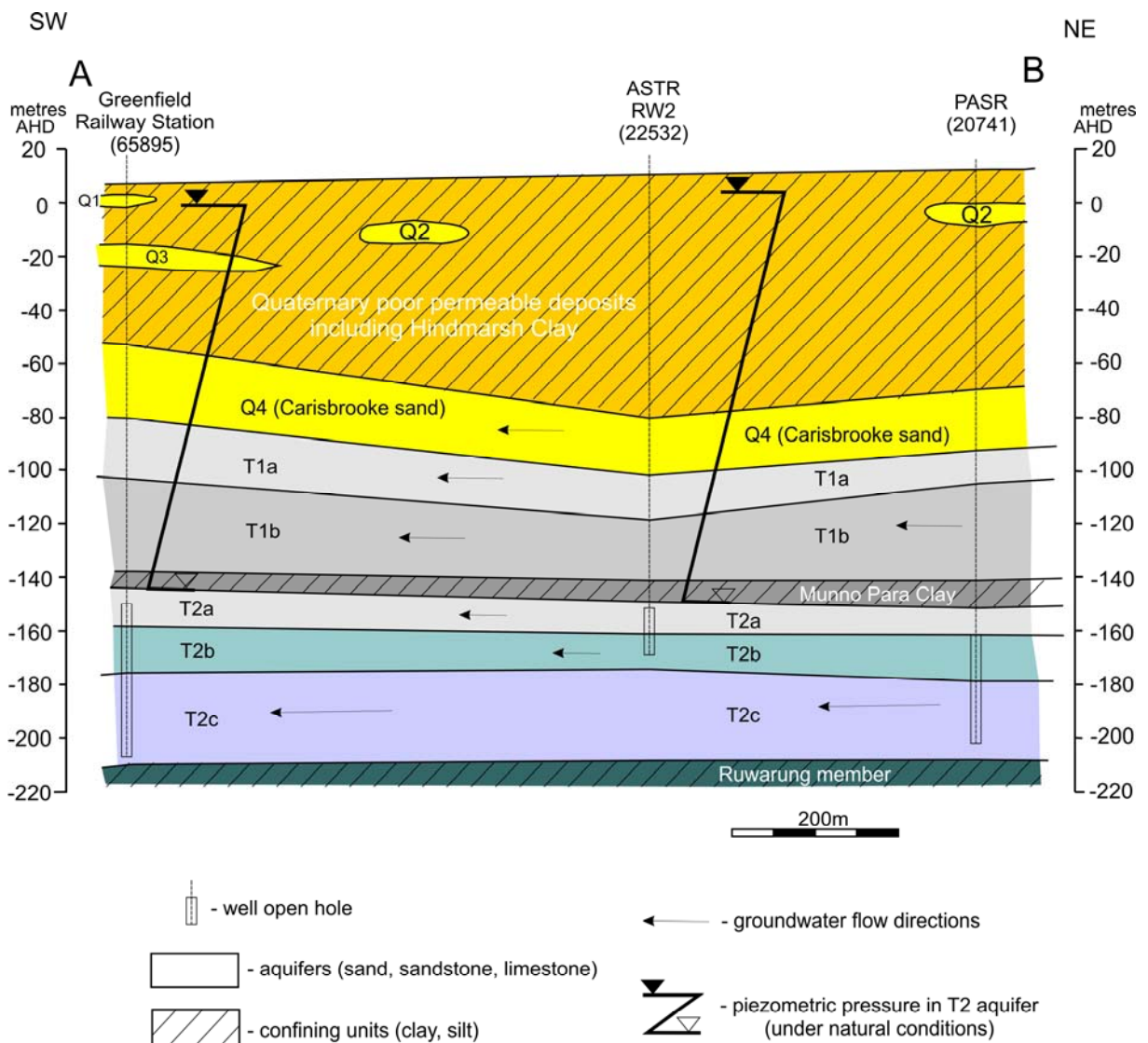


**Figure 2 Hydrogeological cross-section through Quaternary and Neogene aquifers in the ASTR site area. Groundwater flow directions and pressures are relevant for the natural conditions (when the ASTR system is not operating). Line of the cross section is shown in Figure 1.**

The ambient regional groundwater flow occurs approximately from east to west in T2 at the ASTR site, with a hydraulic gradient of 0.0015 (Pavelic *et al.* 2004), without significant seasonal variations. A stronger local gradient is possible due to the nearby Parafield ASR scheme. The ambient groundwater in the T2 aquifer is brackish, with total dissolved solids (TDS) measured at approximately 2000 mg/L (electrical conductivity (EC); specific conductance approximately 3600  $\mu\text{S}/\text{cm}$ ) at the ASTR site in May 2006 prior to injection.

**Table 1 Generalised hydrogeological setting at the ASTR site (modified from AGT 2007)**

Interval (m bgs)	Lithology	Stratigraphic unit	Aquifer
0 – 9	Top soil and clay	-	Confining beds
9 – 90	Clay, silt, sand	<i>Hindmarsh Clay</i>	Q1, Q2, Q3 aquifers and confining units
90 – 105	Fine sand (pale olive grey) lignite	<i>Carisbrooke Sand</i>	Q4 aquifer
105 – 120	Fine grained sandstone (light grey) lignite at bottom	<i>Hallet Cove Formation</i>	T1a subaquifer
120 – 152.5	Limestone	<i>Upper Port Willunga Formation</i>	T1b subaquifer
152.5 – 160	Clay (dark grey, olive, dark blue)	<i>Munno Para Clay</i>	Confining beds
160 – 172	Limestone (grey to white) moderately cemented		T2a subaquifer
172 – 187	Limestone (grey to yellow) well cemented interbedded with sand/silt	<i>Lower Port Willunga Formation (T2)</i>	T2b subaquifer
187 – 220*	Limestone, sand highly fossiliferous		T2c subaquifer
220 – >222**	Clay	<i>Ruwarung Member</i>	Confining beds

\* According to drillings in the area, 2m highly fissured layer occurs at the depth of 195-197 m (Gerges 2005). However, the existence of this layer was not confirmed while drilling P2 piezometer at the ASTR site.

\*\* Max thickness of Ruwarung member is 22 m (Geoscience Australia 2004).

## 2.3. Operational schedule

### 2.3.1. ASTR well field

Following the recommendations of modelling work by Pavelic *et al.* (2004), an ASTR well-field was progressively established between 2006 and 2007 at the Parafield Gardens Oval within the City of Salisbury, nearby two existing ASR wells which currently produce non-potable water supplies from the same stormwater harvesting facilities (Figure 1). The ASTR well field is a six-well system involving two inner recovery wells (RW) referred to as RW1 and RW2, and four outer injection wells (IW), herein referred to as IW1, IW2, IW3 and IW4, with inter-well distance of 50 m between inner and outer wells (Figure 3). RW1, RW2 and IW3 were first drilled in May 2006, while IW1, IW2 and IW4 were drilled in January 2007. In July 2008, three piezometers, herein referred to as P1, P2 and P3 were drilled for monitoring purposes along the IW1-RW1 transect, respectively 10, 20 and 30 m from RW1 (Figure 3).

The ASTR wells partially penetrate the T2 aquifer with the aim of precluding the low recovery efficiency and preferential flow that would invariably occur if the lower interval of the target aquifer (T2c) exhibiting higher hydraulic conductivity was intercepted (Kremer *et al.* 2008). The six ASTR wells are completed within units T2ab over an open interval of approximately 18 m from 165 to 182 m bgs. Piezometers P1 and P3 are open in unit T2a from 165.5 to 169 m bgs; while piezometer P2 is open in unit T2c from 210 to 215 m bgs. All injection/extraction wells were cased using 200 mm PVC casing to the depth of the top of the open hole, and then successfully pressure cemented (AGT 2007). Airlifting was performed at all ASTR wells after drilling for approximately four hours, each well produced a small amount

of sand and estimated well yields were approximately 10 L/s. The wells used for injection during the ASTR operations were not redeveloped between September 2006 and April 2009. IW3 was airlifted prior to its use as an injection well (June 2008).

Piezometers were cased using 200 mm PVC casing over the first six metres below the top of casing, and then using 100 mm PVC casing to the depth of the top of the open hole, and were pressure cemented.

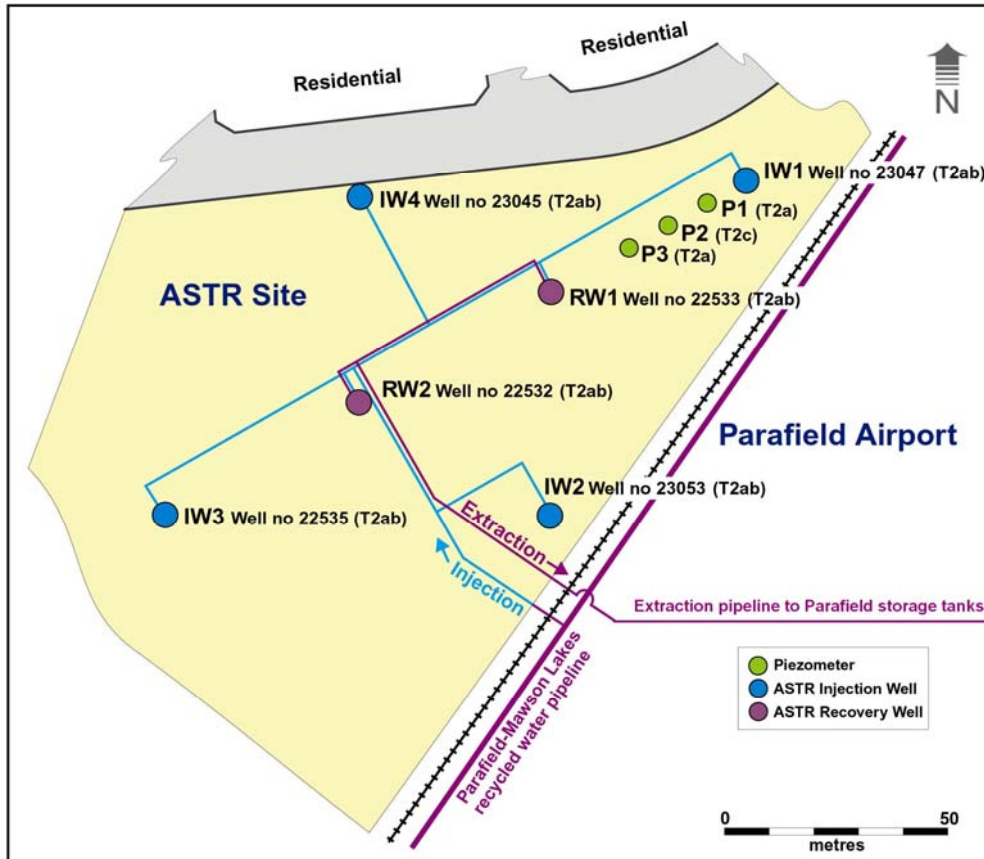


**Figure 3 Close up of the ASTR well-field showing four outer injection wells (IW1-IW4), two inner recovery wells (RW1-RW2) and three piezometers (P1-P3) (from Kremer *et al.* 2008)**

Groundwater samples from piezometers P1 and P3 had a pH of approximately 12 following drilling and development in July 2008. This suggested a contamination of the aquifer with cement used for well grouting. Extensive redevelopments of P1 and P3 were performed in September and October 2008. Groundwater sampled after 16 October 2008 showed that pH subsequently improved with values of approximately pH 8, but still gave evidence of cement contamination. Similar contamination was not apparent in piezometer P2 or any of the ASTR wells.

### 2.3.2. Water balance

The first phase of the ASTR operations conducted between September 2006 and June 2008 was a conditioning (flushing) phase which aimed to drive brackish water out of the storage area to create a plume of fresh water. This is to prevent extensive mixing between the injected water and the ambient groundwater when the storage and recovery of water occurs. The conditioning phase involved injection through the two inner wells RW1 and RW2, with 377 ML injected by June 2008 (Figure 4).

After the conditioning phase the second phase was undertaken in operational mode. Injection in the outer IWs began in September 2008, with 30 ML injected by the end of January 2009. After a total of 407 ML had been injected, the first recovery phase began in

February 2009. By end of April 2009, 106 ML has been recovered from the RW wells. It has to be emphasised that all the flushing, injection or recovery phases include multiples periods of variable duration when the pumps were off. Details of quantities of water injected and extracted in the ASTR well system and dates of events are presented in Table 2.

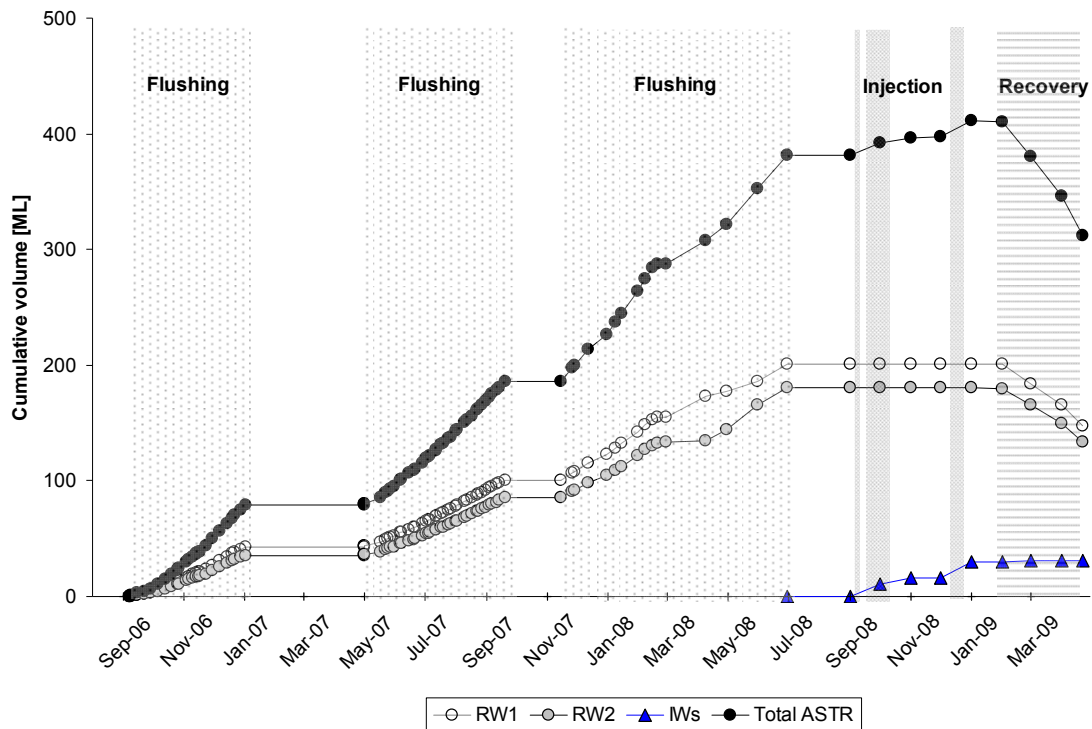


**Figure 4** Cumulative volume injected and recovered from the start of ASTR operation in September 2006 up to April 2009. This includes flushing phase (injection into RW - September 2006–June 2008), injection into IW (September - December 2008), and recovery (February-April 2009).

Between 2006 and 2008, mean injection rates were measured of 5.2 L/s at RW1 and 4.6 L/s at RW2. In 2008, during injection via IWs, mean flow rates were measured of 5 L/s at IW1, 4.4 L/s at IW2, 2.8 L/s at IW3 and 4.6 L/s at IW4. Given that lower injection rates were observed at IW3, airlifting was undertaken at this well in June 2008. Very little material was removed from IW3 and injection rates did not improve. Extraction rates were constant at 9.9 L/s at RW1 and RW2 between February and April 2009.

**Table 2 Quantities of water injected and extracted in the ASTR system, from September 2006 to March 2009 (from Page *et al.* 2009)**

Month	Injected (ML)							Extracted (ML)			Date: Event	
	Monthly Totals		Cumulative volume injected - RW	Monthly Totals				Cumulative volume injected - IW	Monthly Totals			Cumulative volume extracted
	RW1	RW2		IW1	IW2	IW3	IW4		RW1	RW2		
Sep-06	3.6	2.9	6.6	0	0	0	0	0	0	0	0	7: Injection started (RW) - reedbed water
Oct-06	9.4	7.8	23.8	0	0	0	0	0	0	0	0	3: Switched to Parafield ASR water
Nov-06	14.1	11.9	49.8	0	0	0	0	0	0	0	0	14: Switched to reedbed water
Dec-06	13.9	13.0	76.7	0	0	0	0	0	0	0	0	
Jan-07	2.1	0.0	78.8	0	0	0	0	0	0	0	0	2: Injection stopped
Feb-07	0.0	0.0	78.8	0	0	0	0	0	0	0	0	
Mar-07	0.0	0.0	78.8	0	0	0	0	0	0	0	0	
Apr-07	0.0	0.0	78.8	0	0	0	0	0	0	0	0	
May-07	9.2	7.6	95.6	0	0	0	0	0	0	0	0	1: Injection started (RW) – reedbed water
Jun-07	11.0	9.2	115.8	0	0	0	0	0	0	0	0	
Jul-07	12.2	13.2	141.1	0	0	0	0	0	0	0	0	
Aug-07	16.1	11.4	168.6	0	0	0	0	0	0	0	0	20: Switched to Parafield ASR water
Sep-07	6.5	5.9	181.0	0	0	0	0	0	0	0	0	29: Injection stopped
Oct-07	0.0	0.0	181.0	0	0	0	0	0	0	0	0	
Nov-07	8.7	7.6	197.2	0	0	0	0	0	0	0	0	19: Injection started (RW) – Parafield ASR water
Dec-07	15.7	13.8	226.7	0	0	0	0	0	0	0	0	10: Injection stopped 19: Injection started – Parafield ASR water
Jan-08	20.1	17.5	264.3	0	0	0	0	0	0	0	0	
Feb-08	11.9	11.7	287.9	0	0	0	0	0	0	0	0	
Mar-08	14.6	0.7	303.1	0	0	0	0	0	0	0	0	
Apr-08	4.5	9.4	317.0	0	0	0	0	0	0	0	0	25: Switched to reedbed water
May-08	8.8	21.9	347.6	0	0	0	0	0	0	0	0	
Jun-08	14.9	14.3	376.9	0	0	0	0	0	0	0	0	30: Injection stopped
Jul-08	0	0	376.9	0	0	0	0	0	0	0	0	

Month	Injected (ML)			Monthly Totals				Cumulative volume injected - IW	Extracted (ML)			Date: Event
	Monthly Totals		Cumulative volume injected - RW	IW1	IW2	IW3	IW4		Monthly Totals		Cumulative volume extracted	
	RW1	RW2							RW1	RW2		
Aug-08	0	0	376.9	0	0	0	0	0	0	0		
Sep-08	0.1	0	377.0	3.3	3.6	0.5	3.0	10.3	0.3	0.7	1.0	3: Injection started (IW) – Parafield ASR water 5: Injections stopped 19: Injection started (IW) - Parafield ASR water
Oct-08	0	0	377.0	1.7	1.9	0.1	1.7	15.6	0	0	1.0	8: Injection stopped
Nov-08	0	0	377.0	0	0	0.1	0	15.8	0	0	1.0	
Dec-08	0	0	377.0	4.1	3.5	2.3	4.1	29.8	0	0	1.0	13: Injection started (IW) - Parafield ASR water 21: Injection stopped
Jan-09	0	0	377.0	0	0	0.2	0	30.0	0	0	1.0	
Feb-09	0	0	377.0	0	0	0.5	0	30.5	11.5	9.6	22.1	1: Extraction started (RW)
Mar-09	0	0	377.0	0	0	0.7	0	31.2	20.0	17.0	59.1	
April-09	0	0	377.0	0	0	1	0	32	25.9	20.7	105.7	30: Extraction stopped

### 3. SOURCE WATER AND GROUNDWATER MONITORING

#### 3.1. Methods

The standing water level (SWL) was monitored at RW1, RW2, IW1 and IW3 by down-hole CTD loggers between June 2007 and April 2008, and also by manual measurement between September 2006 and April 2009. Loggers were not continuously deployed in all locations due to the small number of loggers available to monitor the whole site. Since August 2008 SWL had been observed at piezometers P1, P2 and P3 from down-hole level loggers and manual measurements. Prior to 16 April 2009, loggers in P2 and P3 were not deep enough to measure drawdown induced by extraction via the RW wells. During periods when SWL was not monitored via loggers, manual measurements were used to assess the extent of the drawdown at P2 and P3.

Monitoring of surface water quality in the cleansing reedbed of the Parafield stormwater harvesting system was performed by the grab sampling at the inlet and outlet of the system. Electrical conductivity of the source water was monitored using field and laboratory measurements from the reedbed outlet or directly at the injection wells, and a conductivity, temperature and depth (CTD) logger at the outlet of the wetland (Page *et al.* 2008).

Groundwater at the ASTR site was sampled using a submersible pump, ensuring that the entire volume of water in the well was displaced at least three times prior to sample collection. In addition to this, down-hole profiling at discrete time intervals in conjunction with continuous data logging with *in situ* CTD probes were conducted. Temperature, EC, dissolved oxygen (DO), pH and redox potential were measured directly in the field using a TPS 90FLMV field analyser and a flow-through cell during pumping. Samples were collected once these values had stabilised. Down-hole EC and temperature profiles were performed using an YSI 600 down-hole water quality analyser on the aquifer profile (Appendix B).

During the flushing phase, from September 2006 to August 2008, sampling and profiling of the IWs was performed on an approximately monthly basis. CTD loggers were installed in IW1 and IW3 at a depth of ~175 m (-165 m AHD) from June 2007 to April 2008 to detect the spread of the freshwater plume during injection into the RWs.

Since September 2008 when injection commenced into the IWs, profiling of all IWs and piezometers were performed on an approximately monthly basis. Additional down-hole level loggers were established in September 2008 in piezometers P1, P2 and P3, at depths 167, 213, and 167.5 m bgs, respectively. Sampling of the groundwater was performed at P1, P2 and P3 after the drilling of the piezometers in July 2008.

Since there is a relation between salinity of water expressed as total dissolved solids (mg/L) and electrical conductivity (specific conductance; in  $\mu\text{S}/\text{cm}$ ), the latter is used as a degree of salinity of water. Normally, both salinity and electrical conductivity are given in the report and then TDS is calculated on the basis of EC according to the formula given by Hem (1985).

#### 3.2. Comparison of sampled versus *in situ* EC

Flushing of the brackish aquifer with stormwater was monitored by sampling, profiling and *in situ* logging methods. Sampling coincident with profiling or logging (collected immediately prior to the sampling event) allows an assessment of the precision of EC measurements. While sampling gives an EC that represents the flux-averaged (FA) salinity of the adjacent groundwater, profiled or *in situ* EC measures the volume-averaged (VA) concentration within the well.

FA and VA EC data collected at the four IWs and the three piezometers are reasonably well correlated as presented in Figure 5. Data collected at IW1 and IW3 in July 2007 at the highest salinity concentration showed that FA EC were higher than VA EC by up to 517  $\mu\text{S}/\text{cm}$ . Conversely, from September 2007, after 181 ML had been injected via the RWs, FA EC at the four IWs appeared to underestimate the breakthrough of fresh water measured

by VA data by up to 1013  $\mu\text{S}/\text{cm}$ . At the freshest salinity concentration observed in April 2009, FA EC at P1, and P3 slightly overestimated the VA measurement with a maximum variation of 68  $\mu\text{S}/\text{cm}$  for piezometer P3 in April 2009.

Results at P2 showed a different relationship between FA and VA EC compared with previously described results for IWs, P1 and P3. Results at P2 prior to recovery in February 2009 (green triangles on Figure 5) showed fresher VA values than FA measurements, with an overestimation by up to 1,951  $\mu\text{S}/\text{cm}$  on 23/09/2008. Whereas, results at P2 on the 16/04/2009, after recovery occurred, showed a similar correlation to other wells, with FA overestimating VA EC by 810  $\mu\text{S}/\text{cm}$  while both measurements showed saline groundwater.

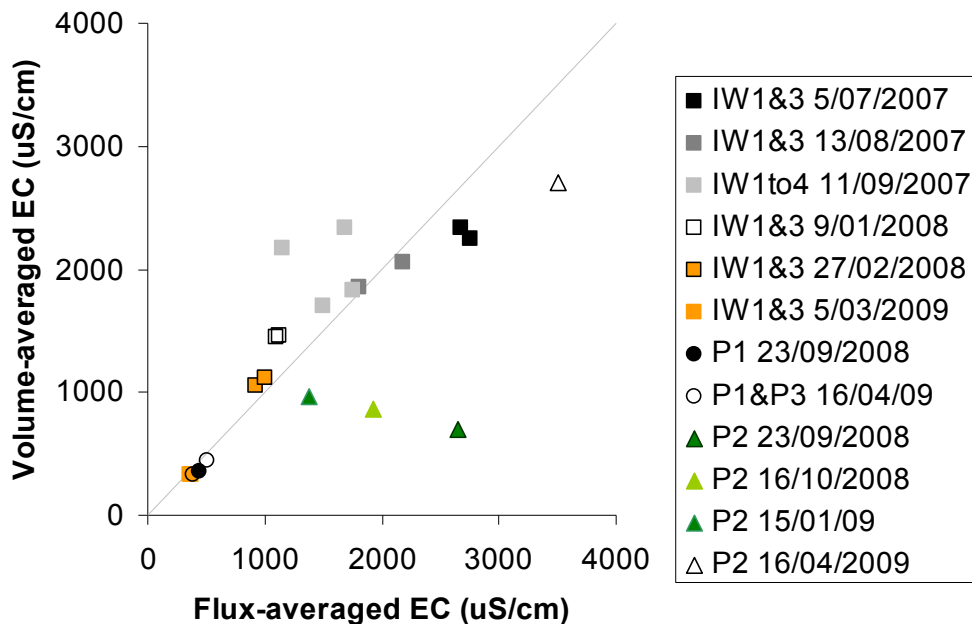


**Figure 5 Volume-averaged versus flux-averaged EC, measured at IWs, P1, P2 and P3 between July 2007 and April 2009**

Not surprisingly, the more the fresh plume breaks through the observation zone, the more FA EC approximates the VA EC. Indeed, when pumping occurred, a greater proportion of flow came from the more permeable layer. Thus as more of the breakthrough front passed the observation wells, the mean of the VA EC measured within the well deviated from the FA EC of the adjacent groundwater measured during sampling. Therefore, the underestimation of FA EC relative to VA EC suggested that the more permeable layer contains fresher water, confirming the breakthrough of the injected water within the heterogeneous aquifer.

### 3.3. Source water salinity

Source water for both ASR and ASTR projects is reedbed-treated stormwater from the Parafield Wetlands system. The detailed description on reedbed water quality and quantity is covered in Page *et al.* (2009). Extracted water from Parafield ASR system was at times used as source water for ASTR after recirculation through the reedbed prior to injection, due to unavailability of stormwater to flush the ASTR well field (Figure 6).

Average EC measured during injection into the RWs between September 2006 and June 2008 was  $233 \pm 58 \mu\text{S}/\text{cm}$  (Figure 6). As no loggers were available between November 2007 and July 2008, salinity of the source water was not constantly monitored. During this period, grab samples showed that salinity increased as observed in February 2008 (Figure 6). This is understood to be due to the source water switching from stormwater to Parafield ASR

water. Despite this, the salinity of the injected water remained below 500 mg/L TDS (EC ~890  $\mu\text{S}/\text{cm}$ ) which is the threshold fixed by the site operator for shutdown of injection.

Average salinity between September and December 2008 during the injection period at the IWs was  $218 \pm 67 \mu\text{S}/\text{cm}$ . Salinity decreased quickly during the last period of injection in December 2008, dropping from 440  $\mu\text{S}/\text{cm}$  on the 13<sup>th</sup> December to 210  $\mu\text{S}/\text{cm}$  on 21<sup>st</sup> December due to low contribution of Parafield ASR water in the mixture.

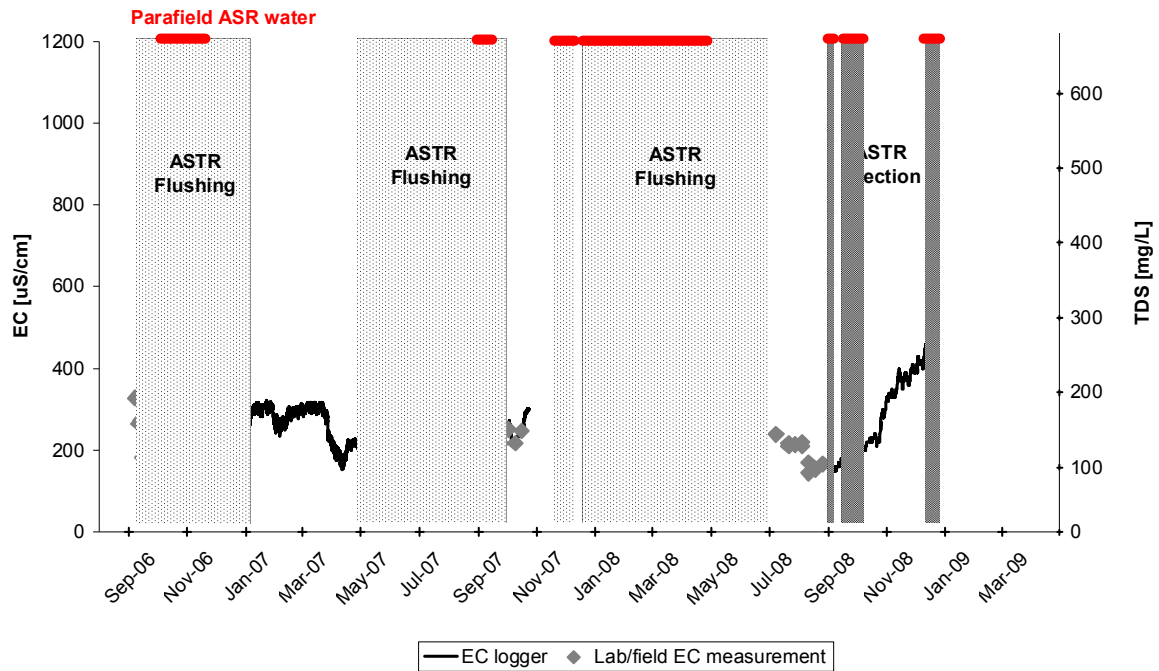


**Figure 6 Salinity of the source water versus time measured from logger and laboratory and field measurements from the wetland. Periods of injection at the RWs (flushing) and IWs (injection) are also presented, as well as periods when Parafield ASR water was used as source water for injection at ASTR.**

### 3.4. Groundwater level and salinity

#### 3.4.1. Hydraulic head observations

Groundwater level in the T2 aquifer prior to operation of the ASTR site was approximately 5 m AHD. During injection into the RWs, an increase in water level up to approximately 60 m AHD at both RWs was observed. Injection pressure in the aquifer resulted in all IW wells becoming artesian with SWLs up to 15 m AHD and site ground elevations of 9-10 m AHD (Figure 7).

Storage periods resulted in the stabilisation of the SWL level at approximately 5-6 m AHD.

During extraction from the RWs between February and April 2009, water level in the aquifer dropped to approximately -11.5 m AHD in the IW1 and IW3 wells and -14.5 m AHD in the IW2 and IW4 wells. This difference is attributed to the heterogeneity of the aquifer, and operations at the Parafield ASR site nearby.

SWL was observed at piezometers P1, P2 and P3 from down-hole level loggers and manual measurements (Figure 8). Prior to 16 April 2009, loggers in P2 and P3 were not deep enough to measure drawdown induced by extraction via the RW wells. During periods when

SWL was not monitored via loggers, manual measurements were used to assess the extent of the drawdown at P2 and P3.

SWLs at all piezometers are correlated with ASTR and nearby ASR operations as shown on Figure 8. Injection at the four IWs with flow rates per well ranging between 2.8 and 5 L/s led to increases in hydraulic head from 10 to 20 m at P1, from 1 to 3 m at P2 and from 6 to 10 m at P3 (marked (a) on Figure 8). Extraction at the nearby ASR wells can also be observed in SWL variations at the three piezometers when no ASTR operations occur (marked (c) on Figure 8). Injection at the two ASR wells at an average rate of 25 L/s led to increases of hydraulic head of about 4 m at P1, P3 and P2.

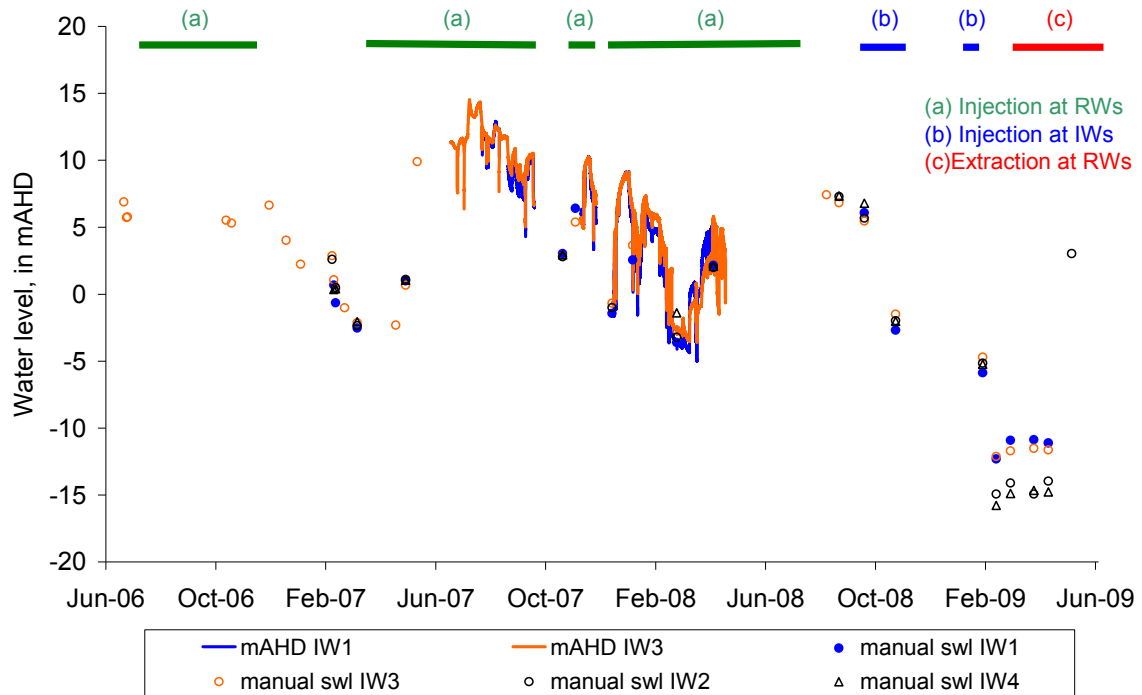


**Figure 7 Water level versus time in IW1 (10.4 m AHD), IW2 (10.1 m AHD), IW3 (10.0 m AHD) and IW4 (10.3 m AHD). Operations periods at ASTR are also shown for information.**

Water level responses at P2 (in T2c) differ from that at P1 and P3 (in T2ab) in terms of magnitude when injection or recovery occurs at the ASTR site (Figure 8 during (a) or (b)). When there is no operation at the ASTR and ASR sites, SWL responses at P1, P2 and P3 are similar (e.g. in January 2009 on Figure 8).

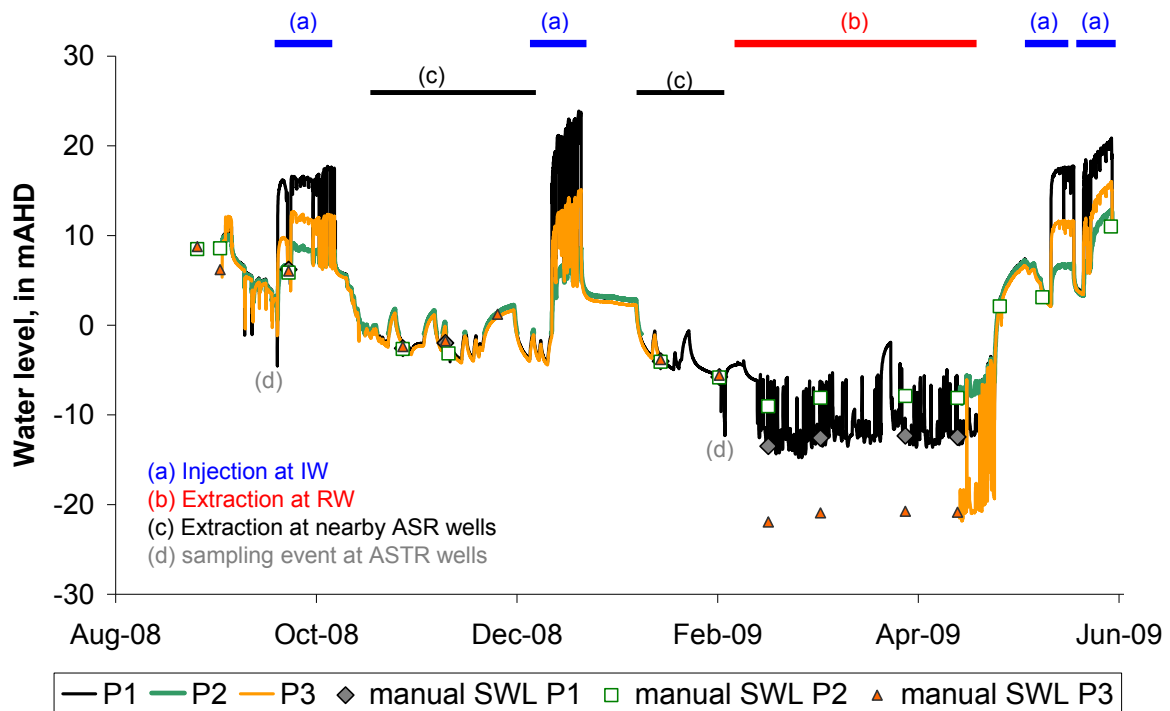


**Figure 8 Water level versus time in P1 (10.2 m AHD), P2 (11.1 m AHD) and P3 (11.2 m AHD), and manual SWL measurements between August 2008 and June 2009. Operations at ASTR and at nearby Parafield ASR are also presented for information.**

Between August 2008 and April 2009, the maximum SWL observed at the piezometers during injection at the IWs was ~24 m AHD at P1, ~8 m AHD at P2 and ~15 m AHD at P3. The elevations of the top of casing of ASTR and piezometers range between 10 m AHD for IW3 and 11 m AHD for P2. Thus, ASTR wells and piezometers can be artesian during injection at ASTR and/or nearby ASR wells.

### 3.4.2. Solute observations

#### ***Observations during the flushing phase (September 2006 to August 2008)***

Salinity of ambient groundwater within T2c aquifer at the ASTR site is 2000 mg/L which corresponds to electrical conductivity of ~3600  $\mu\text{S}/\text{cm}$ .

As a result of the site operation EC decreased from 3620  $\mu\text{S}/\text{cm}$  in June 2006 to 591  $\mu\text{S}/\text{cm}$  in August 2008 (Figure 9). The first drop in salinity was observed at IW3 on 19 December 2006, 104 days after the beginning of injection via RWs on 7 September 2006, and after 70 ML had been injected.

No significant increase in EC occurred during storage intervals between injection events (white areas in Figure 9) suggesting that any ambient groundwater remaining in the less permeable parts of the aquifer is likely either to be small or to diffuse slowly, and that no significant movement of the fresh plume as a result of groundwater gradients occurs. Most significant increases in salinity observed during stoppage periods occurred in early 2007 when the fresh plume had only just begun to reach the IWs.

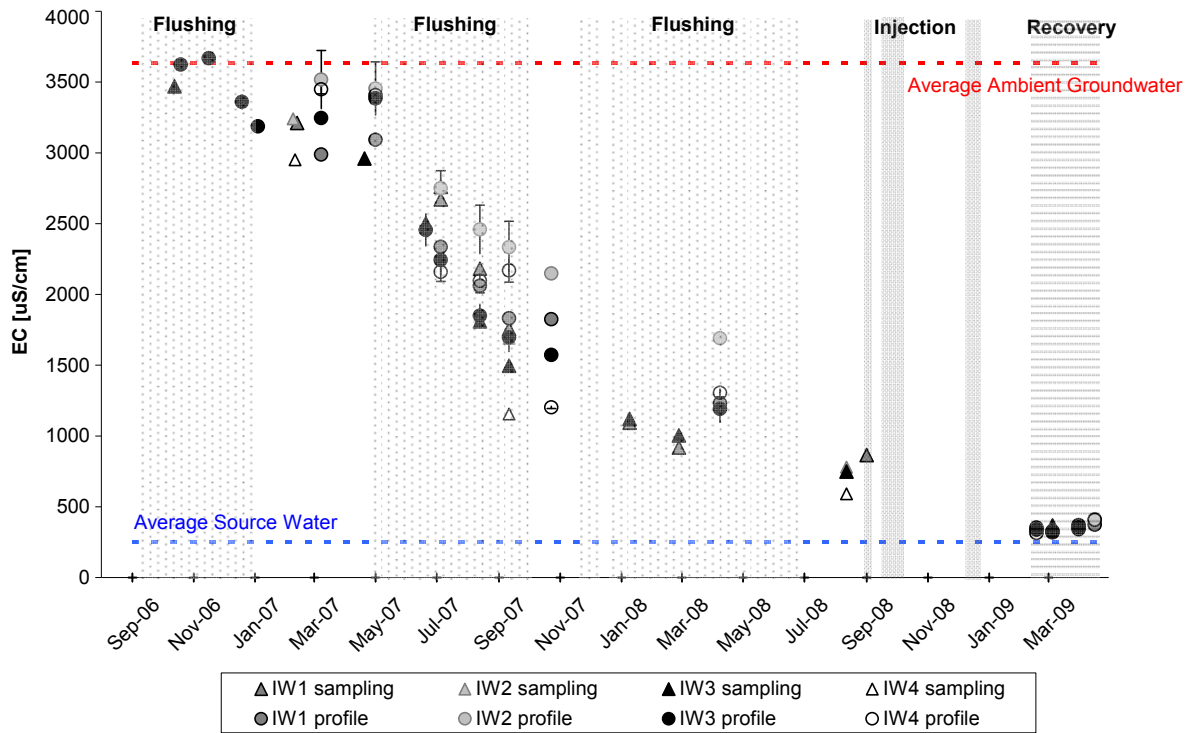


**Figure 9** Depth-averaged EC data versus time obtained from down-hole profiles over the open intervals, and EC data collected during sampling, at the 4 IW during the flushing phase. Flushing periods are presented as grey areas.

The pore volume of each well is shown in Figure 10, where the mixing fraction 'f' for each sampling event is plotted against volume injected. The mixing fraction represents the proportion of injected water in any sampled mixture. Based on the results from well IW1 and IW3 which were monitored more frequently, one pore volume is  $\sim 190 \text{ ML} \pm 10 \text{ ML}$ . Wells IW2 and IW4 were monitored less frequently and as such results showed greater variation, however, IW2 did appear to show a delayed breakthrough response.

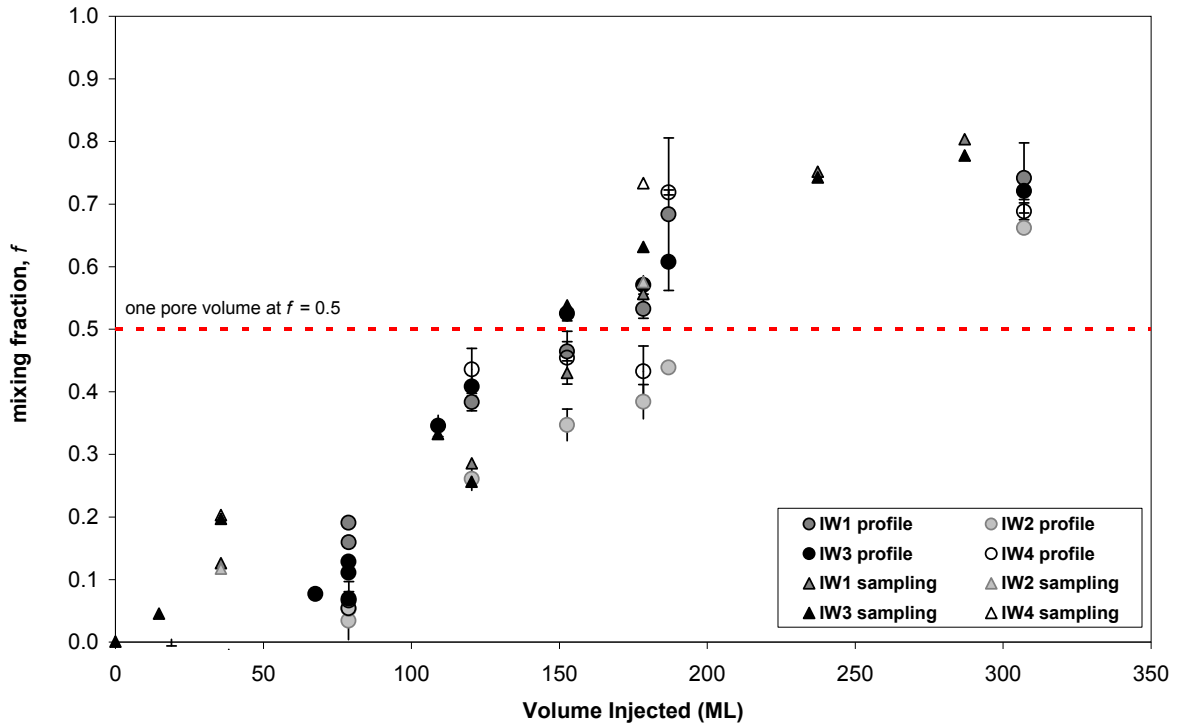
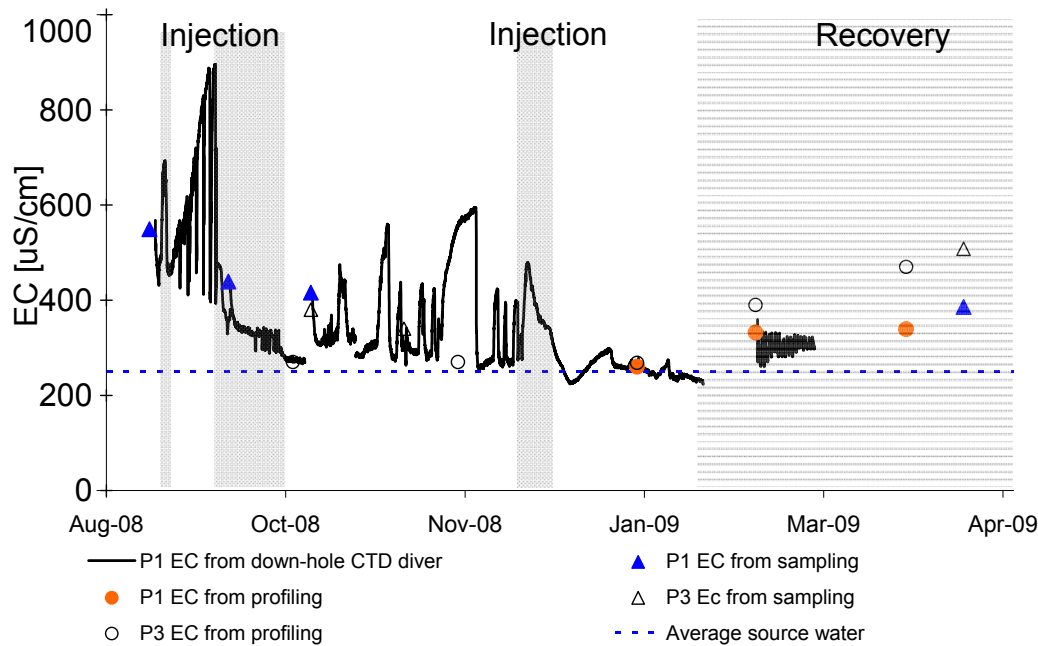


Figure 10 Mixing fraction ' $f$ ' measured in the IW wells as a function of volume injected

**Solute observations in T2ab during the first injection phase (September 2008-January 2009)**

From September 2008 to January 2009, 30 ML was injected via the four IWs in two injection events. During this injection phase, averaged EC at the four IWs dropped from 870  $\mu\text{S}/\text{cm}$  (two days before injection in IWs – 1/09/2008) to 430  $\mu\text{S}/\text{cm}$  (58 days after end of injection in IWs – 17/02/2009). While injecting via the IWs, breakthrough of injectant in T2ab was assessed using EC data from sampling of piezometers P1 and P3 (Figure 11), as well as profiled and *in situ* data after redevelopment of the piezometers and cement contamination was controlled.



**Figure 11 EC over time observed at P1 from a down-hole CTD diver; and EC data collected at P1 and P3 from sampling and profiling measurement, between August 08 and March 2009**

Data collected during sampling both at P1 and P3 are stable over time, with mean sampled EC values of  $313 \pm 55 \mu\text{S/cm}$  and  $397 \pm 111 \mu\text{S/cm}$ , respectively. EC data collected from the down-hole CTD logger in P1 shows large variations over time between August and December 2008. Stabilisation of the logger salinity signal can be observed in September and December 2008, during or just after injection into IWs.

Large fluctuations observed in August and September 2008 are related to SWL variations due to sampling events at the ASTR wells (Figure 7), and notably linked with development of P1 in September and October 2008 that was undertaken to remove the cement contamination discussed previously.

Fluctuations observed between October and December 2008 in between the injection events can be related to SWL variations resulting from extraction at the ASR site (Figure 7). This suggests that variations in EC are likely to be due to the displacement of the fresh plume created by injection firstly into RWs and then IWs.

#### ***Solute observations in T2ab during the first recovery phase (February 2009-April 2009)***

From February to April 2009, 105.7 ML was extracted from the two RWs. Salinity of the recovered water monitored at RWs met the target value of 500 mg/L TDS ( $\sim 890 \mu\text{S/cm}$ ) with mean EC calculated at  $532 \pm 108 \mu\text{S/cm}$  (Figure 12). Not surprisingly, salinity of the recovered water increased during extraction from  $305 \mu\text{S/cm}$  in February 2009 to a maximum of  $617 \mu\text{S/cm}$  on the 8<sup>th</sup> April 2009. Nevertheless, salinity stopped increasing approximately from the 8<sup>th</sup> April and approached steady state until the end of the recovery period with an EC of  $577 \mu\text{S/cm}$  on the 28<sup>th</sup> April. The extraction stopped on the 30<sup>th</sup> April 2009 when stormwater became available for irrigation/other intended uses, and injection began again.

Salinity measured at P3 located 20 m from RW1 presented the same pattern as observed at RW1 with an increase in salinity during the first part of the extraction period from  $390 \mu\text{S/cm}$  on the 17<sup>th</sup> February to  $550 \mu\text{S/cm}$  on the 19<sup>th</sup> March 2009, and then a constant decrease in salinity down to  $420 \mu\text{S/cm}$  on the 22<sup>nd</sup> April by the end of the recovery period. Salinity observed at P1 (40 m from RW1) and IW1 (50 m from RW1) showed a different pattern with a stable signal without significant variations (Figure 12). Salinity histories at the three other IWs were very similar to the one observed at IW1, with an average salinity value calculated

at  $375 \pm 38 \mu\text{S/cm}$  for the four IWs from four profiling events (between February and April 2009).

The salinity of the recovered water is expected to increase as the portion of brackish ambient groundwater recovered increases and is generally greatest on the outer edges of the storage zone. However in this case the opposite is observed and IW1 freshens with recovery.

It is predicted that the EC trend for recovered water salinity relates to the salinity variations in the last 196 ML injected in RWs during the final flushing phase from November 2007 to July 2008. Unfortunately, there is inadequate data to verify this assertion.

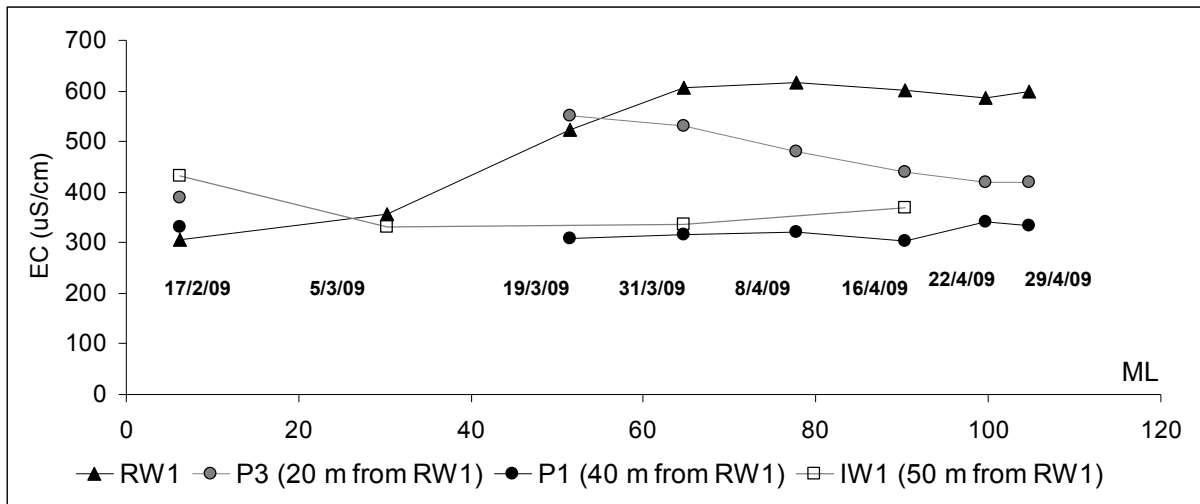


**Figure 12 EC versus volume measured at RW1, P3, P1 and IW1 showing the evolution of salinity on the transect RW1-IW1 during recovery of 104.7 ML via RWs between February and April 2009 (date of data collection is also presented)**

### **Solute observation at P2 in T2c**

EC data from piezometer P2 showed a clear breakthrough of injectant in the bottom part of the aquifer not intersected by the ASTR wells, with values collected during sampling decreasing from  $2700 \mu\text{S/cm}$  in September 2008 to  $1380 \mu\text{S/cm}$  in January 2009 during the injection phase (Figure 13). Data obtained from the down-hole CTD logger appeared to be in agreement with the freshening of T2c, and profiling and sampling measurements at P2. Consistent increases in salinity when pumping P2 for sampling suggest the presence of a highly transmissive layer which induces flow from a more transmissive media beyond the perimeter of the drilled well. Nevertheless, the variation in EC data from the down-hole CTD logger at P2 (Figure 13) does not show any correlation with Parafield ASR operations, contrary to SWL variations (Figure 8), suggesting that the layer intersected by P2 is homogeneously flushed so that no variation in EC appears when the fresh plume is moving due to the gradient observed in SWL variations.

From February 2009, the salinity at P2 increased rapidly which is likely due to reversal flow induced from the extraction from the RWs. By May 2009, EC at P2 had returned to the initial ambient value of  $\sim 3630 \mu\text{S/cm}$  found in T2ab prior to any injection at the ASTR site (Figure 13). No data are available to characterise water salinity in T2c at the ASTR site before the injection of fresh water. Nonetheless it is assumed that salinity in T2c was equivalent to salinity observed T2ab. At the nearby Parafield ASR site, the 'PASR 20741 well' which intercepts T2abc from 174 to 197 m bgs, showed an initial EC of  $3640 \mu\text{S/cm}$  in April 2003, prior to any injection operations.

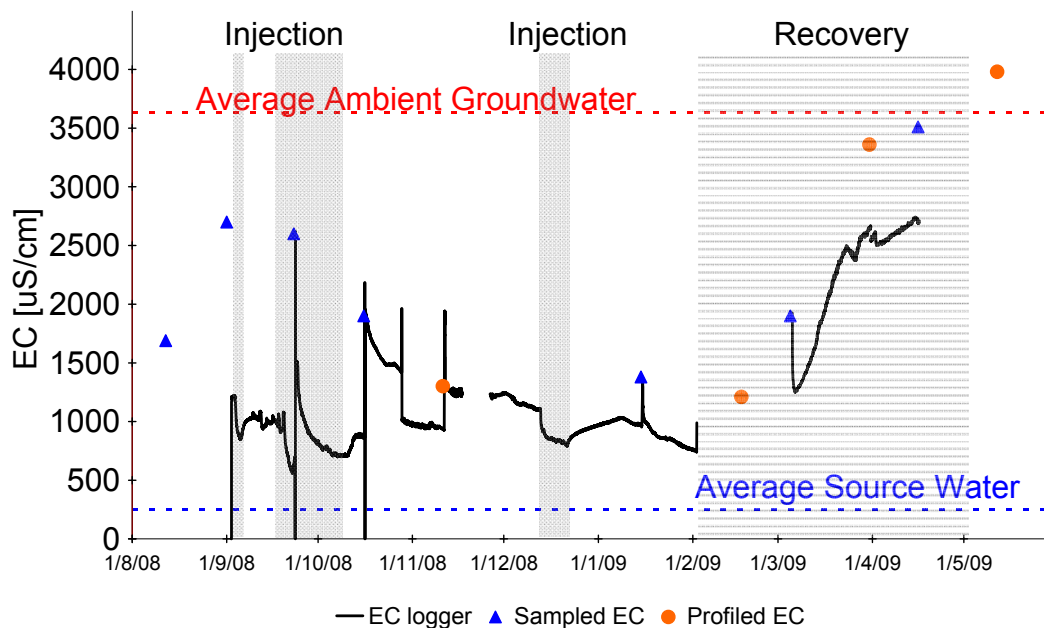


**Figure 13 EC versus time observed at P2 from a down-hole CTD diver; and EC data collected at P2 from sampling and profiling measurement, between August 08 and June 09. Average EC values of ambient groundwater and source water are also presented.**

## 4. GROUNDWATER MODELLING

Three dimensional groundwater flow and conservative solute transport modelling was developed for the ASTR site to simulate mixing and residence time of the injected water within the aquifer. A previous study by Pavelic *et al.* (2004) aimed to design the optimal well-field configuration of the ASTR scheme using a 2D model based on available data prior to site establishment. A second study by Kremer *et al.* (2008) used a 3D ASTR field-based model to provide an initial assessment of the ASTR operations including predictions of the flushing effect on the system efficiency.

In this study, the previous 3D modelling is revised and validated using additional data from the previously unstudied lower part of the T2 aquifer and operational input data, including injection in the four IWs and recovery from the two RWs, as per normal operational mode. Revised and validated modelling provides a powerful field-based predictive tool which is able to simulate the fate of injected water within the aquifer to assess the viability of the ASTR scheme under various operational scenarios.

### 4.1. Simulation package

Groundwater flow and solute transport modelling for the ASTR site was undertaken using commercial code FEFLOW Version 5.1 (Diersch 2005), which is a three dimensional finite-element package that has a built-in grid design, problem editing and graphical post processing display modules that allow rapid model development, execution and analysis. All simulations were done under saturated porous media conditions in a confined aquifer. Due to the succession of injection and extraction phases at the different wells, simulations were transient both for flow and transport. Density effects were not taken into account in the model as the salinity contrast between the injected water and the ambient groundwater was considered insufficient to warrant inclusion (Ward *et al.* 2008; 2009). A 3D model was needed to account for the six injection/extraction wells which involved different operational inputs and to accommodate the plume over the entire T2 aquifer including unit T2c.

## 4.2. Methods of analysis

### 4.2.1. Mixing fraction

Any conservative solute for which the concentration in the injected water differs sufficiently from the concentration in the native groundwater can be used as a tracer to quantify the movement and the mixing of the injected water within the aquifer. A mixing fraction ( $f$ ), representing the proportion of the injectant in any sampled mixture, can be estimated from the following simple mass balance equation:

$$f = \frac{C_{amb} - C_{mix}}{C_{amb} - C_{inj}} \quad \text{Equation 1}$$

Where  $C_{amb}$  is the conservative solute concentration in the native groundwater,  $C_{mix}$  is the conservative solute concentration in the mixture and  $C_{inj}$  is the concentration of a conservative solute in injected water. The mixing fraction can be expressed in terms of an absolute value, from 0 to 1, or in percentage terms (where a value of 1 corresponds to 100% of injected water).

In this study, salinity was assumed to behave as a conservative tracer. Moreover, the pronounced distinction between ambient and injected concentrations and the abundance of EC data allows one to calibrate the solute transport model. In the following discussion, the salinity is expressed as the mixing fraction which is calculated using average EC data from ambient groundwater and injected water, set as initial conditions of 3,633  $\mu\text{S/cm}$  and 250  $\mu\text{S/cm}$ , respectively.

For the sake of simplicity, mixing fractions were calculated and implemented in FEFLOW using a 'relative' solute concentration ranging from 0 to 1 mg/L, set at the value 0 for the ambient groundwater (EC = 3633  $\mu\text{S/cm}$ ) and the value 1 for the injected water (EC = 250  $\mu\text{S/cm}$ ). EC of the mixture can be calculated from the mixing fraction value by the use of formula:

$$EC_{mix} = f * EC_{inj} + (1 - f)EC_{amb} \quad \text{Equation 2}$$

Where  $f_x$  - mixing fraction,  
 $EC_{inj}$  - electrical conductivity of injected water,  
 $EC_{amb}$  - electrical conductivity of ambient groundwater.

### 4.2.2. Residence time

The computation of residence time of the injected water in the aquifer is required to assess the degree of attenuation of potential contaminants between injection and recovery periods. In the case under examination, a modified method of direct simulation of groundwater age was used (Goode 1996; Varni and Carrera 1998; Diersch 2005). The method was adapted by assuming a biodegradable tracer present at some defined concentration in the injected water but absent in the ambient groundwater. That tracer exhibits a simple exponential decay as described by the following equation (Pavelic *et al.* 2004):

$$\frac{C(t)}{C_o} = e^{-\lambda t_{eff}} \quad \text{Equation 3}$$

Where  $t_{eff}$  is the effective residence time of the water in the aquifer, uncorrected for mixing with the ambient groundwater (d),  $\lambda$  is the decay rate constant (1/d),  $C(t)$  is the tracer concentration at some time  $t$  (mg/L) and  $C_o$  is the tracer concentration in injected water (mg/L).

The aforementioned method takes into account the effects of dispersion and mixing within the aquifer which tends to exaggerate the minimum residence time of the recovered water by

decreasing the tracer concentration used in Equation 3. On the other hand, the calculated residence time can be overestimated since some contaminants, including bacteria and viruses, can be transported via preferential flow paths in aquifers (Rehmann *et al.* 1999; Mailloux *et al.* 2003). When estimating the fate of contaminants in the aquifer, one should consider the changes in temperature of groundwater as a result of injection operations.

### 4.3. Previous groundwater modelling at the ASTR site

Pavelic *et al.* (2004) developed a 2D FEFLOW groundwater model based on limited data to characterise the aquifer from nearby Parafield ASR and Greenfields Railway Station (GRS) sites (Figure 1), and validated by a semi-analytical method derived from Theis equations (Table 3). This initial groundwater model was used to establish the optimal well-field design of the ASTR scheme assuming two key constraints. Firstly, a residence time of injected water within the aquifer greater than 200 days was required to ensure inactivation of pathogens, which are potential hazards within the source water. Secondly, recovered water, which is a mixture of native groundwater and injected water, should contain no more than 10% native groundwater to achieve a target quality of less than 300 mg/L total dissolved solids (TDS). The results revealed that the configuration which best met the required criteria was a six-well system of four outer injection wells and two inner recovery wells all equidistant with an inter-well separation distance of 75 m.

However, modelling subsequent to the Pavelic *et al.* (2004) study following the collection of local aquifer hydraulic conductivity data from a newly constructed well and two existing wells led to a revision of the conceptual model of the aquifer. This revision indicated that a reduction in the inter-well spacing from 75 m to 50 m was required to reduce the amount of mixing with ambient groundwater (Kremer *et al.* 2008). The construction of partially-penetrating wells was also recommended to preclude the low recovery efficiency and preferential flow that would invariably occur if the lower interval of the target aquifer with high hydraulic conductivity was also intercepted.

3D flow and solute modelling detailed in Kremer *et al.* (2008) was developed based on previous data and additional aquifer characterisation at the ASTR site, and solute breakthrough data collected during the flushing phase between September 2006 and October 2007 (Table 3). The investigations of the aquifer at the site were performed within the upper parts of the aquifer only (T2a and T2b). Additional flowmeter analysis, undertaken approximately 300 m from the study area at Parafield ASR and GRS wells, indicated higher hydraulic conductivity values in the bottom part of the aquifer which is not intersected by the ASTR wells (T2c).

On the basis of the aquifer characterisation study performed until October 2007 (AGT 2007), 3D groundwater flow and solute modelling exercises involved the development of two conceptual models that used a layered structure to describe the vertical heterogeneity of the aquifer (Figure 14). These models differed by representing either only the part of the aquifer intersected by the open interval of the ASTR wells (conceptual model CM1) or the entire aquifer (conceptual model CM2). Thus, the latter model included that part of the profile which was not intersected by the open interval of the wells. Calibration of the numerical models followed by verification indicated that the assumption of a no-flow boundary in the bottom of T2b unit (CM1) is not a valid representation of the hydrogeological system. For this reason CM2 was adopted in subsequent exercises. Nevertheless, the calibration and verification of this model resulted in non-unique solutions being obtained. As such two numerical models (A and B) were proposed that both corresponded reasonably well with the field data (Kremer *et al.* 2008). Both of them included a highly permeable layer within T2c aquifer.

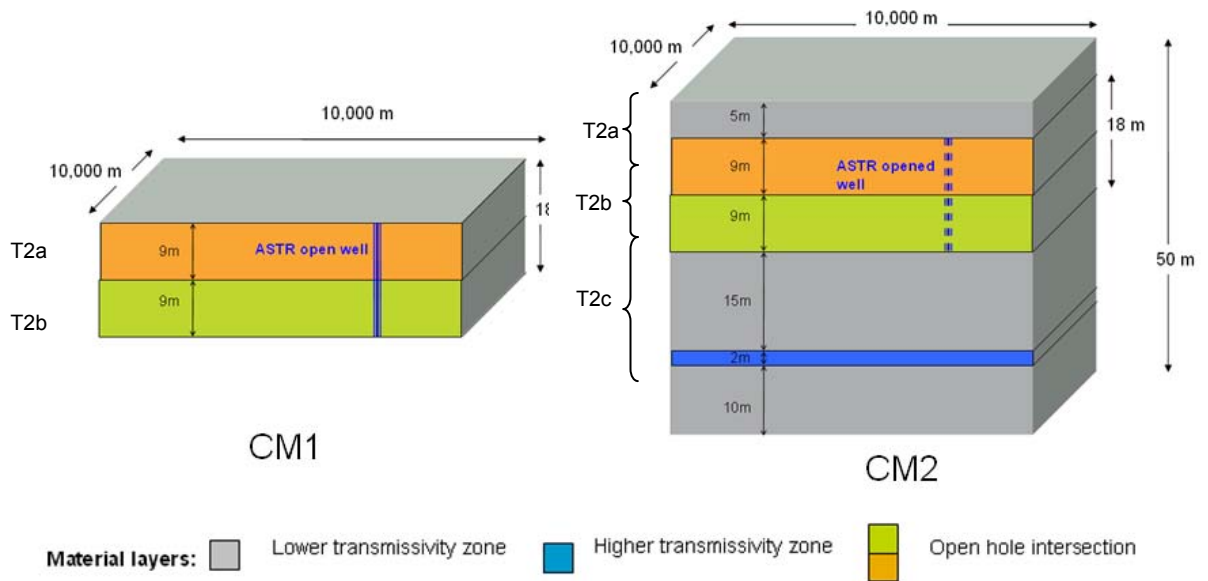


**Figure 14 Schematic 3D view of conceptual models CM1 & CM2 (from Kremer *et al.* 2008)**

The two alternative set of parameters used in the model A and B appeared to be consistent for the predictive scenarios with very similar breakthrough curves, and led to the same management recommendations. Nevertheless, by the end of the study there were too few field data to determine which of the models was the more appropriate, especially as no data were available from the bottom part of the aquifer (Kremer *et al.* 2008).

A summary of the modelling studies undertaken at the ASTR site is presented in Table 3 showing the differences in objectives and hydrogeological and operational data available for each study.

**Table 3 Summary of modelling works undertaken at the ASTR site between 2004 and 2009 and field data used for each study**

<b>Modelling Objectives</b>	<b>Source</b>	<b>Modelling method</b>	<b>Hydrogeological data</b>	<b>Operational input data</b>	<b>Solute observations</b>
Establishment of the optimal well-field design of the ASTR scheme	Pavelic <i>et al.</i> 2004	2D numerical flow and solute transport modelling + semi-analytical modelling	Lithological log, geophysical logs, pump test and flowmeter analysis at nearby Parafield ASR and GRS wells (Figure 1) (T2abc over ~40 m)	None	None
Initial assessment of the performance and viability of the ASTR system	Kremer <i>et al.</i> 2008	3D numerical flow and solute transport	Above + Lithological log, geophysical logs, pump test and flowmeter analysis at RWs and IWs (T2ab)	Flushing via RWs between 7/09/2006 and 15/11/2007	Observations at IWs, in T2ab
Initial assessment of the performance of the ASTR system using revised conceptual model	This report	3D numerical flow and solute transport	Above + Lithological log at P1 and P3, in T2ab Lithological and geophysical logs at P2 (T2abc over ~60 m)	Pumping test at IW2 for 480 minutes Flushing via RWs between 7/09/2006 and 30/06/2008 Injection via IWs between 3/09/2008 and 21/12/2008 Recovery via RWs between 1/02/2009 and 30/04/2009	Observations at RWs, IWs, P1 and P3 in T2ab Observations at P2 in T2c

## 4.4. Revised conceptual model

Incorrect understanding of the hydrogeological system would undoubtedly lead to inaccurate predictions of ASTR site operation. Therefore, collection of new field data was required to improve the conceptual model and consequently an accuracy of predictions. Geological logs and solute data that had been obtained since October 2007 were used to revise conceptual model CM2 into CM3.

Surprisingly, a higher conductive conductivity layer apparent within T2c unit at Parafield ASR site and Greenfields Railway Station was not clearly identified on the geophysical logs collected in P2 (Appendix A). Nevertheless, the head dropped during drilling of this borehole at the depth ~220 m which suggests that the zone of high permeability does occur in the bottom of T2c unit. It is, however, possible that the lack of detection of the high permeable unit by the geophysical equipment was due to clogging of the borehole with the drilling fluid beforehand.

In the model CM3 used for the simulation (Figure 15), coarser vertical discretisation was applied. Thickness of the entire model was extended from 50 to 60 m. The vertical division of the model into 5 material layers is based on the up-to-date understanding of groundwater system. The five material layers are derived from units T2a (layer 1), T2b (layer 2 and two slices of layer 3) and T2c (the remainder of layer 3 as well as layers 4 and 5). Flow and transport parameters were adjusted during the calibration process.

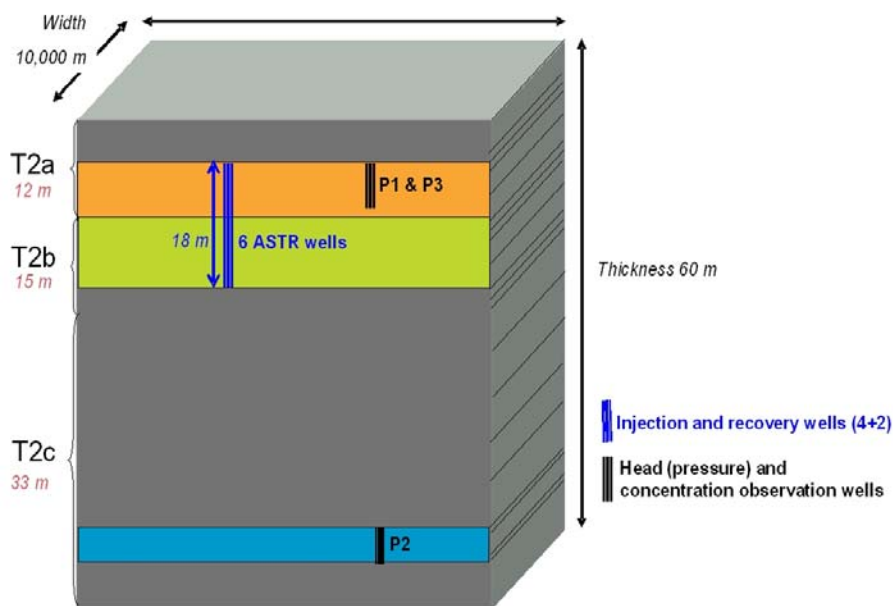


Figure 15 Schematic 3D view of conceptual model CM3

## 4.5. Revised numerical model and input data

### 4.5.1. Spatial discretisation

On the horizontal extent, the numerical model used a triangular finite-element mesh on a 10,000 m x 10,000 m ( $10^4$  ha) domain with the ASTR well-field positioned at its centre. An irregular mesh was used to refine simulation around the ASTR site to manage the scale difference between solute transport and flow simulations, thereby maintaining reasonable run times. Refinement of the mesh was made around the ASTR wells with a minimum element size of ~1 m. Then mesh size was gradually increased with increasing distance from the area

of interest, with a mesh size of ~5 m within the well field, to a maximum mesh length size of ~1700 m on the model boundaries. There are a total of 79 840 elements within the mesh.

On the vertical extent, the five material layers were divided into 20 numerical layers (right side of the cube presented in Figure 15) with a maximum thickness of six metres. Division in this way limited the effect of numerical dispersion. Thin numerical layers of one metre thickness were set at the border between two material layers to refine the simulations. A specific effort was made to refine layers intersected by the ASTR wells.

#### 4.5.2. Input parameters

Input parameters used in the ASTR modelling are a combination of both physical parameters which represent the hydrogeological setting of the system, and operational parameters which can be changed by an operator. Operational parameters include flow rates, injected and recovered volumes, and injection/extraction/stoppage periods at the ASTR and ASR wells (Appendix C). Those parameters are defined as boundary conditions and vary from one simulation to another within the range of realistic values assigned from field data.

Physical parameters include flow and transport parameters and are defined for a given model used later in the predictive modelling. Most of the physical parameters are considered sufficiently well-known to be directly set from field data (e.g. aquifer thickness, regional hydraulic gradient). Some parameters were adjusted during the calibration process within a range of realistic values to fit the best the field data (Table 4).

##### ***Initial and boundary conditions for flow***

To reflect the average regional gradient of 0.0015 from east to west, constant head boundaries were set on the left and right side of the domain, with respective values of +7.5 and -7.5 m. Due to the succession of injection and extraction phases in the ASTR trial involving convergent or divergent flow, all the simulations of ASTR operations are transient both for flow and solute transport. Therefore, an adequate representation of hydrogeological system necessitates the distribution of initial conditions. The initial hydraulic head was calculated from a steady state simulation that incorporated the regional gradient as flow boundary conditions.

To represent the injection and extraction conditions at the different stages of the trial, time-varying specified flux boundaries were used at the ASTR and ASR wells. In a finite element code, the well flux boundary is assigned to a node. In FEFLOW, flux boundaries have to be allocated to the corresponding node on every slice intersected by the opened interval of the well. To reflect the vertical heterogeneity of the aquifer, and so represent the water entering the aquifer at the different depths, flow rates at each node were proportionally defined from the transmissivity of the layers adjacent to that node. Assuming that higher transmissivity layers have a higher proportion of flow, rates were defined as:

$$Q_i = \frac{T_i}{T} Q \quad \text{Equation 4}$$

Where  $Q$  is the total recharge or discharge rate in the well,  $T$  the aquifer transmissivity, and  $Q_i$  and  $T_i$  the recharge/discharge rate and the transmissivity of the layer  $i$ . Finally, to allocate to each slice intersected by the well the corresponding flow rate, the value was set by the mean of the flux  $Q_i$  defined for the two adjacent layers.

##### ***Initial and boundary conditions for transport***

Initial concentration of the ambient groundwater was represented by setting an initial global concentration of 0 mg/L of mixing fraction at every node of the finite-element mesh. To represent the distribution of the solute due to injection of fresh water, a concentration boundary was set for each node of each slice intersecting an ASTR well using specified concentration (Dirichlet condition) set at 1 mg/L. A flow constraint was added to every concentration boundary of the injection well to ensure that no condition was applied to the well when no injection occurred. No boundary condition was set at the ASR well as field data

suggested that the injectant plume of the ASR scheme was unlikely to reach the ASTR trial area.

### **Physical flow and transport input parameters**

To represent vertical heterogeneity of the aquifer, flow parameters, such as hydraulic conductivity or storage coefficient, are assigned on each material layer of the conceptual model based on the present understanding of the flow system derived from pumping tests and EM flowmeter analyses developed previously in Kremer *et al.* (2008). Hydraulic conductivities initially set from the aquifer characterisation study were adjusted during the calibration process to fit the observed drawdown as detailed in Table 4. The ratio between the different conductivities initially set in each layer was kept fixed between the different simulations. The storativity was assigned from average field data  $S=2.7 \times 10^{-4}$  analysed from pumping tests (AGT 2007).

The anisotropy of aquifer's transmissivity, defined as the vertical conductivity to horizontal conductivity ratio ( $K_v/K_h$ ), influences the vertical mixing and, in this case, determines the flux to and from T2c. A global value of 0.1 was initially set and adjusted during the calibration process (Table 4).

No field data were available to assess the solute transport parameters such as porosity, dispersivity and diffusion coefficient. For a sandy-limestone sedimentary aquifer, realistic values of porosity range from 0.2 to 0.5 (Zheng and Bennett 2002). Longitudinal dispersivity was adjusted within a range of realistic values for this scale of interest (Gelhar *et al.* 1992; Zheng and Bennett 2002). The ratio between transverse and longitudinal dispersivity was set at 0.1 from the literature (Gelhar *et al.* 1992; Zheng and Bennett 2002). Diffusion coefficient was set to the default value  $1 \times 10^{-9} \text{ m}^2/\text{s}$  (Zheng and Bennett 2002).

## **4.6. Revised model calibration and verification**

### **4.6.1. Calibration strategy**

With a view to using the model for the predictive simulations of ASTR system operations, the boundary conditions were adjusted towards the observed distribution of hydraulic heads and concentrations. The popular "trial-and-error" approach was used (Anderson and Woessner, 1992). Prerequisite to transport simulations, the first step of the calibration aimed to adjust flow parameters (hydraulic conductivity) using observed drawdown during a pumping test at the ASTR site (AGT 2007). The second step of the calibration process aimed to adjust parameters within a range of realistic values using salinity data collected at the ASTR site between 2006 and 2008 during injection via RWs and IWs.

The accuracy of the model calibration was assessed by the calculation of root-mean-square-error (RMSE) and mean error (ME) of the head (flow performance) and the concentration of solute (flow and solute transport performance) (Zheng and Bennett 2002), using three arbitrary calibration errors, referred to as E1, E2 and E3.

Firstly, error E1 was used to consider flow performance using RMSE calculations of simulated absolute hydraulic head compared with the observed drawdown collected at IW1, IW3, IW4, RW1 and RW2 during a pumping test at IW2 over approximately 8 hours in February 2007 while no operations occurred at the ASTR or nearby ASR site. The pumping test involved injection rates of 3 and 6 L/s for steps of 100 minutes each and 9L/s for 280 minutes. E1 was calculated at the end of the last step ( $t = 480$  minutes) using two absolute head values calculated as the average of the IWs on one hand and RWs on the other hand. Indeed, hydraulic conductivity is assumed to be homogeneous on the horizontal extent.

Once flow-parameters were adequately calibrated, the performance of the simulations was compared with respect to the average solute breakthrough curve at the IWs using error E2. This error represents RMSE and ME of mixing fraction ( $f$ ) at IWs calculated from eight

average EC data derived from 29 depth-averaged EC profiles collected at the IWs on eight dates during the flushing phase.

Finally, to evaluate simulation of groundwater flow and solute transport in the lower part of the aquifer, error E3 represented RMSE of mixing fraction that were calculated on the basis of six EC data collected at P2 between 01/09/2008 and 17/02/2009 during profiling and sampling events.

#### 4.6.2. Calibration results

Summary of adjusted parameters and performance of E1, E2 and E3 of 14 calibration simulations are presented in Table 4. The initial set of flow parameters from the aquifer characterisation study (simulation 1) showed low performance in representation of the flow system with E1 equalling 0.57. The initial aquifer parameterisation was based on analyses of pumping tests as though the wells fully penetrated the aquifer. Noting that fresh injected water penetrating deep below these wells to T2c in piezometer P2, the permeability was reduced to compensate for the additional effective thickness of the transmissive zone. Decreasing the hydraulic conductivity by half (simulation 2) and then three-quarters (simulation 3) improved the performance of the models. Finally, the best fit E1 was 0.02 for simulation 3.

Simulation 3 was then calibrated for solute transport (simulation 3 to 3f in Table 4). E2 showed very good performance with RMSE values ranging between 0.06 and 0.22 suggesting a robust representation of the mixing occurring within the storage area. A best fit RMSE of 0.06 was found for simulations 3b and 3f. These two simulations differ in porosity and dispersivity values of material layers 3, 4 and 5, but have the same parameterisation in layers 1 and 2 (Table 4).

Simulations 3 to 3f were then compared using E3. Results ranged between 0.15 and 0.40. Not surprisingly, given the uncertainties of aquifer characterisation in the lower part of T2, simulations were consistently better in T2ab (E2) than in T2c (E3). While simulations 3b and 3f presented the best fit RMSE in T2ab, simulation 3f represents better fit in the bottom part of the aquifer than simulation 3b. Thus, the change in porosity and dispersivity in layers 3, 4 and 5 was necessary to obtain a better fit between observed and modelled data.

However, given the uncertainty in characterising flow and solute transport in layers 3, 4 and 5, a second set of parameters based on the previous model CM2 with a different flow system in the lower part of the aquifer was calibrated (simulation 7 to 9 in Table 4). While simulations 1 to 6 represented unit T2c as an homogeneous layer, simulations 7 to 9 simulated unit T2c as two low conductive layers (layers 3 and 5) which include a thin higher conductive layer at about 210 m bgs (layer 4).

As previously described, calibration firstly focused on assessing the performance of the flow model using E1. Simulation 9 had the best E1 of simulations 4 to 9 with a value of 0.04. Once flow was adequately represented, solute transport performance was estimated using the same indicators E2 and E3. Simulation 9 performed very well to simulate flow and solute processes within the storage area with best fit RMSE of mixing fraction at IWs with E2=0.06 but lower performance at P2 with E3=0.36.

Finally, simulations 3f and 9 presented the best fit for flow and solute transport at the ASTR site with similar performances in simulating flow (Figure 16) and transport (Figure 17) within T2ab, as expected from a similar set of parameters in layers 1 and 2. They differ in simulating groundwater flow and solute transport in the lower part of T2 with E3=0.15 for simulation 3f and 0.36 for simulation 9 (Figure 18).

It is well-known that the calibration process can lead to the non-uniqueness problem, which describes the fact that different conceptual models and different sets of parameterisation can fit the field data equally well (Chavent 1974; Yeh 1986; Freyberg 1988). Solutions to solve the non-uniqueness problem included collection of adequate data to constrain the model, limitation of the parameters within a range of realistic values and verification using an

independent set of data. Once constrained, the non-uniqueness problem can become a solution to account for uncertainties resulting from field data and for judging the reliability of model prediction, by offering two different approximations of the behaviour of the aquifer system when insufficient data is available.

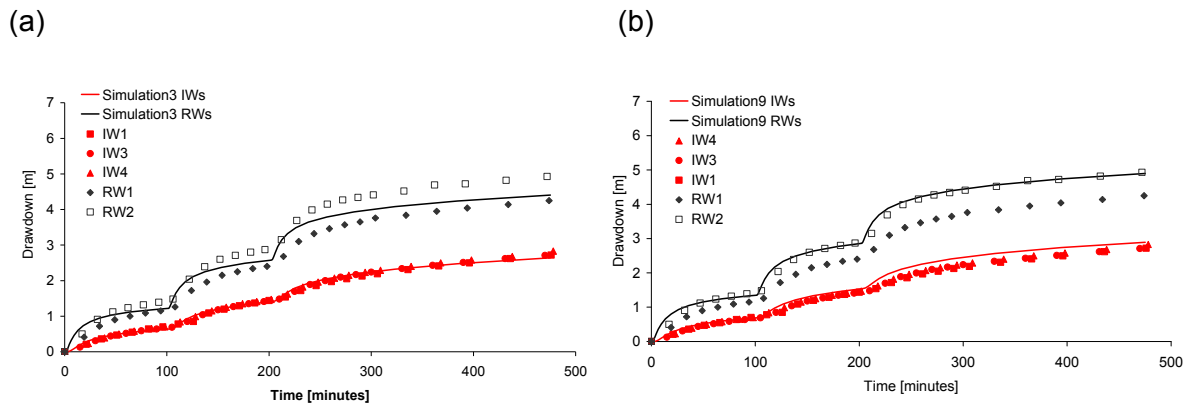


**Figure 16 Comparison of simulated and observed drawdown at IW1, IW3, IW4, RW1 and RW2 during pumping test at IW2 for simulations 3 (a) and 9 (b)**

Thus far, limited data is offered from injection/recovery cycles to assess the impact of leakage to and from T2c on the stored water and so to allow for model validation between the two alternative representations of simulations 3f and 9. Therefore, the choice was made to use the two alternative models to account for the uncertainties to represent flow and solute processes within layers 3, 4 and 5. In the following, simulations 3f and 9 will be referred to as model C and D, respectively to follow on from model A and B used in Kremer *et al.* (2008).

**Table 4 Summary of adjusted parameters and changes in errors of mixing fraction and hydraulic head during the calibration simulation constrained by hydraulic head and EC data observed at the ASTR site. Simulations 1, 2 and 4 to 8 simulate only flow while simulations 3 (a to f) and 9 simulate flow and solute transport.**

Adjusted parameters	Conductivity [1e-4 m/s]				Anisotropy [-]		Porosity n [-]		Dispersivity $\alpha$ [m]		Error E1*	Error E2**	Error E3***
	1	2	3, 5	4	1, 2	3, 4, 5	1, 2	3, 4, 5	1, 2	3, 4, 5	[-]	[-]	[-]
Layer	1	2	3, 5	4	1, 2	3, 4, 5	1, 2	3, 4, 5	1, 2	3, 4, 5	1, 2	1, 2	4
SIMU_1	0.333	0.209	0.82	0.82	0.1	0.1	-	-	-	-	<b>0.57</b>	-	-
SIMU_2	0.167	0.105	0.41	0.41	0.1	0.1	-	-	-	-	<b>0.23</b>	-	-
SIMU_3a	0.125	0.078	0.31	0.31	0.1	0.1	0.35	0.35	2	2	<b>0.02</b>	<b>0.08, -0.02</b>	<b>0.40</b>
SIMU_3b	0.125	0.078	0.31	0.31	0.1	0.1	0.35	0.35	8	8	<b>0.02</b>	<b>0.06, +0.01</b>	<b>0.28</b>
SIMU_3c	0.125	0.078	0.31	0.31	0.1	0.1	0.35	0.35	15	15	<b>0.02</b>	<b>0.07, +0.04</b>	<b>0.24</b>
SIMU_3d	0.125	0.078	0.31	0.31	0.1	0.1	0.25	0.25	8	8	<b>0.02</b>	<b>0.17, +0.17</b>	<b>0.18</b>
SIMU_3e	0.125	0.078	0.31	0.31	0.1	0.1	0.45	0.45	8	8	<b>0.02</b>	<b>0.12, -0.1</b>	<b>0.37</b>
SIMU_3f Model C	0.125	0.078	0.31	0.31	0.1	0.1	0.35	0.25	8	2	<b>0.02</b>	<b>0.06, +0.01</b>	<b>0.15</b>
SIMU_4	0.333	0.209	0.1	0.1	0.1	0.1	-	-	-	-	<b>0.16</b>	-	-
SIMU_5	0.333	0.209	0.1	0.1	0.1	1	-	-	-	-	<b>0.21</b>	-	-
SIMU_6	0.333	0.209	0.1	0.1	1	1	-	-	-	-	<b>0.26</b>	-	-
SIMU_7	0.333	0.209	0.1	5	0.1	1	-	-	-	-	<b>0.54</b>	-	-
SIMU_8	0.167	0.105	0.05	2.5	0.1	1	-	-	-	-	<b>0.19</b>	-	-
SIMU_9 Model D	0.125	0.078	0.0375	1.875	0.1	1	0.35	0.25	8	2	<b>0.04</b>	<b>0.06, +0.04</b>	<b>0.36</b>

\* Error E1 is represents absolute RMSE of hydraulic heads calculated at ASTR wells during a pumping test at IW2

\*\* Error E2 represents RMSE and ME of concentrations calculated at IWs during injection via RWs

\*\*\* Error E3 represents RMSE of concentrations calculated at P2 during injection via IWs

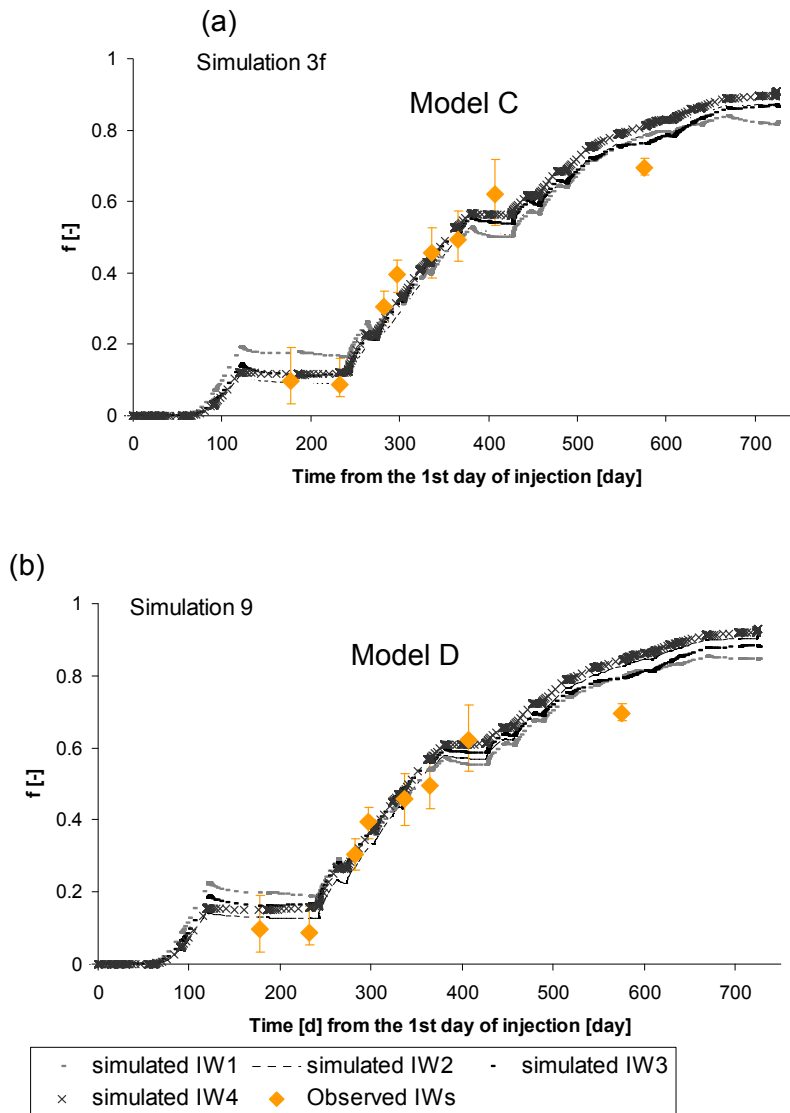


**Figure 17 Comparison of observed (dot) and simulated (lines)  $f$  at IWs during injection at RWs for calibration simulations 3f (a) and 9 (b) which presented the best overall fit during the calibration process**

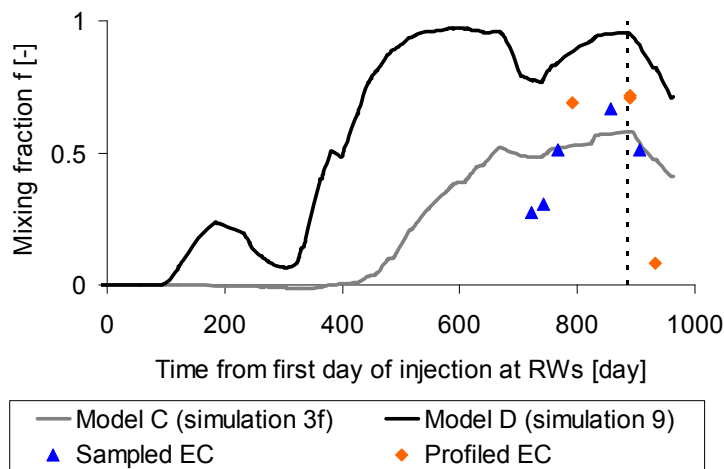


**Figure 18 Observed and simulated  $f$  at P2 during injection at the ASTR site for calibration simulation 3f and 9 (day 0 to day 886), and extraction via RWs for verification simulations 3f (model C) and 9 (model D), (day 886 to 964)**

### 4.6.3. Calibration sensitivity analysis

Owing to the uncertainties in the conceptual model and the input data used in the calibration process, a sensitivity analysis helps to enhance a better understanding of the numerical problem and so establish greater confidence in the calibration. Few numerical studies on ASR and ASTR systems in similar hydrogeological settings have described the influence of important parameters, such as dispersivity or porosity, on the simulated mixing processes occurring within the aquifer which affect solute transport (Pavelic *et al.* 2002; Pavelic *et al.* 2004; Lowry and Anderson 2006; Kremer *et al.* 2008). Summary of a qualitative review of a sensitivity analysis performed on the main input parameters during the calibration process is presented in Table 5.

**Table 5 Qualitative review of a sensitivity analysis of input data adjusted in CM3 during the calibration process**

Condition varied	Range tested	Results
Hydraulic conductivity* [m/s]	$0.1 \times 10^{-4} - 8.2 \times 10^{-4}$	Major effect on head; minor effect on mixing
Storativity [-] $S = S_s * b$ , where $S_s$ – specific storage $b$ – thickness	$2 \times 10^{-4} - 8.4 \times 10^{-4}$	Minor effect on head and mixing for range tested within realistic values
Porosity [-]	0.2-0.5	Major effect on mixing, increasing porosity increases mixing
Longitudinal dispersivity [m]	2-20	Effect on mixing, especially extent of the fresh plume
Influence of Parafield ASR operations	On and off	Major effect on the displacement of the fresh plume when no operations occurred at the ASTR site, minor effect when ASTR operation occurs - effects of ASR decrease as the fresh plume gets bigger
Influence of a regional gradient	On and off	Major effect on the displacement of the fresh plume when no operations occurred at the ASTR site, minor effect when ASTR operation occurs
Influence of highly conductive layer in T2c unit	On and off	Major effect on the plume distribution in the vertical direction, minor effect on recovery efficiency and travel times

\* Ratio between the conductivities initially set in material layers of CM3 was kept fixed between the different simulations involving different hydraulic conductivity values

### 4.6.4. Model Verification

A short recovery period over 72 days occurred from February to April 2009 involving the extraction of 105.7 ML of groundwater via the RWs. Salinity data collected at the RWs, IWs and piezometers during this period were used to verify the performance of the two alternative models to predict the quality of the recovered water. Models C and D showed relatively similar performance to simulate the mixing fraction of the recovered water with RMSE in the mixing fraction at the RWs of 0.05 for both models (Figure 19a).

The simulated mixing fraction at the RWs appeared to over-predict the salinity of the recovered water by up to 0.07 suggesting that not enough mixing occurred between the injected water and the ambient groundwater. Nevertheless, it is expected that the differences between observed and simulated mixing fractions are mainly due to variations in EC of the injected water which are not taken into account in the simulations.

RMSEs in mixing fraction calculated at the IWs during the extraction period are 0.11 for model C and 0.12 for model D (Figure 19b). Conversely to simulated mixing fractions at

RWs, mixing fractions at the IWs clearly under-predicted observed data by up to 0.13 for model C and 0.14 for model D (day 948 on Figure 19b). However, this is in good agreement with the observed variations of salinity of injected water (Figure 6). Indeed, the average salinity of 218  $\mu\text{S}/\text{cm}$  calculated during injection through IWs is lower than the value of 250  $\mu\text{S}/\text{cm}$  used in the modelling.

Given the uncertainties in input parameters, results of verification simulations from both models appeared to reliably simulate mixing fraction at the ASTR site.

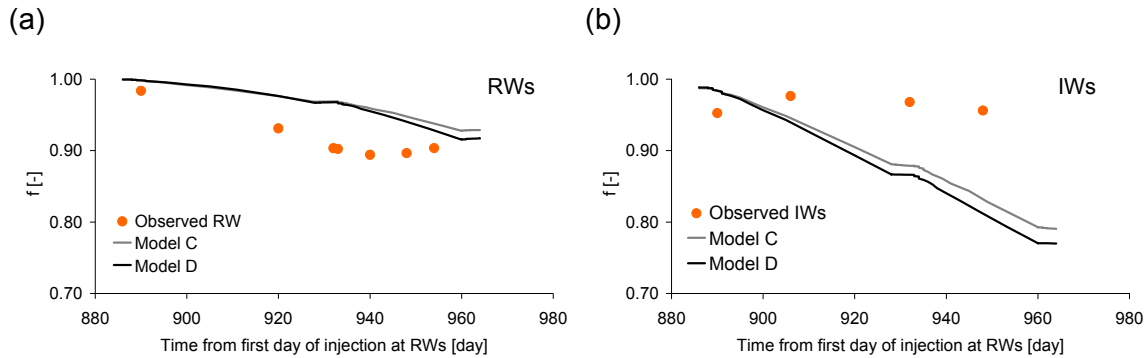


**Figure 19 Observed and simulated mixing fraction at RWs (a) and IWs (b), during extraction via RWs over 72 days, using models C (grey line) and D (black line)**

A comparison of cross-sectional distribution of mixing fraction for models C and D is presented for before (Figure 20) and after recovery (Figure 21). As expected, given that the same parameters are set in layers 1 and 2 on both models C and D, differences in the distribution of mixing fraction mainly occur in the lower part of the aquifer. Model C, which presents a homogeneous distribution of parameters in layers 3, 4 and 5, simulated a very compact plume. Whereas model D, which involves a heterogeneous distribution of parameters in the same layers, presented a more mixed distribution of mixing fraction, notably in layer 4 where the fresh plume tends to drift as a result of regional hydraulic gradient enhanced by the high hydraulic conductivity set in this layer.

Model C predicts fresher water at the IWs and RWs than model D, as shown on Figure 19. The distribution of mixing fraction at the end of the recovery period, especially in model D (Figure 20), suggests that more saline water tends to move from T2c towards the storage area. Therefore, the differences in simulated mixing fraction at the ASTR wells are mainly due to the representations of unit T2c on the models (layers 3, 4 and 5).

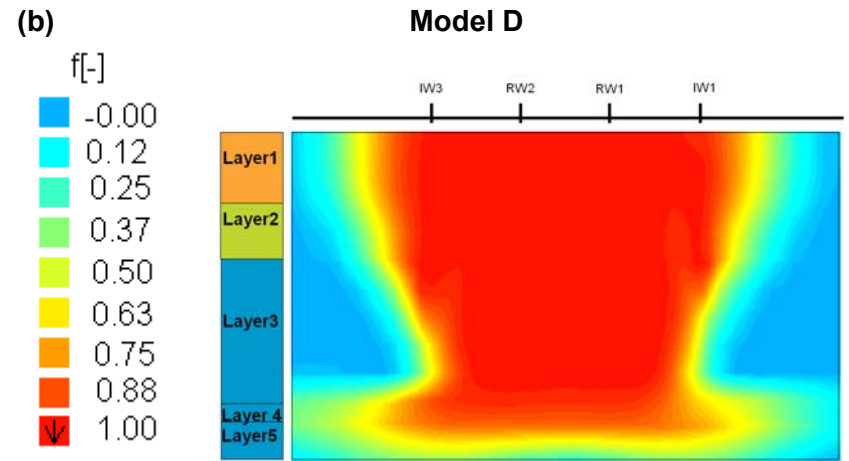
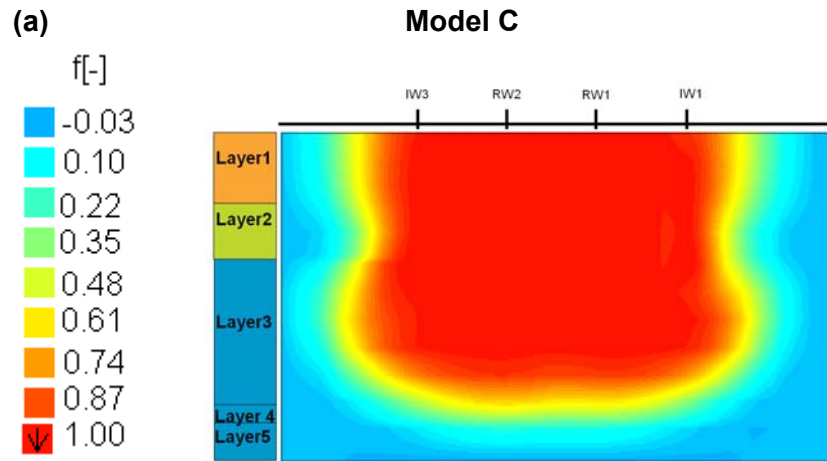


Figure 20 Cross-sectional distribution of mixing fraction at the end of the injection period simulated with models C (a) and D (b). Horizontal scale: 300 m, vertical scale: 60 m.

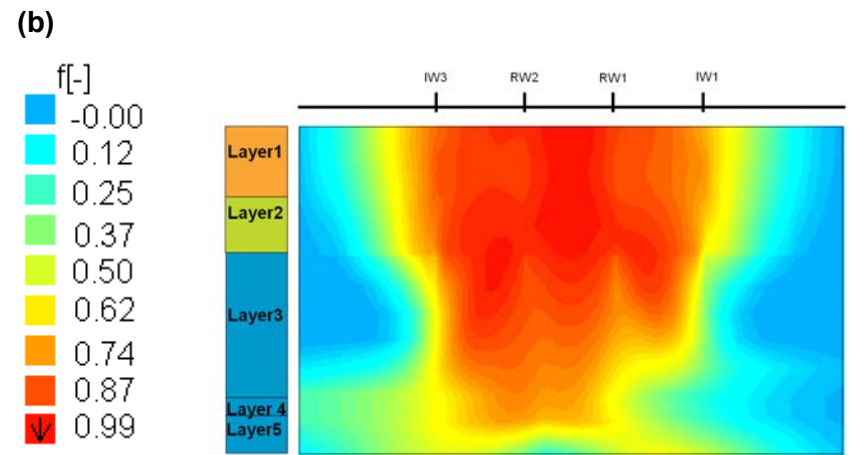
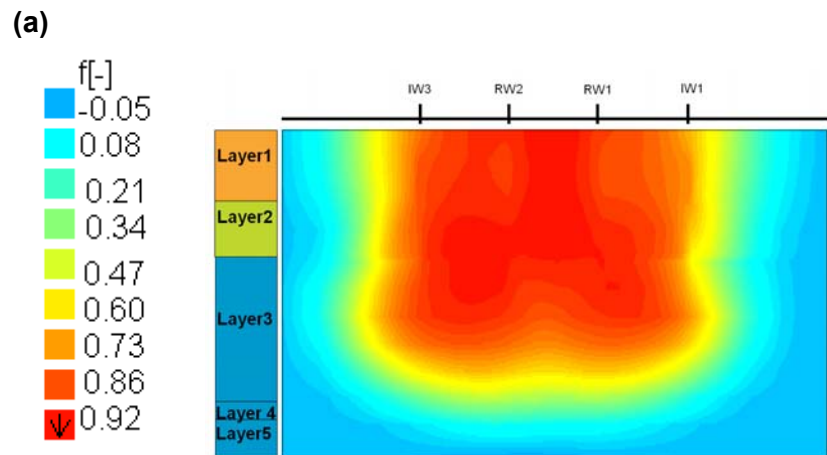


Figure 21 Cross-sectional distribution of mixing fraction at the end of the recovery period simulated with models C (a) and D (b). Horizontal scale: 300 m, vertical scale: 60 m.

## 4.7. Numerical modelling predictions

Calibrated and verified models described in the previous section were employed to run several predictive scenarios. Distribution of solute in the post-flushing period was used as an initial condition. The comparison of those results with the findings of Kremer *et al.* (2008) must be done with caution because different volumes of water were injected during the flushing period in the simulations executed for models A and B.

### 4.7.1. Prediction of mixing fraction

#### *Predictive scenarios*

Three scenarios, referred to as ‘normal’, ‘wet’ and ‘drought’, were used to simulate the effect of different operational conditions on the salinity of the recovered water. Predicted salinities were then compared using two threshold concentrations: 300 and 500 mg/L TDS. The 300 mg/L limit was established to meet acceptance criteria for recovered water entering the Mawson Lakes Mixing Tank as per the site operator’s requirements. The 500 mg/L limit was established to meet acceptance criteria for drinking water supplies based on Australian Drinking Water Guidelines.

The three scenarios differ by the volume of fresh stormwater injected per year: 200 ML for the normal scenario, 300 ML for the wet scenario and 100 ML for the drought scenario (Table 6). Annual volumes of injection were based on history of water availability at the harvesting facilities in an agreement with the site operator, combined with field average injection rate and realistic number of days of stormwater availability.

Recovery volume was defined using a recovery efficiency parameter (RE) representing the ratio of recovered volume to injected volume. Initially, for each scenario, RE was specified at 80% to ensure a good buffer against the brackish water in the storage zone over the following year. Values of 60, 100 and 120% were also tested.

Each scenario involved six cycles of injection/extraction designed to correspond to seasonal variations of water supplies. Each cycle describes over 365 days an injection period, a first storage period, an extraction period and a storage period before the next cycle. Volume and length of the different periods defined in each cycle for normal, wet and drought scenarios are presented in Table 6.

Injection occurs at the four IWs at a flow rate of 5 L/s while extraction occurs at the two RWs at a flow rate of 10 L/s. For each model, initial conditions of head and solute distribution are based on the distribution obtained at the end of the verification simulation. Time in all simulations is expressed in days, from the first day of injection at the ASTR site as used previously in the calibration simulations.

**Table 6 Summary of recovery efficiency and volume and length of injection and extraction periods of each cycle for scenarios normal, wet and drought**

Scenario	Recovery efficiency [%]	Injection		Storage Duration [days]	Recovery		Storage Duration [days]	Total days
		Volume [ML]	Duration [days]		Volume [ML]	Duration [days]		
Normal	60	200	116	37	120	69	142	365
	80	200	116	37	160	93	191	365
	100	200	116	37	200	116	96	365
	120	200	116	37	240	139	73	365
Wet	80	300	174	10	240	139	42	365
Drought	80	100	58	64	80	46	196	364

### ***Effect of Parafield ASR operations on prediction of recovered water salinity***

To assess the impact of the nearby Parafield ASR scheme on predicted solute transport at the ASTR site, two simulations representing three years of operations under normal conditions of use were run on both models C and D. The first simulation “with ASR” took into account ASR operations based on data from the field, while the second simulation “without ASR” did not take the ASR scheme into account. Comparisons of simulated mixing fraction at the RWs for simulations ‘with ASR’ and ‘without ASR’ are presented on Figure 22.

Results for salinity at the RWs for a given model are almost always similar, and differ only during the storage period following recovery. Not surprisingly, differences in mixing fraction at the RWs occur when the plume is smaller (end of recovery) and are affected by local hydraulic gradient as a result of no operations at the ASTR wells. When the following injection period occurs, differences in breakthrough of injectant at the RWs disappear.

Simulated mixing fraction during the recovery period represents the salinity of the recovered water. It does not differ between simulations ‘with ASR’ and ‘without ASR’, for both models C and D (Figure 22). This suggests that prediction of salinity of the extracted water is not affected by nearby Parafield operations. Therefore, given that the purpose of the modelling is the prediction of recovered water quality, Parafield ASR operations need not be taken into account in the following predictive simulations of ASTR operations.

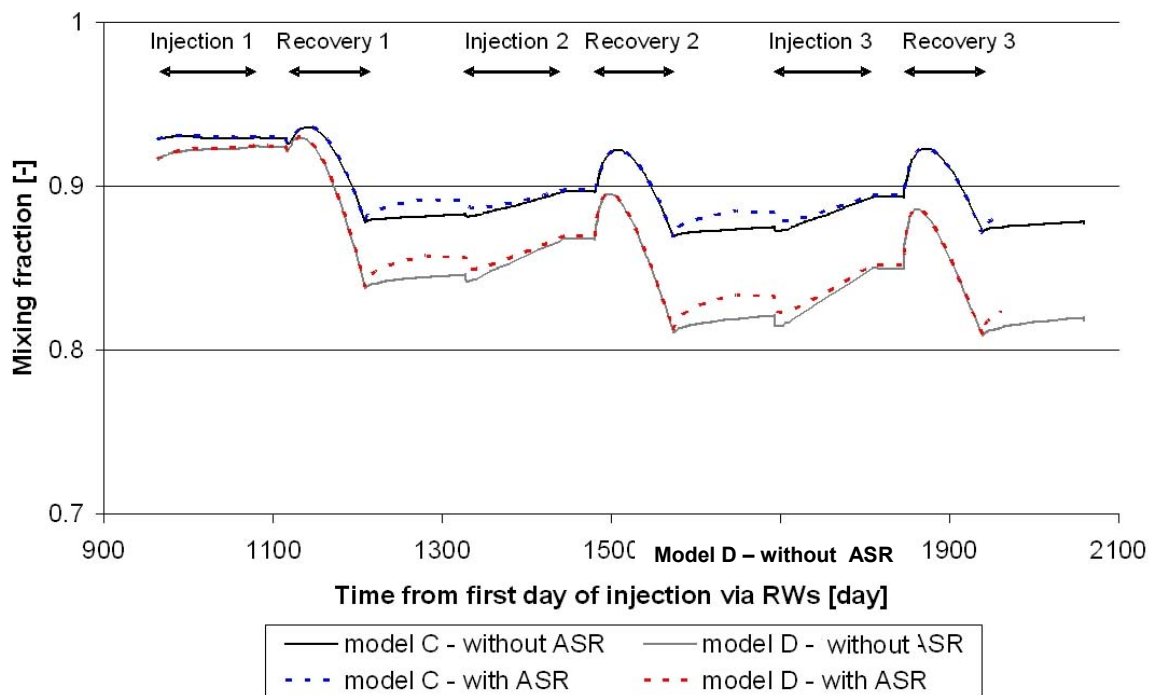


**Figure 22** Mixing fraction at RWs versus time during 3 injection/recovery cycles with (dot lines) and without (plain lines) influence of Parafield ASR scheme simulated on model C and D. Periods of injection and recovery at ASTR are also presented.

### ***Prediction of recovered water salinity***

The minimum mixing fraction predicted at RW1 and RW2 for a given recovery phase represents the maximum salinity of the extracted water during this period. Comparison of minimum mixing fraction at the RWs for each recovery phase of the six injection/extraction cycles for normal, drought and wet scenarios, calculated on models C and D, for 80% of recovery efficiency, are presented on Figure 23.

Maximum predicted salinity of the recovered water differed between models C and D with a fresher water simulated on model C. The differences between the prediction simulated on models C and D are greater than the differences between the conditions of use normal, wet or dry.

Model C showed the salinity of the recovered water to be below 500 mg/L TDS for all cases tested. Model D predicted concentrations slightly above 500 mg/L TDS for each of the scenarios tested, with a maximum salinity of ~520 mg/L TDS. None of the cases tested with recovery efficiency set at 80% showed maximum salinity of the recovered water below 300 mg/L TDS.

Both models C and D presented the same pattern in the evolution of the minimum mixing fraction for the different cycles and scenarios. At the beginning of the six-year operations, both models C and D showed that the normal and wet scenarios simulate smaller minimum mixing fractions than the drought scenario. After the first three years of operations, the scenarios involving greater additional volume stored in the aquifer result in fresher recovered water (Figure 23). This suggests that, at the beginning stage of operations, the salinity of the recovered water is very sensitive to the volume extracted. After three years of operations and additional water stored in the ground, the salinity of the recovered water is clearly less sensitive to the volume extracted, reflecting an improvement of the fresh buffer within the trial area.

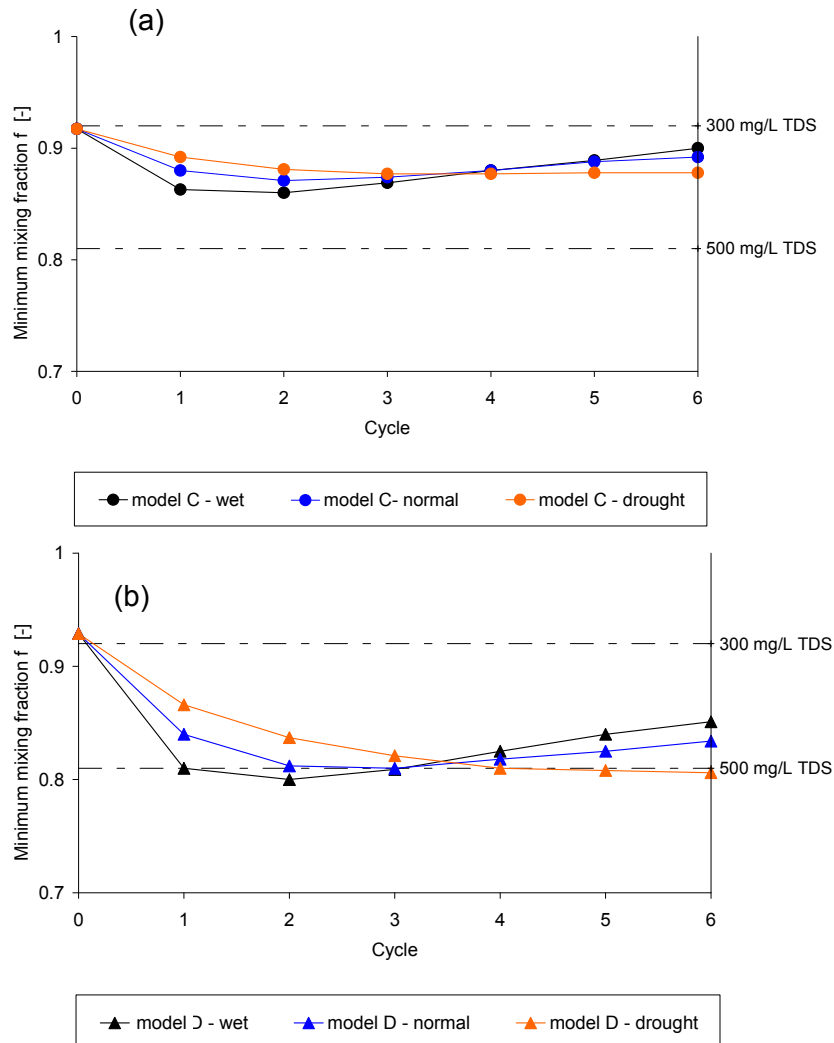


**Figure 23 Minimum mixing fraction predicted at RWs in function of the cycle, over 6 cycles, simulated on models C (a) and D (b), under normal, dry and wet conditions for recovery efficiency of 80%. Thresholds of 300 and 500 mg/L TDS are also presented.**

Comparison of minimum mixing fractions at the RWs for each recovery phase of the six injection/extraction cycles under the normal scenario for recovery efficiencies of 60, 80, 100 and 120%, calculated by models C and D, are presented in Figure 24.

As observed previously, model C simulates a fresher mixing fraction than model D in all cases tested. Nevertheless, in contrary to previous observations, differences between predictions by models C and D are smaller than the differences between the recovery efficiency tested.

For both models C and D, simulations set with REs of 60 and 80% showed maximum salinity of the recovered water to be below the threshold of 500 mg/L TDS; while simulations set with REs of 100 and 120% resulted in maximum salinities higher than the threshold of 500 mg/L TDS. The worse case with a salinity of ~850 mg/L TDS ( $f=0.62$ ) was obtained using model D and an RE of 120% (cycle 4). Conversely, a recovery efficiency of 60% simulated by model C lead to salinity under the threshold of 300 mg/L after the second year.

Not surprisingly, given that RE lower than 100% involve additional storage of fresh water within the aquifer, evolution of the minimum salinity over the years for REs of 60 and 80% indicated, for both models C and D, a decrease in the salinity of the extracted water after the first cycle. In contrast, REs of 100 and 120% tend to simulate an initial increase in the salinity of the extracted water, which then plateaus after the fourth cycle.

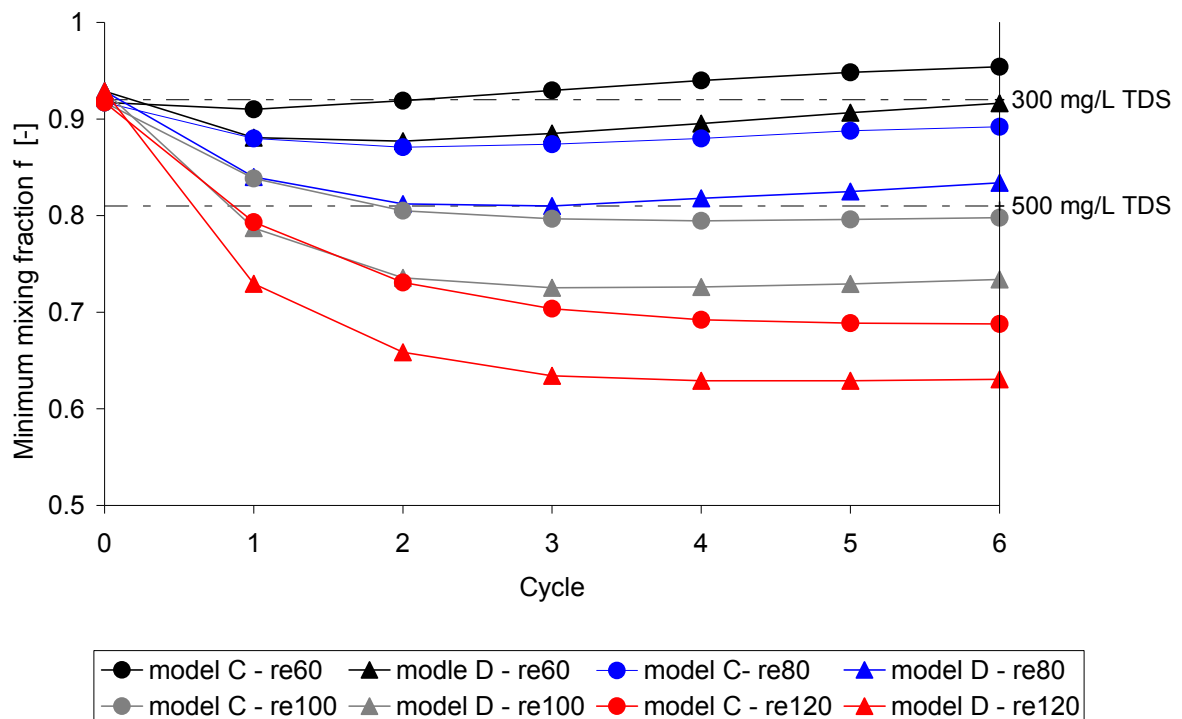


**Figure 24** Minimum mixing fraction predicted at RWs in function of the cycle, over 6 cycles simulated on models C and D involving injection of 200 ML per cycle and a recovery efficiency of 60, 80, 100 and 120%. Thresholds of 300 and 500 mg/L TDS are also presented.

**Prediction of the behaviour of the fresh injected plume**

The distribution of the fresh plume on the horizontal extent is presented on Figure 25, at the end of the 6<sup>th</sup> cycle injection period (a) and of the 6<sup>th</sup> cycle recovery period (b), for the “normal” scenario on model D. Due to the fact that the same parameters have been set in layers intersected by the ASTR wells, behaviour of the fresh injected plume during an ASTR injection/recovery cycle are similar for models C and D. Therefore, only distributions on model D are addressed in the present section. Vertical distribution of the fresh plume was discussed in Section 4.6.4.

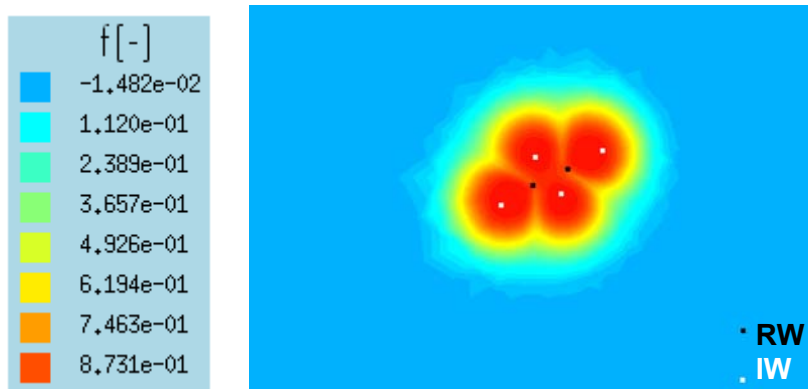
Distribution of mixing fraction showing the fresh injected plume at the end of an injection period shows that the size of the plume is about 500 m on the horizontal extent (Figure 25a). As expected at the end of injection, fresher water concentrates around each IW with some more saline water remaining from the last recovery period trapped between two plumes.

The shape of the plume at the end of a recovery period is presented on Figure 25b. The length of the plume decreases by about 100 m. Intrusion of more saline water into the fresh plume can clearly be observed between the plumes created previously by injection via the IWs. It should be noted that no saline water appears to be trapped between the RWs.

Comparison of the extent of the plume for the wet and drought scenarios was made. Both scenarios showed the same pattern of the fresh injected plume as the normal scenario, but with more saline water trapped between the fresh plumes for the drought scenario, and almost no saline water trapped for the wet scenario. As shown on Figure 23, the wet scenario predicted fresher water than normal and drought scenarios (6<sup>th</sup> cycle). This clearly illustrates that the volume of injection and extraction impacts the intrusion of more saline water within the plume and so the recovery efficiency of the ASTR scheme by influencing the mixing between the two end-members before recovery.

Intrusion of saline water within the plume can be a result of insufficient injection or excessive extraction. So far, the observation wells at the ASTR site have been unable to indicate if more saline water enters the plume, as fresher water concentrates around the IWs, the RWs, and the transect between IWs and RWs (as seen on Figure 25b), notably where the piezometers are located.

(a)



(b)

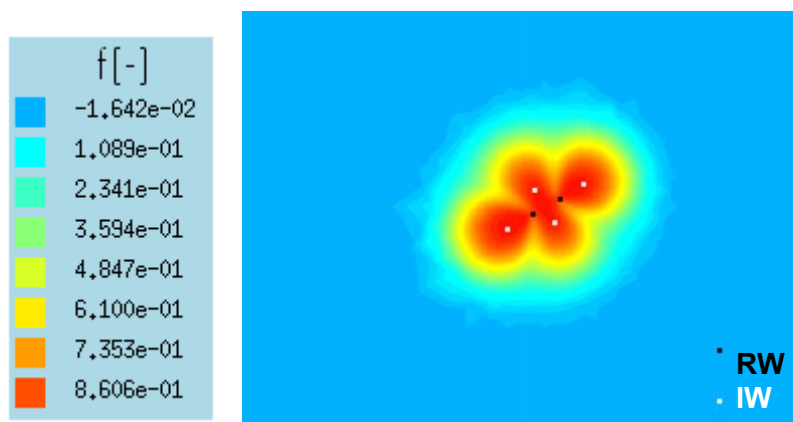


**Figure 25** Distribution of mixing fraction at the end of the 6<sup>th</sup> injection period (a) and of the 6<sup>th</sup> recovery period (b) for scenario normal on model D (numerical layer 5; scale: 1,000 m).

### Sensitivity of the predictions of mixing fraction

Simulations were made to determine the sensitivity of the predicted maximum salinity of the recovered water. Physical input parameters of the models that were shown to have a major effect on flow and solute transport during the calibration process were tested, including porosity and dispersivity. Comparison of those simulations allows assessment of the reliability of the predictions of future ASTR operations as a function of uncertainties in the input parameters.

Each of the tested parameters was changed individually while keeping the others unchanged. Sensitivity of the models to variations in parameters was assessed using the minimum mixing fraction calculated during the third cycle under normal conditions for both models C and D.

Effective porosity determines the storage volume in the aquifer and hence influences the viability of the ASTR scheme by impacting on the mixing occurring within the fresh plume and the effective travel time. Porosity was tested in layers 1 and 2 at values of 0.25, 0.45 and 0.55, with proportional changes in porosity in layers 3, 4 and 5. Not surprisingly, for both models C and D, the more porosity is increased, the more mixing that occurs, which increases the maximum salinity of the recovered water (Figure 26).

Dispersivity influences the viability of ASTR by controlling the propagation of the breakthrough front and the extent of the plume. Dispersivity values in layers 1 and 2 were tested at 4, 12 and 16, with proportional changes in dispersivity in layers 3, 4 and 5. Not surprisingly, for both models C and D, an increase in dispersivity increases mixing and increases the maximum salinity of the recovered water (Figure 26).

Porosity and dispersivity appeared to be equally important in the prediction of the maximum salinity of the recovered water. Differences in representing T2c between models C and D have a greater impact on the simulations of mixing fraction of the recovered water than changes in porosity and dispersivity.

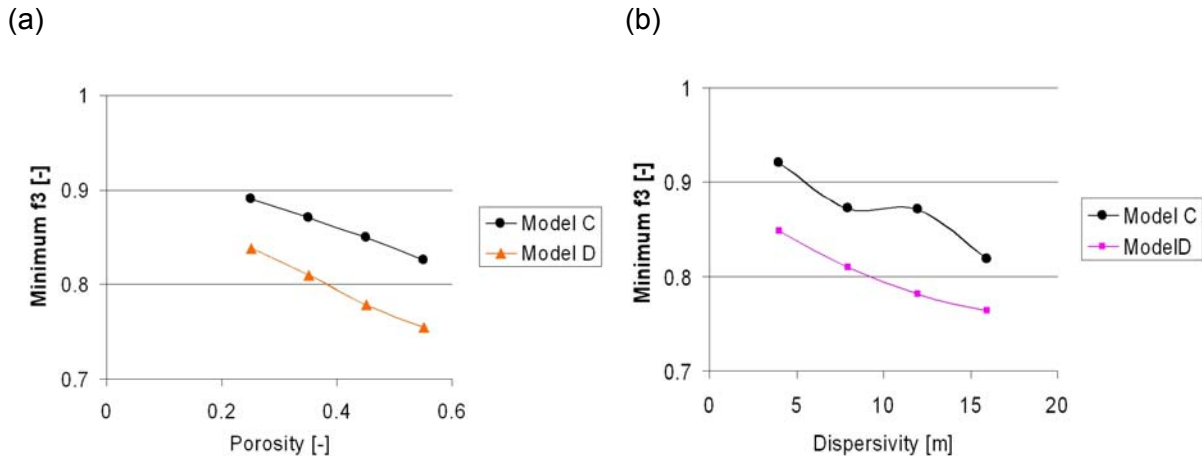


Figure 26 Change in minimum simulated mixing fraction at RWs after 3 years of ASTR operations in function of porosity (a) and dispersivity (b) for models C and D

### 4.7.2. Prediction of residence time

#### Predictive scenarios

Two scenarios, referred to as normal and wet, were used to simulate the residence time of the injected water within the aquifer before recovery using the tracer decaying method. Simulations were performed by using an input concentration of 1.0 mg/L and a decay rate of  $6.93 \times 10^{-3}$ /day (equivalent to a half-life of 100 days). Both predictive scenarios involve two cycles of injection/extraction. Scenarios did not take into account any storage periods between the end of injection and the beginning of recovery which are likely to occur under

normal use, and which would lead to an increase in the residence time of the water within the aquifer. Time in all simulations is expressed in days from the first day of injection of the first cycle. Injection occurs at the four IWs at a flow rate of 5 L/s while extraction occurs at the two RWs at a flow rate of 10 L/s.

The normal scenario involves, per cycle, the injection of 200 ML and the extraction of 160 ML. Each normal cycle runs over 210 days: the injection phase lasts 116 days and the recovery lasts 93 days. The wet scenario involves, per cycle, the injection of 300 ML and the extraction of 240 ML. Each wet cycles runs over 314 days: the injection phase lasts 174 days and the recovery lasts 139 days.

### Calculation of residence time

Predicted residence time of the recovered water from the second cycle for normal and wet scenarios, for models C and D, is presented on Figure 27. All cases predicted a similar pattern, with an initial decrease in residence time and a subsequent increase following a linear evolution over time. This result shows that, by the end of the injection period, the fresh injected water concentrates around the IWs and does not intersect the RWs. In a normal year, when 200 ML of water is being injected via four injection wells during a single injection cycle, a radius of influence of an individual well does not exceed 50 m which is the distance between injection and recovery wells. The minimum residence time observed on Figure 27 corresponds to the breakthrough of the last injected water at the RWs. Comparison of simulated residence time at wells RW1 and RW2 showed that the distributions of residence time are identical between the two wells.

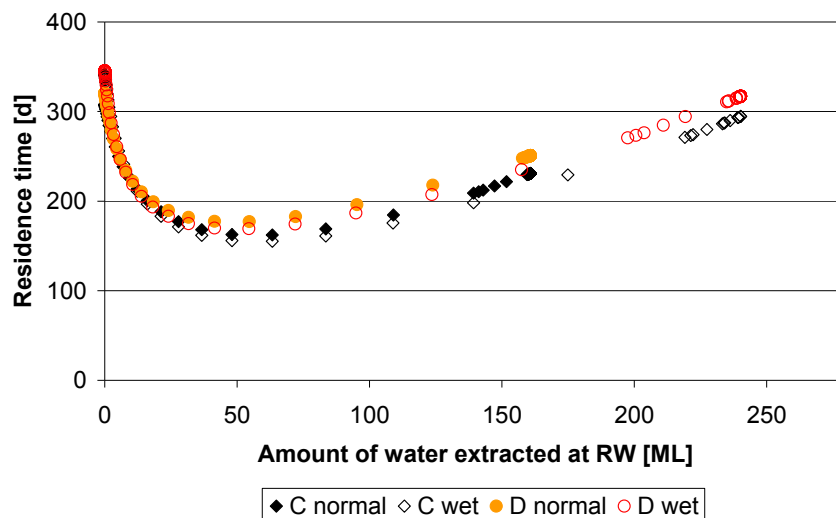


**Figure 27 Distribution of residence time within the aquifer of the recovered water as a function of the volume extracted at RW1 and RW2, without a storage period between the end of injection at IW and recovery via RW**

Not surprisingly, because the same parameters have been set in layers intersected by the ASTR wells, models C and D produced fairly similar predictions of residence time of the recovered water with a lower minimum residence time for model C (Figure 27). Model C predicted minimum residence times of 162 days under normal conditions of use and 155 under wet conditions, while model D simulated 177 days and 169 days, respectively. Mean residence time for the models are as follows: C normal 254.9 days, C wet 293 days, D normal 267.7 days and D wet 305.6 days.

In all cases, the minimum residence time occurs after about 50 ML has been extracted (about 30 days at an extraction rate of 10 L/s). As expected, comparison of the normal and wet scenarios showed that the greater the injected – and extracted – volume, the younger

the recovered water is (Figure 27). Nevertheless, the difference between the minimum residence times predicted by the two scenarios is small, only seven days for model C and eight days for model D.

### **Sensitivity of the predictions**

A sensitivity analysis was conducted to assess the likely errors in the prediction of residence time of the recovered water due to uncertainties in the input parameters. Focus was put on transport parameters as the method used the solute transport equation to calculate the age of the injected water. Sensitivity simulations were compared with results from the normal scenario using model C.

Porosity was tested using realistic values of 0.25, 0.45 and 0.55 for layers 1 and 2, with proportional changes in dispersivity in layers 3, 4 and 5 for a given sensitivity run. All cases tested presented the same pattern of distribution of the residence time, with changes in values, especially of the minimum residence time. Results showed a linear dependency between the minimum residence time predicted and the porosity, with smaller predicted values for lower porosity (Figure 28a). Minimum residence time predicted for porosity of 0.25 is 127 days. For the range of realistic values that porosity could take, sensitivity of the predictions to porosity is acceptable.

Prediction of residence time is not sensitive to dispersivity (Figure 27b). Sensitive simulations involved tested values of 2, 4 and 12 m set in layers A and B. Change in prediction of the minimum residence time is in the order of a day in all cases.

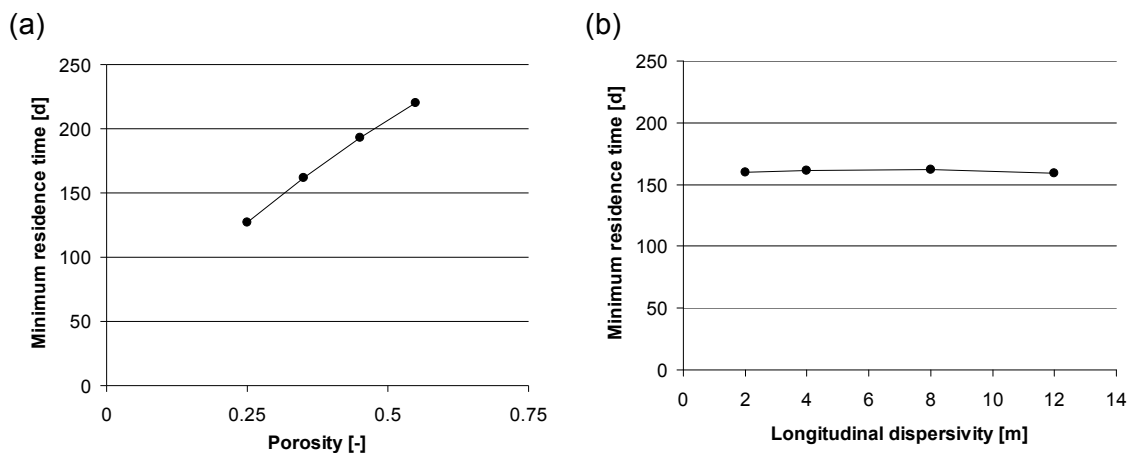


**Figure 28 Change in minimum residence time of the injected water before recovery in function of porosity (a) and dispersivity (b) values, using model C**

### **4.7.3. Limitations of the model**

Confidence in the predictions can be limited by a number of factors that can be described in two categories: hydrogeological data and modelling method.

Hydrogeological data relate to the understanding of the flow and solute transport system at the study site. As discussed previously, improvement of the representation of the system is required to constrain errors in the predictive simulations. Among the hydrogeological issues limiting the modelling, the most important include:

- Incomplete understanding of the distribution of hydraulic conductivity, especially within T2c, to quantify the fluxes occurring between the storage area (T2ab) and the lower part of the aquifer not intersected by the ASTR well (T2c) (heterogeneity, anisotropy); and
- Lack of field information of porosity values and knowledge of fractures, less permeable areas or dead-end pores that would impact the flow and solute transport processes at macro and micro scale (effective porosity, mobile/immobile domain)

Limitations of the modelling method comprise:

- Assumption of constant salinity of the injectant; and
- Use of single-domain that does not account for non-dispersive mixing (versus dual-domain; Coats and Smith 1964, Haggerty and Gorelick 1995; Culkin *et al.* 2008). Single domain does not represent small-scale geological heterogeneities which could lead to heterogeneous flushing of the aquifer. Indeed, saline water could remain in the dead-end pores or so-called immobile domain not sensitive to advection. The trapped solute would then be released by diffusion during the storage period and would increase the salinity of the stored water, lowering the predicted efficiency of the ASTR system.

It must be highlighted that both model C and D generate similar predictions which indicates that the inclusion of high permeable layer within the T2C unit does not largely increase the sensitivity of the model.

## 4.8. Analytical modelling predictions

The calibrated FEFLOW model represents the best use of information to predict mixing fraction and residence time of recovered water as shown in Section 4.7. However, for operational management of the ASTR site, use of FEFLOW would require commencing simulations from the outset of operations for each operational scenario to be taken into account.

It was considered that a simple analytical rule could be developed to determine the volume of water recoverable at an acceptable salinity based on the volume of water injected in the most recent injection cycle. Such a model could be calibrated by using the FEFLOW model to make predictions under a range of scenarios. Model C was the sole model adopted.

### **Methods**

Three new scenarios of injection were used to develop the analytical model. These scenarios were set using the volume injected per year as follows:

1. three wet years (300 ML/yr recharge) followed by three dry years (100 ML/yr recharge),
2. a random sequence of wet and dry years (300, 200, 80, 270, 70, 180 ML/yr recharge in sequence), and
3. alternating years of high and low recharge (300, 100, 300, 100, 300, 100 ML/yr recharge in sequence).

For each year of each scenario, the extracted volume was defined using a threshold of maximum salinity of 500 mg/L TDS ( $f=0.81$ ) for the recovered water. Therefore, the recovery was ceased for each run once the critical mixing fraction of 0.81 was reached.

Injection and recovery was undertaken at the same rate (20 L/s) and commenced on the same day each year with recovery commencing exactly six months after the start of injection. Hence in low flow years the duration of the storage period between recharge and recovery was longer than in wetter years.

### **Results**

The results of the three sequences of simulations are shown on Figure 29. It is immediately striking that the volume of water recoverable is very similar to the immediately preceding recharge volume. It is expected that this is caused by the consistent use of a single critical mixing ratio to shut down recovery. This would have left a very similar freshwater buffer in the aquifer each year at the end of recovery. The effect of this is to erase any memory of the aquifer of preceding injection and recovery cycles. Additional small variations in recovery volume, particularly those evident in successive years in scenario 1, suggest that

approximations made in modelling such as variations in the length of time steps at the time of shut down, can influence results.

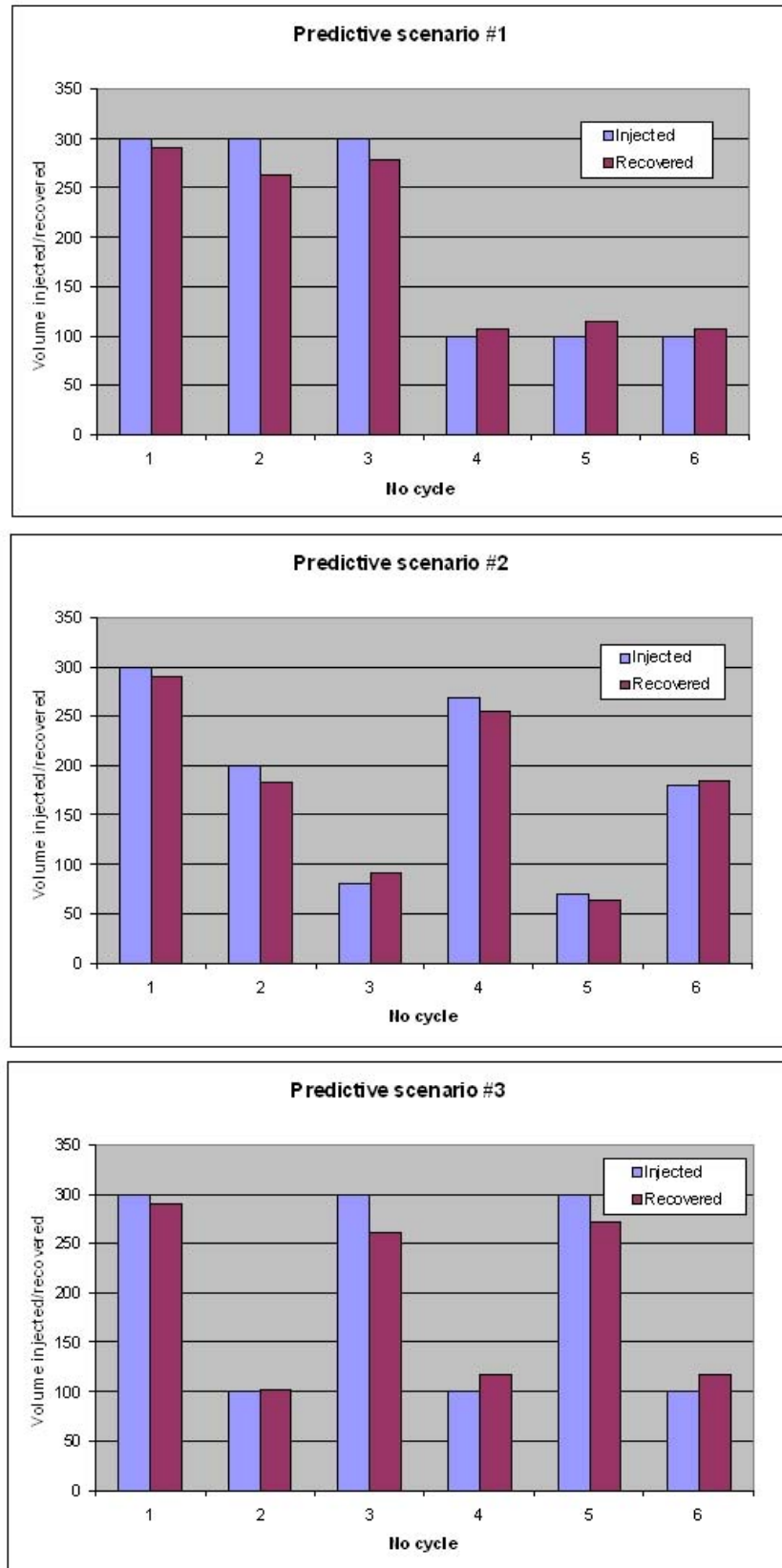


**Figure 29** Amount of injected and recovered water in three predictive scenarios

Plotting the volume recovered at  $f \geq 0.81$ , versus the immediately preceding injection volume (Figure 30a) shows an approximate equality.

Recovery efficiency defined on the threshold of  $f = 0.81$  is found to exceed 86% for all cases (Figure 30b). In years with below average injection the proportion recoverable appears to be buoyed by additional water left in the aquifer in years when larger volumes were injected and correspondingly larger dispersion occurred leaving more residual freshwater in the aquifer. This suggests that if there was greater value in recovering water in years of low recharge than in years of high recharge, an alternative recovery rule could be more efficient.

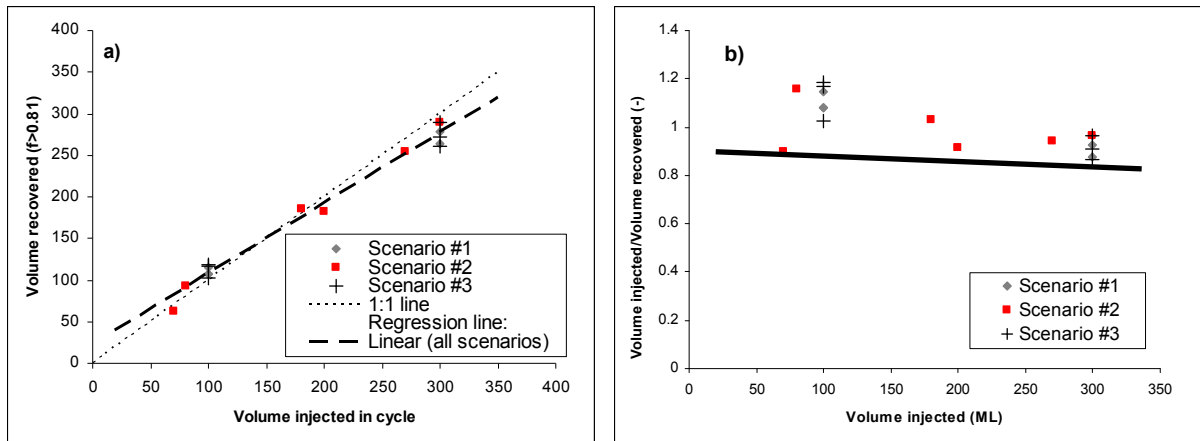


**Figure 30** Volume recovered versus volume injected in the each cycle. a) direct comparison, b) recovery efficiency in function of amount of injected water. Solid line in fig. b indicates min achievable recovery

As an example, recovering a fixed volume or changing the critical mixing ratio could be more useful as a buffer against single drought years. Although not evaluated, a model of the type:

$$\begin{aligned}
 f_{\text{crit}} &= 0.81; V_{\text{inj}} \leq 100\text{ML} \\
 &= 0.76 + 0.0005 \cdot V_{\text{inj}}; 100 \leq V_{\text{inj}} \leq 300\text{ML} \\
 &= 0.91; V_{\text{inj}} > 300 \text{ML},
 \end{aligned}$$

is likely to yield substantially higher volumes in the first year of any low flow sequence ( $V_{\text{inj}} < 100 \text{ ML}$ ). The approach is graphically presented in Figure 31.

Operating rules such as drawing a constant volume of water from the aquifer will have a volume-reliability relationship (where reliability represents the proportion of water or years when the mixing fraction exceeds its critical value, i.e. salinity less than target volume).

These have not been explored but it is suggested that the objective function would need to be defined in order to allow optimisation of such operating rules.

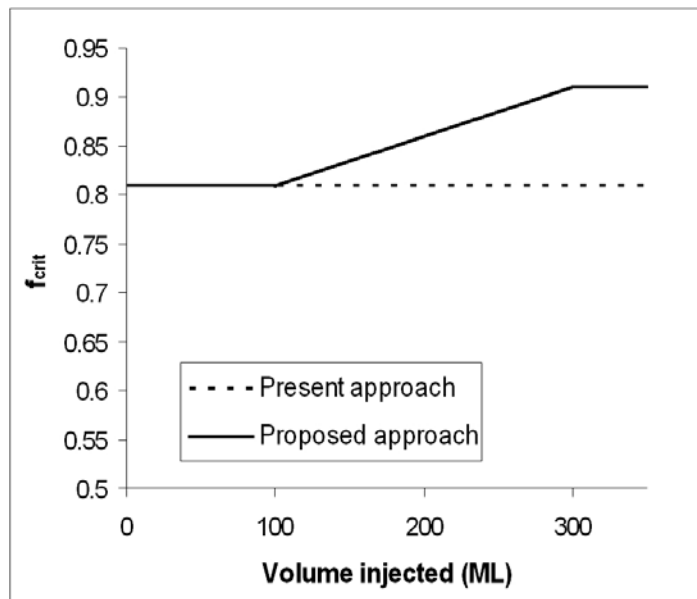


**Figure 31 Comparison of the operational approaches of the ASTR system. The new approach allows one to generate a “dry weather buffer” which would increase the effectiveness of the system in dry years.**

## 5. CONCLUSIONS AND RECOMMENDATIONS

### *Field trial*

Between 2006 and 2009, the ASTR trial included a flushing phase that aimed to drive the brackish water out of the storage area by injecting 377 ML of fresh stormwater via the RWs between September 2006 and June 2008; an injection phase that involved injection of 30 ML into the IWs between September and December 2008; and a first recovery period between February and April 2009 when 105.7 ML was extracted from RWs.

During injection into the RWs, hydraulic head monitoring showed that maximum water level variations observed were ~60 m AHD at RWs and ~14 m AHD at IWs. Moreover, SWL observed from continuous logging at piezometers P1, P2 and P3 appeared to be related to nearby Parafield ASR operations.

During the flushing phase, EC data collected at ASTR wells showed a clear breakthrough of injectant across the study zone with values at IWs dropping from 3620  $\mu\text{S}/\text{cm}$  in June 2006 to 590  $\mu\text{S}/\text{cm}$  in August 2008. Averaged salinity of the recovered water was measured at 530  $\mu\text{S}/\text{cm}$  with a maximum observed of 620  $\mu\text{S}/\text{cm}$ , largely below the threshold of salinity of drinking water of 500 mg/L (~890  $\mu\text{S}/\text{cm}$ ).

Monitoring of EC during injection and recovery at the ASTR site indicated that the nearby Parafield ASR scheme creates a local gradient within T2 that tends to move the ASTR fresh plume. However, no significant displacement was observed. Fluctuations in EC within the fresh plume could be likely due to the variations in salinity of the injectant.

Additional data collected from a new piezometer opened in the bottom part of the aquifer not intersected by the ASTR wells (T2c) showed a clear breakthrough of fresh water with EC values collected during sampling decreasing from 2700  $\mu\text{S}/\text{cm}$  in September 2008 to 1380  $\mu\text{S}/\text{cm}$  in January 2009, which suggests a flow exchange occurring between the storage area and the lower part of the aquifer. This finding eliminates one of the conceptual groundwater model (CM1) tested in the previous report (Kremer *et al.* 2008).

### ***Flow and solute transport modelling***

Previous 3D flow and transport modelling was successfully revised using new data collected at the ASTR site since October 2007. The new conceptual model is a five-material layered model that encompasses T2abc and, contrary to previous models, takes account of the full thickness of the aquifer over 60 m.

Results of calibration showed the new conceptual model performed well in the simulation of hydraulic head and salinity data observed at the ASTR wells. Two alternative sets of parameters were found to match the field data, which differ in their representations of T2c.

Verification of the two models using independent data collected during the recovery period indicated a satisfying performance in the simulation of salinity of the extracted water for both of the models. Nevertheless, the verification of both models must still be performed with a view to eliminating that one which reproduces the observed data with a lower degree of accuracy. Eventually, one unique model should be obtained and used for predictive simulations.

### ***Predictions of operations for progressing trial***

Results of six-year injection/recovery cycles at the ASTR site with recovery efficiency of 80% under normal, wet and dry conditions indicate that salinity of the recovered water remains mainly below the drinking water criteria of 500 mg/L TDS, even under drought conditions. Additional simulations under normal conditions of use suggest that recovery efficiency greater than 80% led to salinity values greater than the threshold of 500 mg/L TDS.

Mixing occurs at the bottom of the fresh plume due to vertical flow between the storage area and T2c; and within the fresh plume due to intrusion of saline water between the IWs due to an insufficient buffer against the brackish water within the study area. Salinity of recovered water is more sensitive to recovery efficiency (i.e. volume of injection and extraction) than, firstly, to the choice of representation of T2c (models C or D) and, secondly, to the conditions of operations (normal, dry or wet). Prediction of the salinity of the ASTR recovered water over three years is not sensitive to the nearby Parafield ASR operations.

The minimum residence time of the injected water within the aquifer before recovery, under normal conditions without any storage periods taken into account was simulated at 162 days. Ultimately, minimum residence time in the worse case tested was greater than 150 days.

### ***Recommendations***

It is recommended that recovery efficiency should be maintained at no higher than 80% to enhance the buffer against the brackish water within the study area, and to ensure that the salinity of the recovered water can fulfil the drinking water requirements of 500 mg/L TDS reliably over the long term.

To enhance knowledge of the size of the fresh plume within the study area, salinity could be monitored in T2ab equidistant from two IWs, to assess the intrusion of more saline water within the fresh plume during extraction, which, so far, cannot be done using existing ASTR wells and piezometers. Monitoring on the bisector of two IWs would be a powerful tool to estimate the ideal extraction volume while keeping a buffer against the brackish water to ensure the efficiency of the ASTR system in the following years.

## REFERENCES

- AGT (2007) Final draft Parafield ASTR wells completion report and aquifer test results. AGT Report no 2077/22, Australian Groundwater Technologies PTY LTD, Wayville, South Australia.
- Anderson, MP and Woessner, WW (1992) Applied groundwater modeling: simulation of flow and advective transport. Academic Press.
- Chavent, G (1974) Identification of Parameters in Distributed Systems. In: RE Goodson and M Polis (Eds), *Identification of parameters in distributed systems: Proceedings of the Joint Automatic Control Conference*, University of Texas, US, 17-21 June 1974, pp. 31-48, American Society of Mechanical Engineers, New York.
- Coats, KH and Smith, BD (1964) Dead-end pore volume and dispersion in porous media, *Journal of Petroleum Science and Engineering*, vol. 4, pp. 73-84.
- Culkin, SL, Kingha, K and Day-Lewis, FD (2008) Implication of Rate-Limited Mass Transfer for Aquifer Storage and Recovery. *Ground Water*, vol. 46, no. 4, pp. 591-605.
- Diersch, H-JG, 2005. *FEFLOW: Finite Element Subsurface Flow & Transport Simulation System*. WASY GmbH Institute for Water Resources Planning and Systems Research.
- Dillon, P, Page, D, Pavelic, P, Toze, S, Vanderzalm, J, Barry, K, Levett, K, Regel, R, Rinck-Pfeiffer, S, Pitman, C, Purdie, M, Marles, C, Power, N and Wintgens, T (2008) City of Salisbury's progress towards being its own drinking water catchment. In: Singapore International Water Week, Singapore, 23-27 June 2008.
- Freyberg, DL (1988) An exercise in ground water model calibration and prediction. *Ground Water*, vol. 26, no.3, pp. 350-360.
- Gelhar, LW, Welty, C and Rehfeldt, KR (1992) A critical Review of Field-Scale Dispersion in Aquifers. *Water Resources Research*, vol. 28, no. 7, pp. 1955-1974.
- Geoscience Australia (2004) Australian Stratigraphic Names Database. Commonwealth of Australia, viewed October 2009 <[http://dbforms.ga.gov.au/pls/www/geodx.strat\\_units.int](http://dbforms.ga.gov.au/pls/www/geodx.strat_units.int)>.
- Gerges G (2005) Greenfield Railway Station ASTR Project Briefing on Aquifer Tests. Report prepared for ASTR Technical committee by NZG Groundwater consultant, Hallett Cove SA 5158, Australia.
- Gerges G (2006a) Technical specification for drilling and well completion ASTR project at Greenfield's Railway Station (to be read as Parafield Gardens oval) 16th March 2006.
- Gerges G (2006b) Parafield oval ASTR wells completion and aquifer tests results. Preliminary draft for Technical Meeting August 2006.
- Goode, DJ (1996) Direct simulation of groundwater age. *Water Resources Research*, vol. 32, no. 2, pp. 289-296.
- Haggerty, R and Gorelick, SM (1995) Multiple-rate mass transfer for modelling diffusion and surface reactions in media with pore-scale heterogeneity. *Water Resources Research*, vol. 31, no. 10, pp. 2383-2400.
- Hem JD (1985) Study and interpretation of the chemical characteristics of natural water, 3<sup>rd</sup> ed. US Geological Survey Water Supply Paper 2254, 264 pp.
- Kremer, S, Pavelic, P, Dillon, P, and Barry, K (2008) Flow and Solute Transport Observations and Modelling from the First Phase of Flushing Operations at the Salisbury ASTR Site. CSIRO: Water for a Healthy Country National Research Flagship.
- Lowry, CS and Anderson, MP (2006) An Assessment of Aquifer Storage and Recovery Using Ground Water Flow Models. *Ground Water*, vol. 44, no. 5, pp. 661-667.
- Mailloux, BJ, Fuller, ME, Onstott, TC, Hall, J, Dong, H, DeFlaun, MF, Streger, SH, Rothmel, RK, Green, M, Swift, DJP, Radke, J (2003) The role of physical, chemical, and microbial

heterogeneity on the field-scale transport and attachment of bacteria. *Water Resources Research*, Vol. 39, No. 6, 1142.

Page, D, Vanderzalm, J, Barry, K, Levett, K, Kremer, S, Ayuso Gabella, MN, Dillon, P, Toze, S, Sidhu, J, Shackleton, M, Purdie M and Regel R (2009) Operational residual risk assessment for the Salisbury stormwater ASTR project. CSIRO: Water for a Healthy Country National Research Flagship.

Pavelic, P, Dillon PJ and Simmons, CT (2002) Lumped parameter estimation of initial recovery efficiency during aquifer storage and recovery. In: PJ Dillon (Ed.) *Management of Aquifer Recharge for Sustainability*. Swets and Zeitlinger, Lisse, ISBN 90 5809 527 4.

Pavelic, P, Dillon, P and Robinson, N (2004) Groundwater Modelling to Assist Well-Field Design and Operation for the ASTR Trial at Salisbury, South Australia. CSIRO Land and Water Technical Report No. 27/04.

Rehmann, LLC, Welty, C and Harvey RW (1999) Stochastic analysis of virus transport in aquifers. *Water Resources Research*, Vol. 35, No. 7, p. 1987-2006.

Rinck-Pfeiffer S, Pitman C, Dillon, P (2005) Stormwater ASR and ASTR (Aquifer Storage Transfer and Recovery) in practice and under investigation in South Australia. In: *Recharge systems for protecting and enhancing groundwater resources. Proceedings of the 5th International Symposium on Management of Aquifer Recharge*, ISMAR5, 11-16 June 2005, Berlin, Germany, IHP-VI Series on Groundwater No. 13.

Swierc J, Page D, van Leeuwen J, and Dillon P (2005) Preliminary Hazard Analysis and Critical Control Points Plan (HACCP) - Salisbury Stormwater to Drinking Water Aquifer Storage Transfer and Recovery (ASTR) Project, CSIRO Land and Water Technical Report.

Varni, M and Carrera, J (1998) Simulation of groundwater age distribution. *Water Resources Research*, vol. 34, no. 12, pp. 3271-3281.

Ward, JD, Simmons, CT and Dillon, PJ (2008) Variable-density modelling of multiple-cycle aquifer storage and recovery (ASR): Importance of anisotropy and layered heterogeneity in brackish aquifers. *Journal of Hydrology*, vol. 356, pp. 93-105

Ward, JD, Simmons, CT, Dillon, PJ and Pavelic, P (2009) Integrated assessment of lateral flow, density effects and dispersion in aquifer storage and recovery. *Journal of Hydrology*, vol. 370, no. 1, pp. 83-99.

Yeh, WG (1986) Review of Parameters Identification Procedures in Groundwater Hydrology: The Inverse Problem. *Water Resources Research*, vol. 22, no. 2, pp. 95-108.

Zheng, C and GD Bennett (2002) Applied Contaminant Transport Modeling, Second Edition, Wiley-Interscience, New York.

## APPENDIX A: LITHOLOGICAL AND GEOPHYSICAL LOG

From 30/06/2008 to 31/07/2008, three piezometers, P1 (permit number (PN) 149448), P2 (PN 149449) and P3 (PN 149450), were drilled at the ASTR site along the RW1-IW1 transect. P1, P2 and P3 are situated respectively 10, 20 and 30 m from IW1. P1 and P3 were drilled until 171.5 and 171 m bgs, respectively; while P2 was drilled to 228 m bgs. Lithological units intersected during drilling are identical at the three piezometers and in accordance with previous lithological logs collected during drilling of the RWs and IWs at the ASTR site up to 180 m bgs (AGT 2007). P2 allows access to the lithology below 180 m bgs that was previously unknown at the ASTR site and so far assumed from nearby deep wells situated about 300 m from the trial site.

**Table 7 Lithological and stratigraphical units intersected at P2 at the ASTR site (adapted from Well Construction Report and AGT 2007)**

Interval [m bgs] P2	Lithology	Aquifer	Stratigraphy
0 – 2.1	Top soil mound	<i>Confining bed</i>	<i>Recent to Quaternary</i>
2.1 – 9.4	Clay	<i>Confining bed</i>	
9.4 – 10.8	Sand / gravel	<i>Q2 aquifer</i>	
10.8 – 90	Clay	<i>Confining bed – contains Q3 and Q4 sub-aquifers</i>	
90 – 118	Sand / shell grit	T1a	<i>Hallet Cove Sandstone &amp; Dry Creek Sand</i>
118 – 158	<i>Limestone</i>	T1b	<i>Upper Port Willunga Formation</i>
158 – 162	<i>Clay</i>	Confining bed	<i>Munno Para Clay</i>
162 – 222	<i>Limestone / sand</i>	T2	<i>Lower Port Willunga Formation</i>
222 - 228	<i>Clay</i>	<i>Confining bed</i>	<i>Ruwarung member</i>

\* Information from Well Completion report is completed by information from AGT (2007) indicated in *grey italic*.

Field investigations undertaken at P2 included geophysical logs by DWLBC from 0 to about 225 m bgs, and core sampling by CSIRO between 162 and 186 m bgs. Geophysical logs that ran prior to installation of the well casing included natural gamma, neutron, caliper, bulk density, point resistance, spontaneous potential, medium resistivity and deep resistivity. Logs of the target aquifer T2, between 160 and 220 m bgs are presented in Figure 32.

The caliper log can be divided into three intervals: from 164 to 173 m bgs, a diameter of 17.5 cm appeared to be fairly regular without significant variations; from 173 to 188 m bgs, the caliper log presented multiple variations in the range of 15-20 cm; and then, from 188 to 220 m bgs, the log was again regular (~17 cm), with a small increase up to 20.5 cm at 211 m bgs. These observations are in good correlation with depths of units T2a, T2b and T2c defined from previous lithological logs at the ASTR wells (AGT 2007), and confirm the lithological stratigraphy of the target aquifer as Table 1 and Table 7.

The natural gamma values vary in the range of 25-110 API. These values scatter in the profile which could suggest that fine-grained fractions are uniformly dispersed in T2 aquifer. Similar patterns are apparent with respect to neutron and bulk density values. The latter parameters are however influenced by the hole diameter. Relatively large values of bulk density confirm that calcite is the primary mineral phase of the aquifer. The pronounced peaks in neutron, spontaneous potential and point resistance values at the depth of 170 m

are an indication of the existence of high porosity zone. All electrically based parameters (spontaneous potential, point resistance and resistivity values) increase over depth from 160-200m and then decrease from 200-210 m. With respect to the resistivity values the increase is particularly sharp and the decrease quite gentle. These patterns may reflect the differences in electrical conductivity and temperature of groundwater in the aquifer. They may be related with the vertical extension of freshwater plume induced by ASTR site operation in July 2008.

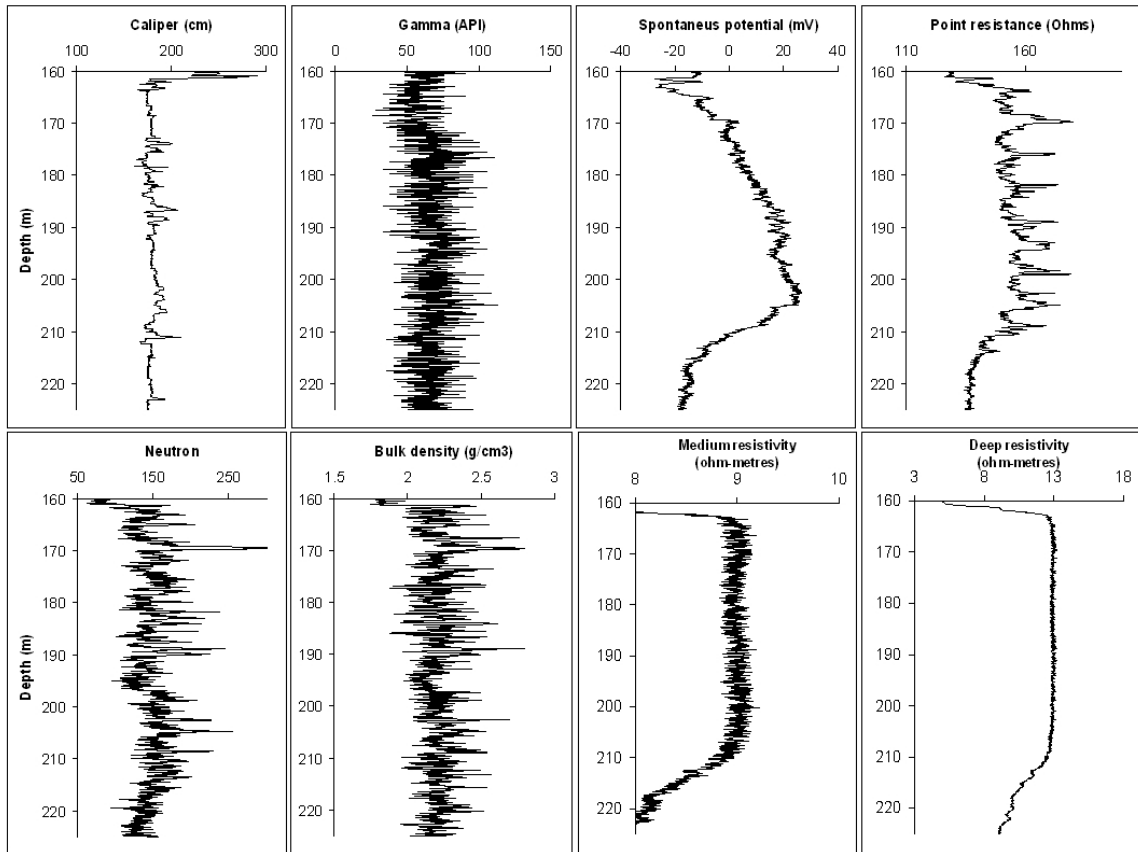


**Figure 32 Geophysical logs as a function of depth (only for 160 to 225 m interval) collected at P2 in July 2008 prior to casing**

# APPENDIX B: PROFILED EC AND TEMPERATURE DATA

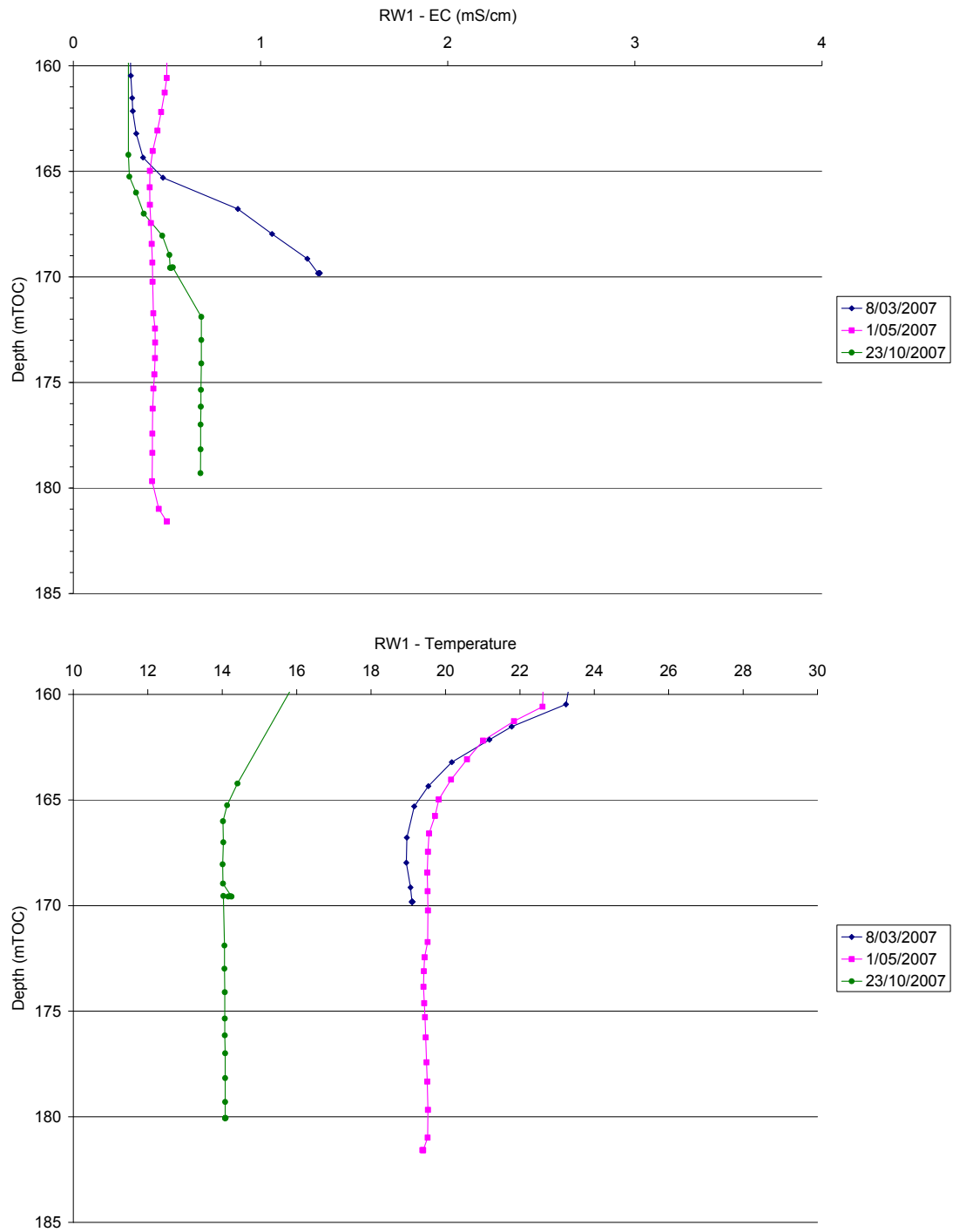
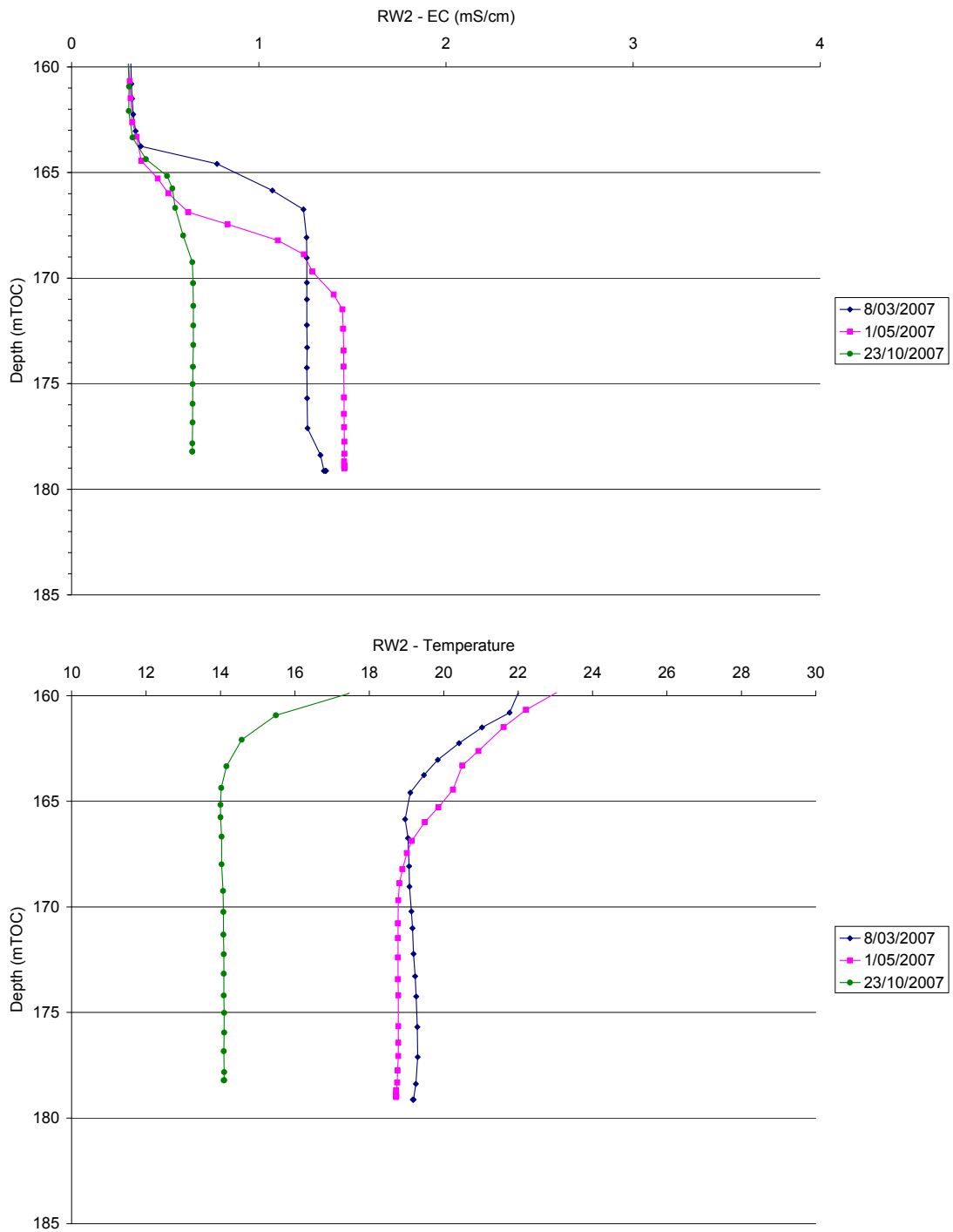


Figure 33 EC and temperature versus depth at RW1 between March and October 2007



**Figure 34 EC and temperature versus depth at RW2 between March and October 2007**

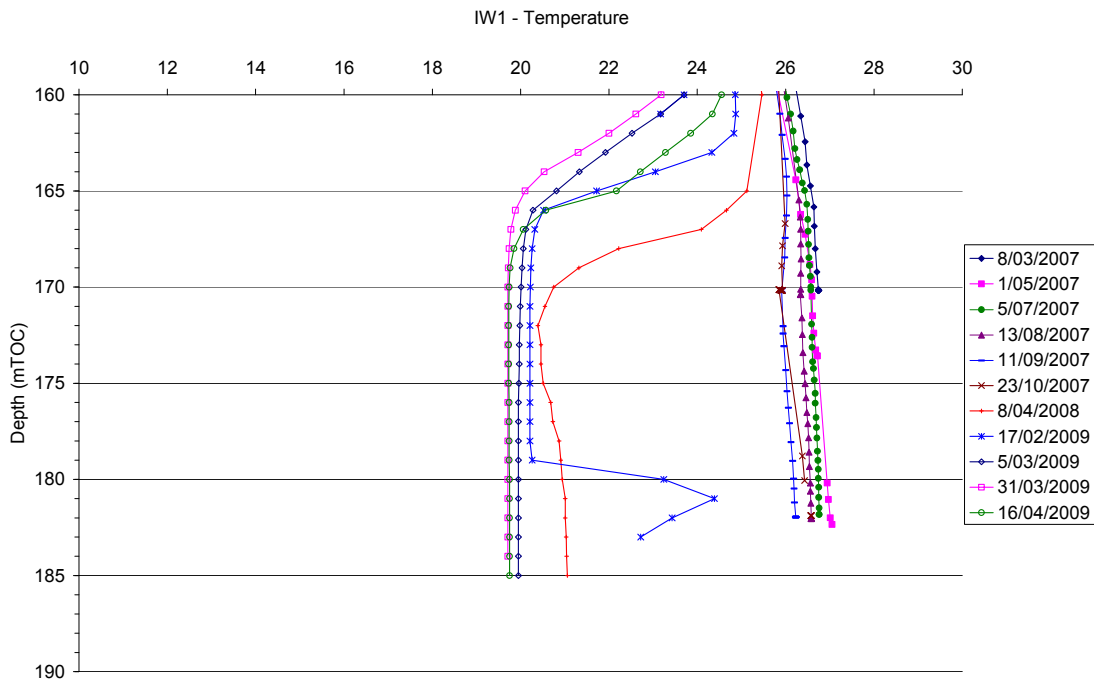
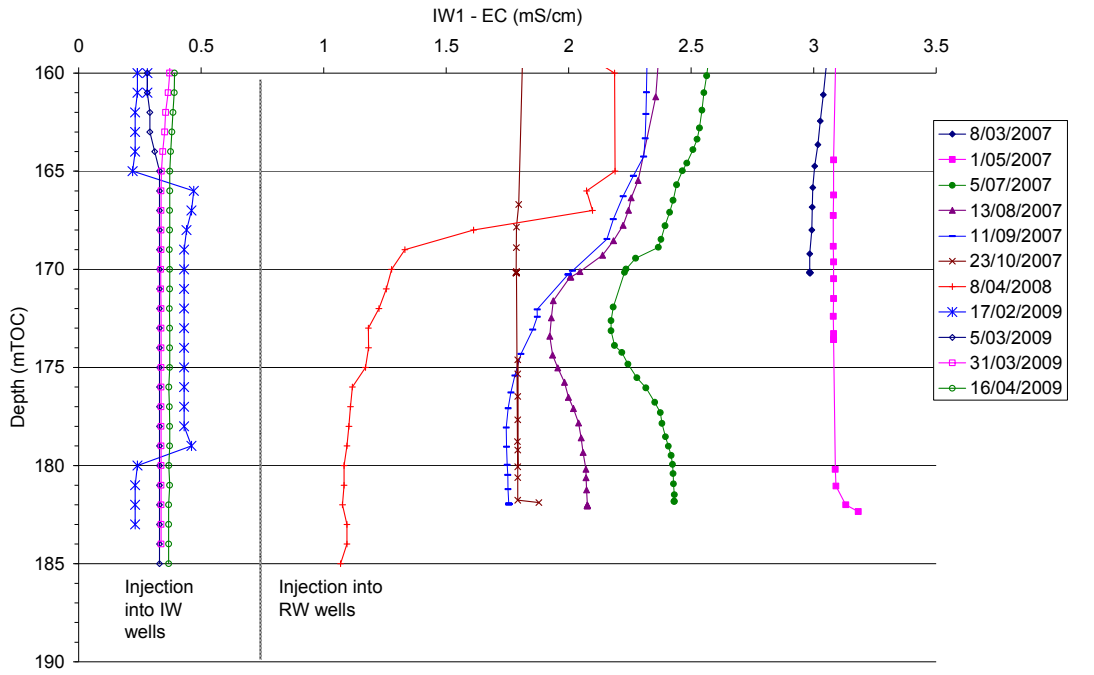
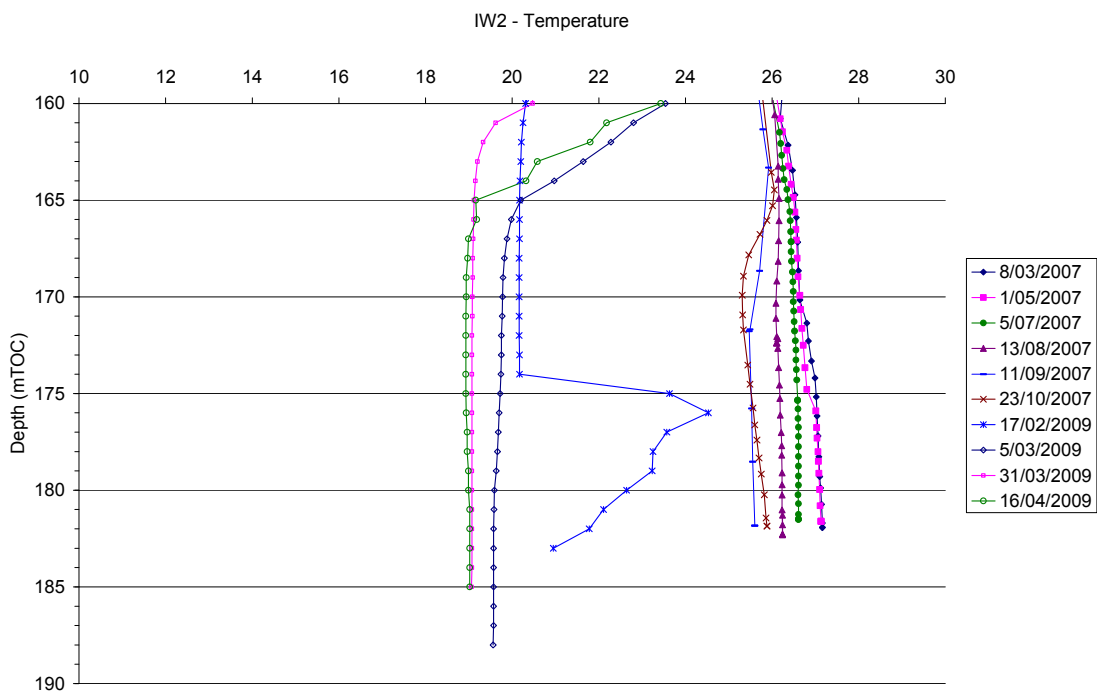
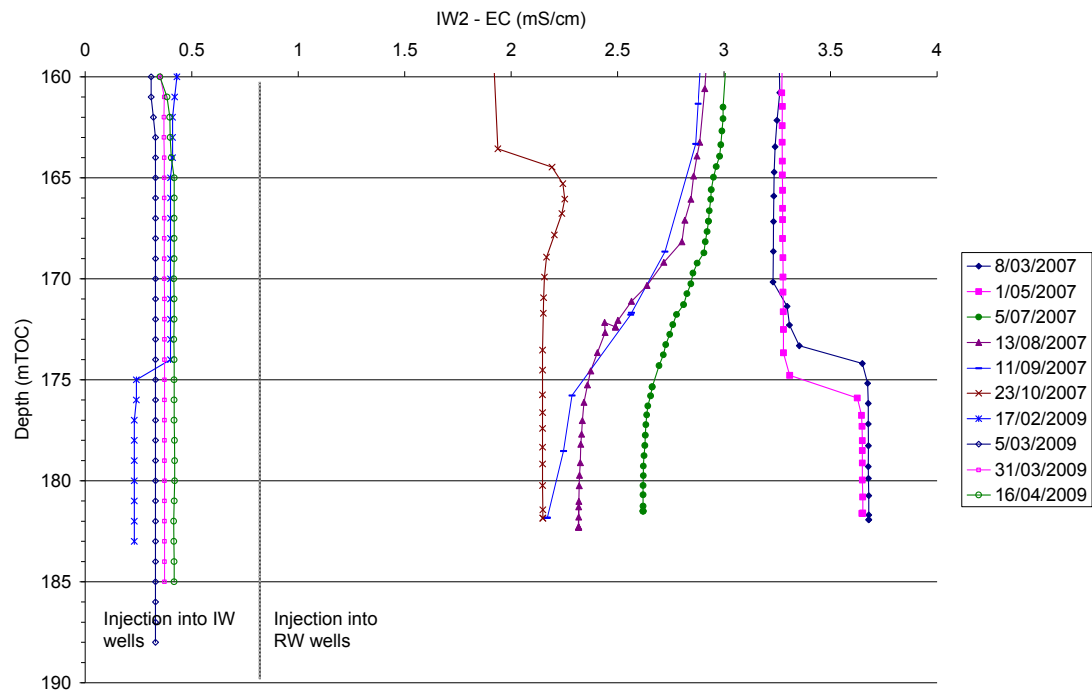
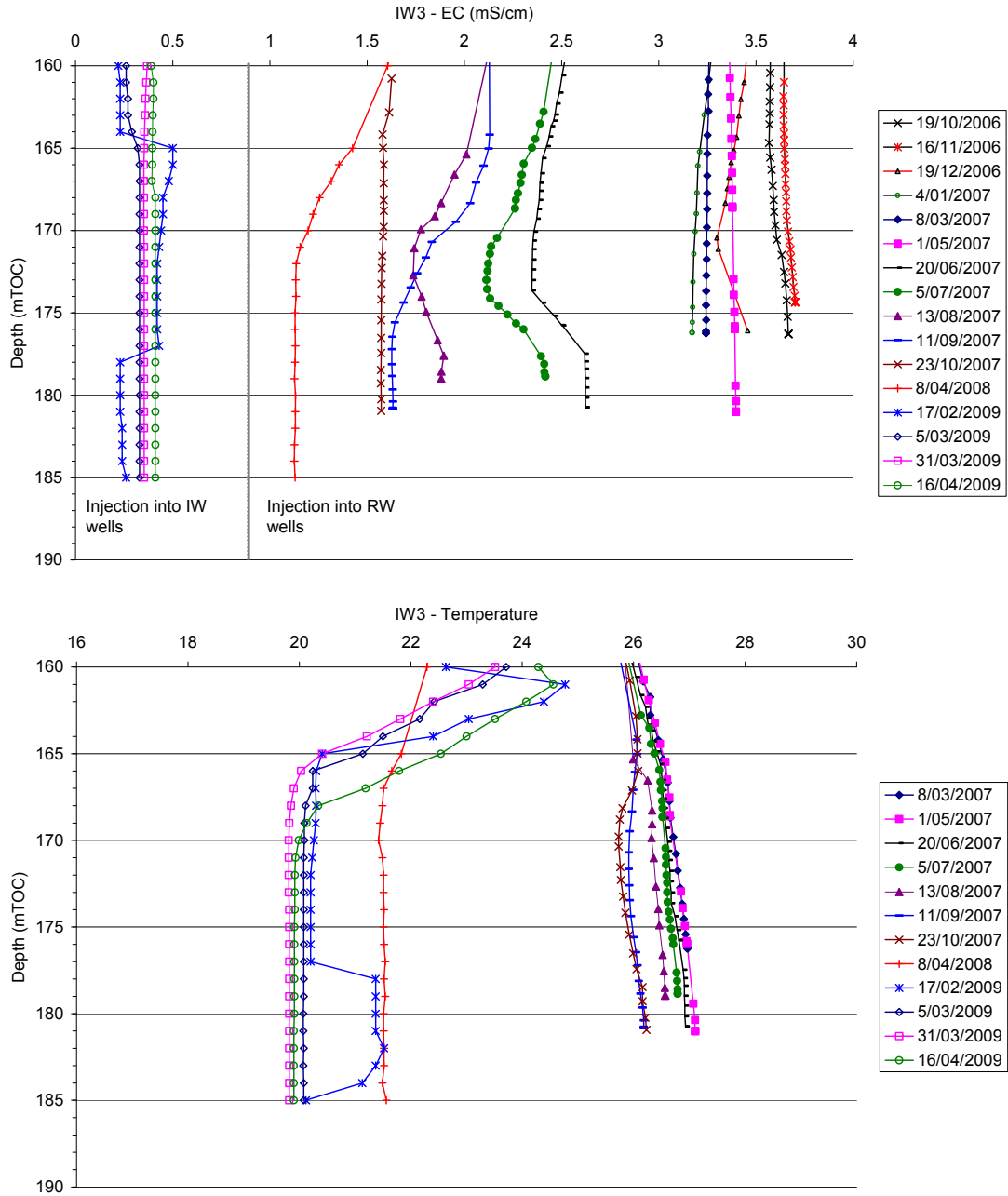


Figure 35 EC and temperature versus depth at IW1 between March 2007 and April 2009. Peak in the profile sampled 17/02/2009 reflects start of recovery on 1/02/2009.



**Figure 36 EC and temperature versus depth at IW2 between March 2007 and April 2009. Sharp increase in the temperature profile sampled 17/02/2009 reflects start of recovery on 1/02/2009.**



**Figure 37 EC and temperature versus depth at IW3 between March 2007 and April 2009. Sharp increase in the temperature profile sampled 17/02/2009 reflects start of recovery on 1/02/2009.**

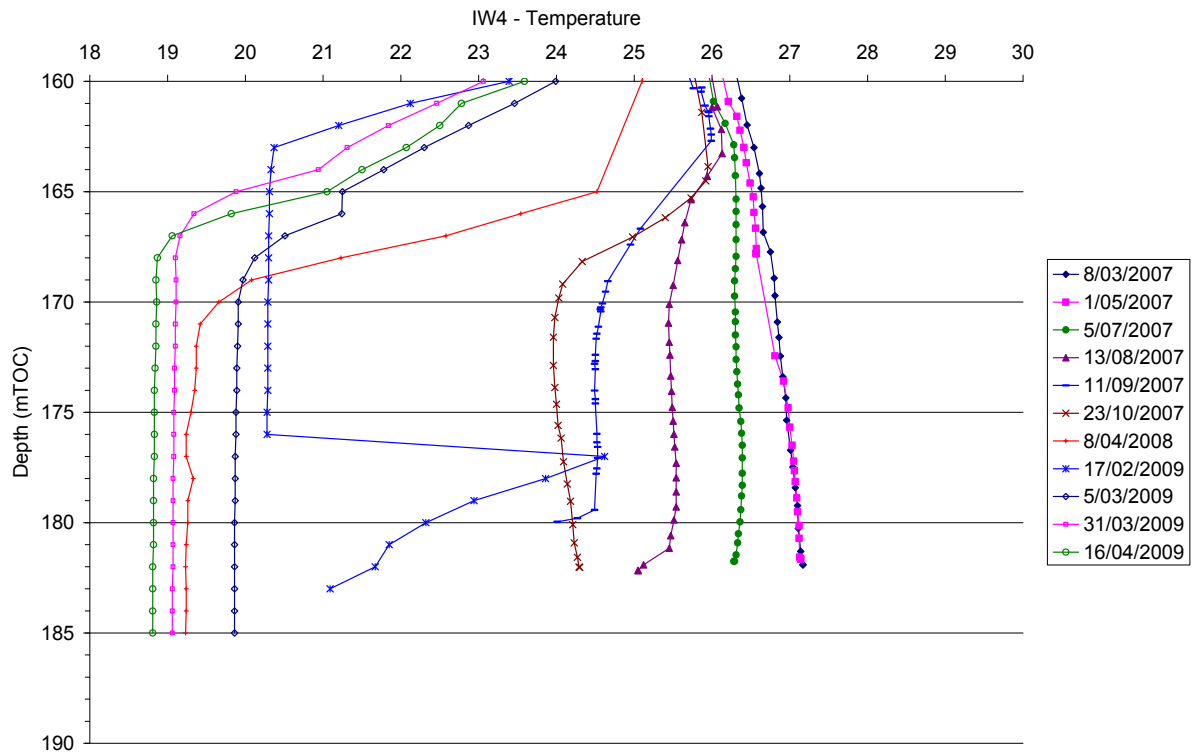
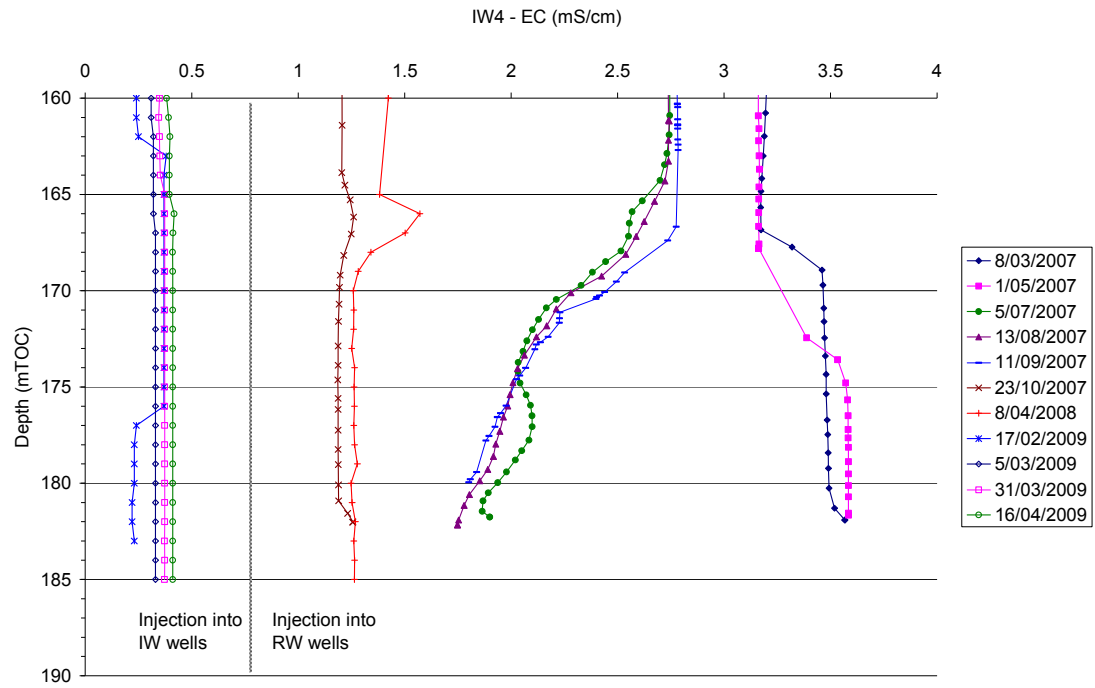
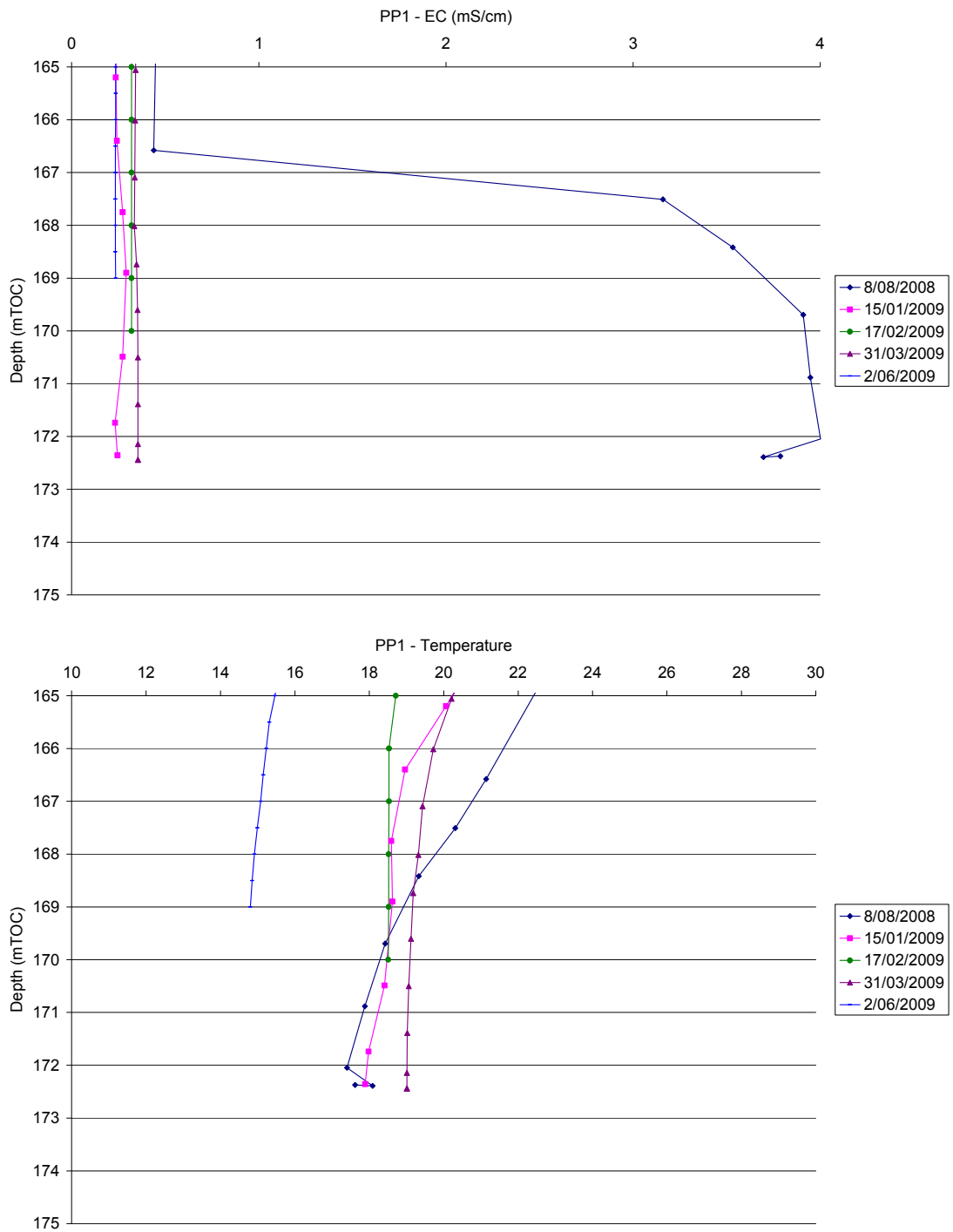


Figure 38 EC and temperature versus depth at IW4 between March 2007 and April 2009. Sharp increase in the temperature profile sampled 17/02/2009 reflects start of recovery on 1/02/2009.



**Figure 39 EC and temperature versus depth at P1 between August 2008 and June 2009**

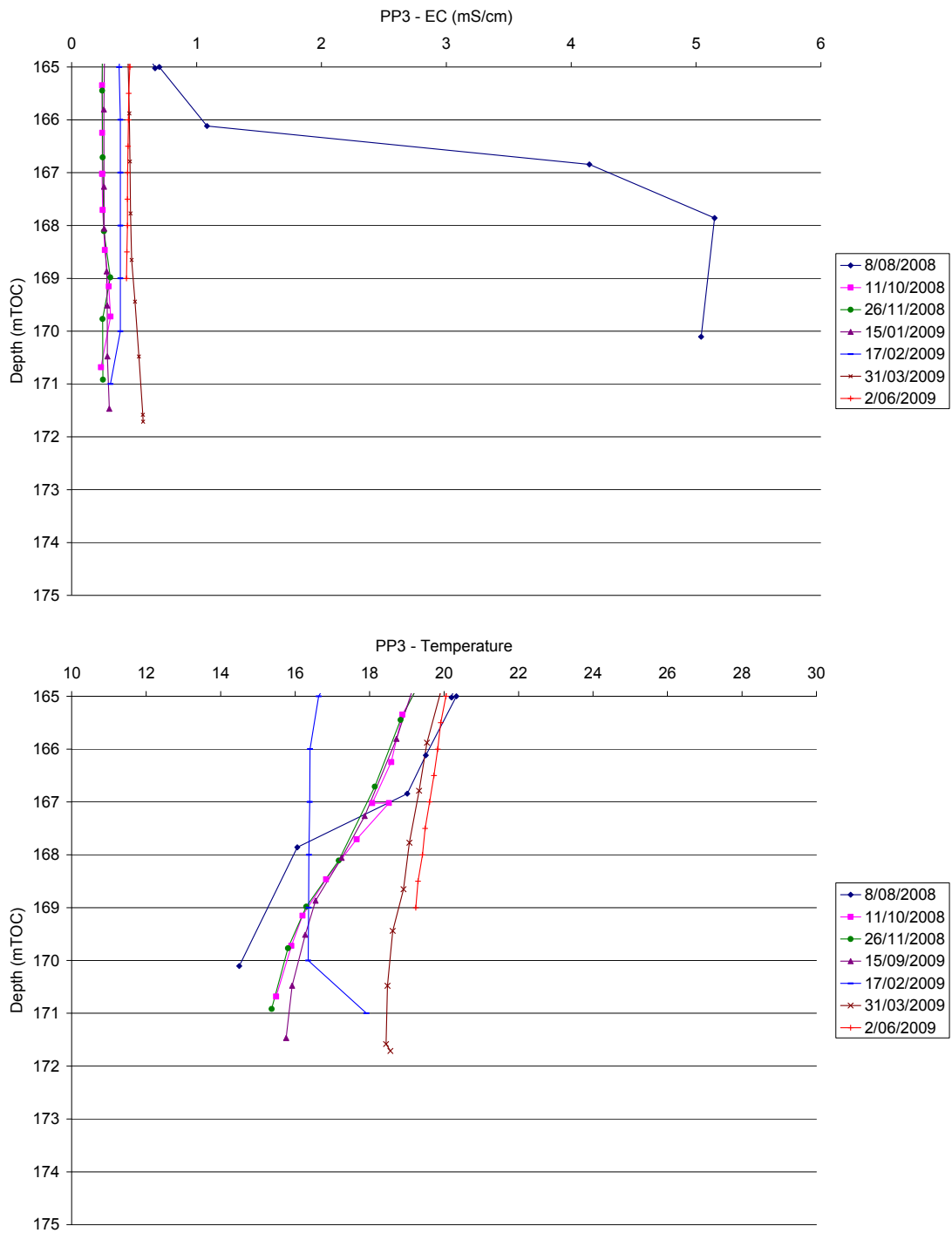
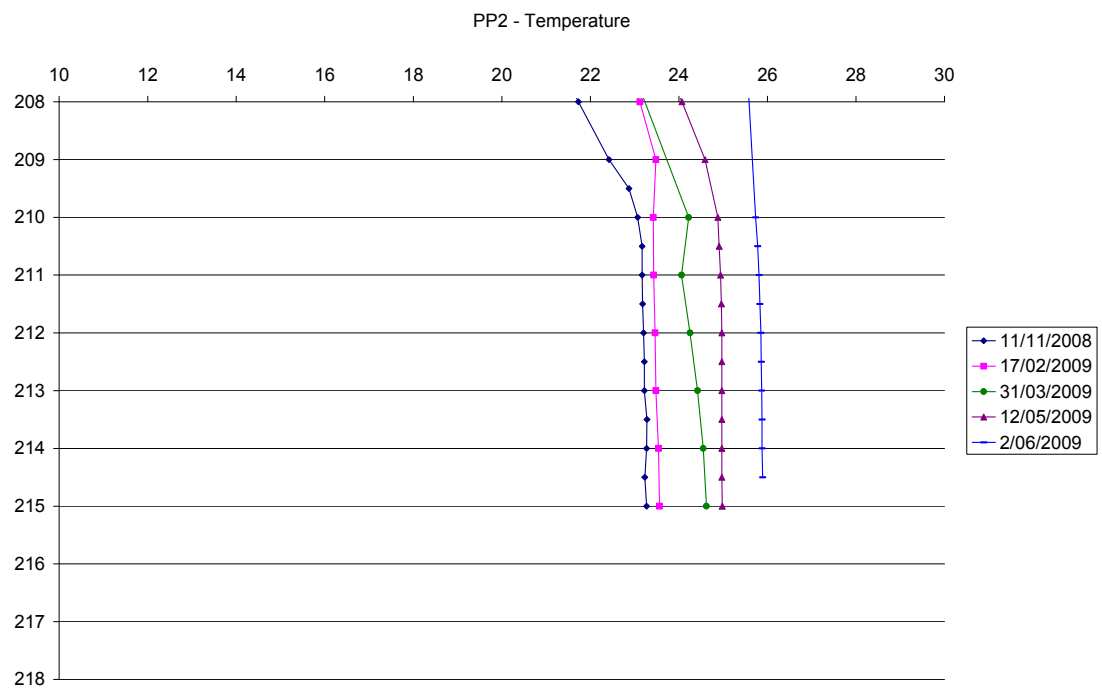
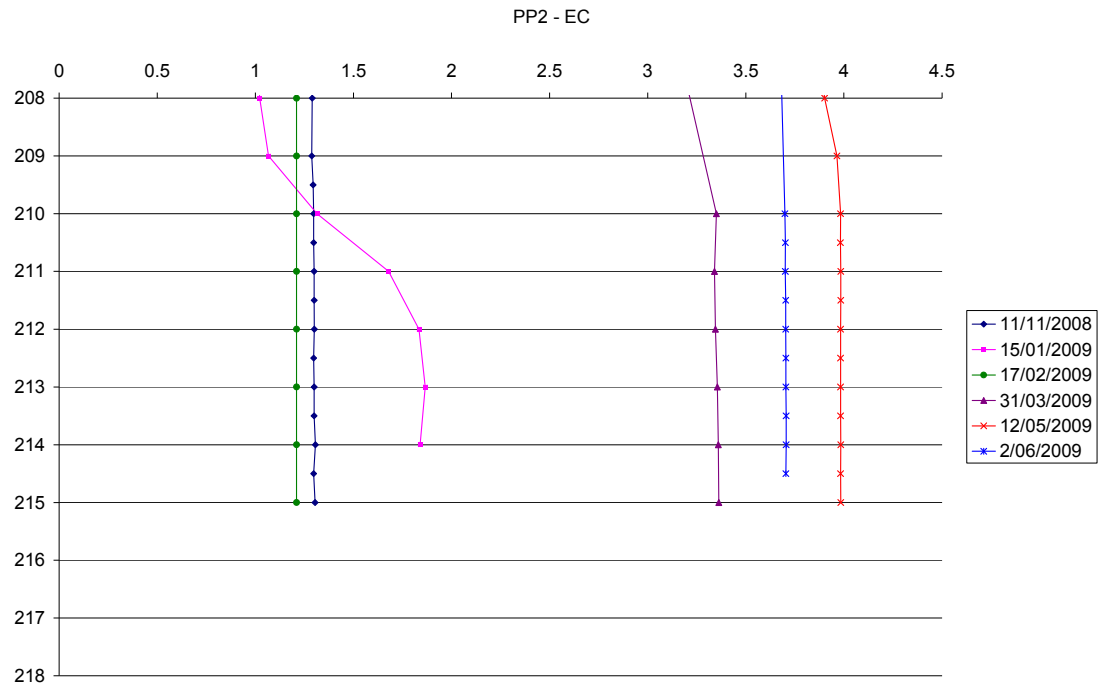


Figure 40 EC and temperature versus depth at P3 between August 2008 and June 2009



**Figure 41 EC and temperature versus depth at P2 between November 2008 and June 2009**

# APPENDIX C: OPERATIONAL INPUT DATA FOR NUMERICAL SIMULATIONS

## C.1 Calibration simulations

Calibration simulations were run over 857 days. Time in all simulations is expressed in days, from the first day of injection at the ASTR site. Operational input data include injection via RWs between 0 and 668.8 days, injection via IWs between 723 and 832 days and injection and extraction at the nearby Parafield ASR scheme between day 24 and day 857. In the following tables, negative flow rates indicate injection, while positive flow rates designate extraction.

Input data for injection at the RWs were based on observed flow rates and cumulative volumes collected monthly. Simulation involved a total injected volume of 195 ML through RW1 and 177 ML through RW2. Details of periods of injection and flow rates used in the simulations are presented in Table 8.

**Table 8 Injection flow rates (Q) and periods of injection at RW1 and RW2 used as input data for the calibration simulation**

RW1			RW2		
From day no.	To day no.	Q [L/s]	From day no.	To day no.	Q [L/s]
0	14.0	-3.0	0	16.8	-2.0
30	55.7	-4.2	30	55.4	-3.6
61	90.4	-5.6	61	90.7	-4.6
91	119.7	-5.6	91	121.2	-5.0
242	262.3	-5.2	242	261.9	-4.4
273	301.8	-4.4	273	300.7	-3.8
303	330.1	-5.2	303	332.3	-5.2
334	363.4	-6.4	334	361.6	-4.8
365	380.1	-5.0	365	380.8	-4.3
426	446.1	-5.0	426	443.5	-5.0
456	478.4	-8.1	456	477.2	-7.5
487	515.5	-8.2	487	513.9	-7.5
518	545.6	-5.0	518	545.1	-5.0
547	576.1	-5.8	547	548.6	-5.0
578	588.3	-5.0	578	599.7	-5.0
608	628.3	-5.0	608	638.0	-8.4
639	668.8	-5.8	639	667.6	-5.8

Input data for injection via IWs were based on observed flow rates and cumulative volumes. Simulations involved 30.5 ML injected via IWs with 9.2 ML, 9.2, 3.1 ML and 9 ML cumulated volume injected at wells IW1, IW2, IW3 and IW4, respectively. Details of periods of injection and flow rates at the IWs are presented in Table 9.

**Table 9 Injection flow rates (Q) and periods of injection at IW1, IW2, IW3 and IW4 used as input data for the calibration simulation**

From day no.	To day no.	Q [L/s]			
		IW1	IW2	IW3	IW4
723	725	0.0	-3.2	-0.4	-2.6
739	750	-3.5	-3.2	-0.4	-2.6
751	758	-2.8	-3.1	-0.6	-2.8
824	832	-6.0	-5.0	-3.4	-6.0

The two Parafield ASR wells were represented in the ASTR modelling by one injection/extraction well situated at equal distance between both ASR wells. Given that usually injection or extraction at the ASR wells do not happen in the same time, the numerical ASR well was set at 25 L/s from the observed average flow rate. Annual injection/recovery volumes of the ASR well were set in the simulation at 200 ML injected in winter, and recovered in summer, based on observed cumulative volume at the ASR site between 2006 and 2008. Details of periods of injection and flow rates at the ASR well from the first day of injection at the ASTR site are presented in Table 10.

**Table 10 Injection and extraction flow rates (Q) and periods of injection at ASR well used as input data for the calibration simulation**

ASR		
From day no.	To day no.	Q [L/s]
24	185	27
232	323	-25
399	582	25
612	704	-25
760	857	25

### C.2 Verification simulations

Verification simulations represented the extraction of 105.8 ML through the RWs that occurred at the ASTR site between February and April 2009 over 72 days. Input data include periods of extraction and flow rates, and were based on observed flow rates and cumulative volume collected approximately fortnightly at the RWs. For each model, initial conditions of head and solute distribution are based on the distribution obtained at the end of the calibration simulation. Time in all simulations is expressed in days, from the first day of injection at the ASTR site used previously in the calibration simulations. In the following, negative flow rates indicate injection, while positive flow rates designate extraction.

**Table 11 Extraction flow rates (Q) and periods of recovery at RW1 and RW2 used as input data for the verification simulation**

From day no.	To day no.	Q [L/s]	
		RW1	RW2
888	928	9.9	9.9
933	960	9.9	9.9

### C.3 Predictive modelling of mixing fraction

Time in all simulations is expressed in days, from the first day of injection at the ASTR site used previously in the calibration simulations. In the following, negative flow rates indicate injection, while positive flow rates designate extraction.

**Table 12 Summary of input data for the simulations of mixing fraction, showing flow rates (Q), total volume injected and extracted per period, and the storage period between two operations at the ASTR site.**

from day	to day	Q [L/s]						Volume injected [ML]	Volume extracted [ML]	storage [day]	periods
		RW1	RW2	IW1	IW2	IW3	IW4				
<b>Scenario normal re80%</b>											
963	1079	0	0	-5	-5	-5	-5	-200.448	0		
1116	1209	10	10	0	0	0	0	0	160.704	37	
1328	1444	0	0	-5	-5	-5	-5	-200.448	0	119	
1481	1574	10	10	0	0	0	0	0	160.704	37	
1693	1809	0	0	-5	-5	-5	-5	-200.448	0	119	
1846	1939	10	10	0	0	0	0	0	160.704	37	
2059	2175	0	0	-5	-5	-5	-5	-200.448	0	120	
2212	2305	10	10	0	0	0	0	0	160.704	37	
2424	2540	0	0	-5	-5	-5	-5	-200.448	0	119	
2577	2670	10	10	0	0	0	0	0	160.704	37	
2789	2905	0	0	-5	-5	-5	-5	-200.448	0	119	
2942	3035	10	10	0	0	0	0	0	160.704	37	
<b>Scenario wet re80%</b>											
963	1137	0	0	-5	-5	-5	-5	-300.672	0		
1147	1286	10	10	0	0	0	0	0	240.192	10	
1328	1502	0	0	-5	-5	-5	-5	-300.672	0	42	
1512	1651	10	10	0	0	0	0	0	240.192	10	
1693	1867	0	0	-5	-5	-5	-5	-300.672	0	42	
1877	2017	10	10	0	0	0	0	0	241.92	10	
2059	2233	0	0	-5	-5	-5	-5	-300.672	0	42	
2243	2382	10	10	0	0	0	0	0	240.192	10	
2424	2598	0	0	-5	-5	-5	-5	-300.672	0	42	
2608	2747	10	10	0	0	0	0	0	240.192	10	
2789	2963	0	0	-5	-5	-5	-5	-300.672	0	42	
2973	3112	10	10	0	0	0	0	0	240.192	10	
<b>Scenario drought re80%</b>											
994	1052	0	0	-5	-5	-5	-5	-100.224	0		
1116	1163	10	10	0	0	0	0	0	81.216	64	
1359	1417	0	0	-5	-5	-5	-5	-100.224	0	196	
1481	1528	10	10	0	0	0	0	0	81.216	64	

from day	to day	Q [L/s]						Volume injected [ML]	Volume extracted [ML]	storage [day]	periods
		RW1	RW2	IW1	IW2	IW3	IW4				
1724	1782	0	0	-5	-5	-5	-5	-100.224	0	196	
1846	1893	10	10	0	0	0	0	0	81.216	64	
2090	2148	0	0	-5	-5	-5	-5	-100.224	0	197	
2212	2259	10	10	0	0	0	0	0	81.216	64	
2455	2513	0	0	-5	-5	-5	-5	-100.224	0	196	
2577	2624	10	10	0	0	0	0	0	81.216	64	
2820	2878	0	0	-5	-5	-5	-5	-100.224	0	196	
2942	2989	10	10	0	0	0	0	0	81.216	64	
<b>Scenario normal re60%</b>											
963	1079	0	0	-5	-5	-5	-5	-200.448	0		
1116	1209	10	10	0	0	0	0	0	120.96	37	
1328	1444	0	0	-5	-5	-5	-5	-200.448	0	142	
1481	1574	10	10	0	0	0	0	0	120.96	37	
1693	1809	0	0	-5	-5	-5	-5	-200.448	0	142	
1846	1939	10	10	0	0	0	0	0	120.96	37	
2059	2175	0	0	-5	-5	-5	-5	-200.448	0	143	
2212	2305	10	10	0	0	0	0	0	120.96	37	
2424	2540	0	0	-5	-5	-5	-5	-200.448	0	142	
2577	2670	10	10	0	0	0	0	0	120.96	37	
2789	2905	0	0	-5	-5	-5	-5	-200.448	0	142	
2942	3035	10	10	0	0	0	0	0	120.96	37	
<b>Scenario wet re60%</b>											
1217	1391	0	0	-5	-5	-5	-5	-300.672	0		
1401	1506	10	10	0	0	0	0	0	181.44	10	
1582	1756	0	0	-5	-5	-5	-5	-300.672	0	76	
1766	1871	10	10	0	0	0	0	0	181.44	10	
1947	2121	0	0	-5	-5	-5	-5	-300.672	0	76	
2131	2236	10	10	0	0	0	0	0	181.44	10	
2313	2487	0	0	-5	-5	-5	-5	-300.672	0	77	
2497	2602	10	10	0	0	0	0	0	181.44	10	
2678	2852	0	0	-5	-5	-5	-5	-300.672	0	76	
2862	2967	10	10	0	0	0	0	0	181.44	10	
3043	3217	0	0	-5	-5	-5	-5	-300.672	0	76	

from day	to day	Q [L/s]						Volume injected [ML]	Volume extracted [ML]	storage [day]	periods
		RW1	RW2	IW1	IW2	IW3	IW4				
3227	3332	10	10	0	0	0	0	181.44	10		
<b>Scenario drought re60%</b>											
1248	1306	0	0	-5	-5	-5	-5	-100.224	0		
1370	1405	10	10	0	0	0	0	60.48	64		
1613	1671	0	0	-5	-5	-5	-5	-100.224	0	208	
1735	1770	10	10	0	0	0	0	60.48	64		
1978	2036	0	0	-5	-5	-5	-5	-100.224	0	208	
2100	2135	10	10	0	0	0	0	60.48	64		
2344	2402	0	0	-5	-5	-5	-5	-100.224	0	209	
2466	2501	10	10	0	0	0	0	60.48	64		
2709	2767	0	0	-5	-5	-5	-5	-100.224	0	208	
2831	2866	10	10	0	0	0	0	60.48	64		
3074	3132	0	0	-5	-5	-5	-5	-100.224	0	208	
3196	3231	10	10	0	0	0	0	60.48	64		
<b>Scenario normal re100%</b>											
963	1079	0	0	-5	-5	-5	-5	-200.448	0		
1116	1232	10	10	0	0	0	0	200.448	37		
1328	1444	0	0	-5	-5	-5	-5	-200.448	0	96	
1481	1597	10	10	0	0	0	0	200.448	37		
1693	1809	0	0	-5	-5	-5	-5	-200.448	0	96	
1846	1962	10	10	0	0	0	0	200.448	37		
2059	2175	0	0	-5	-5	-5	-5	-200.448	0	97	
2212	2328	10	10	0	0	0	0	200.448	37		
2424	2540	0	0	-5	-5	-5	-5	-200.448	0	96	
2577	2693	10	10	0	0	0	0	200.448	37		
2789	2905	0	0	-5	-5	-5	-5	-200.448	0	96	
2942	3058	10	10	0	0	0	0	200.448	37		
<b>Scenario wet re100%</b>											
963	1137	0	0	-5	-5	-5	-5	-300.672	0		
1147	1321	10	10	0	0	0	0	300.672	10		
1328	1502	0	0	-5	-5	-5	-5	-300.672	0	7	
1512	1686	10	10	0	0	0	0	300.672	10		
1693	1867	0	0	-5	-5	-5	-5	-300.672	0	7	

from day	to day	Q [L/s]						Volume injected [ML]	Volume extracted [ML]	storage [day]	periods
		RW1	RW2	IW1	IW2	IW3	IW4				
1877	2052	10	10	0	0	0	0	0	302.4	10	
2059	2233	0	0	-5	-5	-5	-5	-300.672	0	7	
2243	2417	10	10	0	0	0	0	0	300.672	10	
2424	2598	0	0	-5	-5	-5	-5	-300.672	0	7	
2608	2782	10	10	0	0	0	0	0	300.672	10	
2789	2963	0	0	-5	-5	-5	-5	-300.672	0	7	
2973	3147	10	10	0	0	0	0	0	300.672	10	
<b>Scenario drought re100%</b>											
994	1052	0	0	-5	-5	-5	-5	-100.224	0		
1116	1174	10	10	0	0	0	0	0	100.224	64	
1359	1417	0	0	-5	-5	-5	-5	-100.224	0	185	
1481	1539	10	10	0	0	0	0	0	100.224	64	
1724	1782	0	0	-5	-5	-5	-5	-100.224	0	185	
1846	1904	10	10	0	0	0	0	0	100.224	64	
2090	2148	0	0	-5	-5	-5	-5	-100.224	0	186	
2212	2270	10	10	0	0	0	0	0	100.224	64	
2455	2513	0	0	-5	-5	-5	-5	-100.224	0	185	
2577	2635	10	10	0	0	0	0	0	100.224	64	
2820	2878	0	0	-5	-5	-5	-5	-100.224	0	185	
2942	3000	10	10	0	0	0	0	0	100.224	64	
<b>Scenario normal re120%</b>											
963	1079	0	0	-5	-5	-5	-5	-200.448	0		
1116	1255	10	10	0	0	0	0	0	240.192	37	
1328	1444	0	0	-5	-5	-5	-5	-200.448	0	73	
1481	1620	10	10	0	0	0	0	0	240.192	37	
1693	1809	0	0	-5	-5	-5	-5	-200.448	0	73	
1846	1985	10	10	0	0	0	0	0	240.192	37	
2059	2175	0	0	-5	-5	-5	-5	-200.448	0	74	
2212	2351	10	10	0	0	0	0	0	240.192	37	
2424	2540	0	0	-5	-5	-5	-5	-200.448	0	73	
2577	2716	10	10	0	0	0	0	0	240.192	37	
2789	2905	0	0	-5	-5	-5	-5	-200.448	0	73	
2942	3081	10	10	0	0	0	0	0	240.192	37	

from day	to day	Q [L/s]						Volume injected [ML]	Volume extracted [ML]	storage [day]	periods
		RW1	RW2	IW1	IW2	IW3	IW4				
<b>Scenario wet re120%</b>											
963	1108	0	0	-6	-6	-6	-6	-300.44	0		
1109	1318	10	10	0	0	0	0	0	361.152	1	
1328	1473	0	0	-6	-6	-6	-6	-300.44	0	10	
1474	1683	10	10	0	0	0	0	0	361.152	1	
1693	1838	0	0	-6	-6	-6	-6	-300.44	0	10	
1839	2049	10	10	0	0	0	0	0	362.88	1	
2059	2204	0	0	-6	-6	-6	-6	-300.44	0	10	
2205	2414	10	10	0	0	0	0	0	361.152	1	
2424	2569	0	0	-6	-6	-6	-6	-300.44	0	10	
2570	2779	10	10	0	0	0	0	0	361.152	1	
2789	2934	0	0	-6	-6	-6	-6	-300.44	0	10	
2935	3144	10	10	0	0	0	0	0	361.152	1	
<b>Scenario drought re120%</b>											
1248	1306	0	0	-5	-5	-5	-5	-100.224	0		
1370	1440	10	10	0	0	0	0	0	120.96	64	
1613	1671	0	0	-5	-5	-5	-5	-100.224	0	173	
1735	1805	10	10	0	0	0	0	0	120.96	64	
1978	2036	0	0	-5	-5	-5	-5	-100.224	0	173	
2100	2170	10	10	0	0	0	0	0	120.96	64	
2344	2402	0	0	-5	-5	-5	-5	-100.224	0	174	
2466	2536	10	10	0	0	0	0	0	120.96	64	
2709	2767	0	0	-5	-5	-5	-5	-100.224	0	173	
2831	2901	10	10	0	0	0	0	0	120.96	64	
3074	3132	0	0	-5	-5	-5	-5	-100.224	0	173	
3196	3266	10	10	0	0	0	0	0	120.96	64	

## C.4 Predictive modelling of residence time

Time in all simulations is expressed in days, from the first day of the simulation. In the following, negative flow rates indicate injection, while positive flow rates designate extraction.

**Table 13 Summary of input data for the ASTR wells for the simulation of residence time for the “normal” scenario (Q = flow rate)**

From day no.	To day no.	Q [L/s]					
		RW1	R2W	IW1	IW2	IW3	IW4
0	116	0	0	-5	-5	-5	-5
117	210	10	10	0	0	0	0
210	316	0	0	-5	-5	-5	-5
318	420	10	10	0	0	0	0

**Table 14 Summary of input data for the ASTR wells for the simulation of residence time for the “wet” scenario (Q = flow rate)**

From day no.	To day no.	Q [L/s]					
		RW1	R2W	IW1	IW2	IW3	IW4
0	174	0	0	-5	-5	-5	-5
175	314	10	10	0	0	0	0
314	488	0	0	-5	-5	-5	-5
489	628	10	10	0	0	0	0

## APPENDIX D: PARAFIELD ASR OPERATIONS

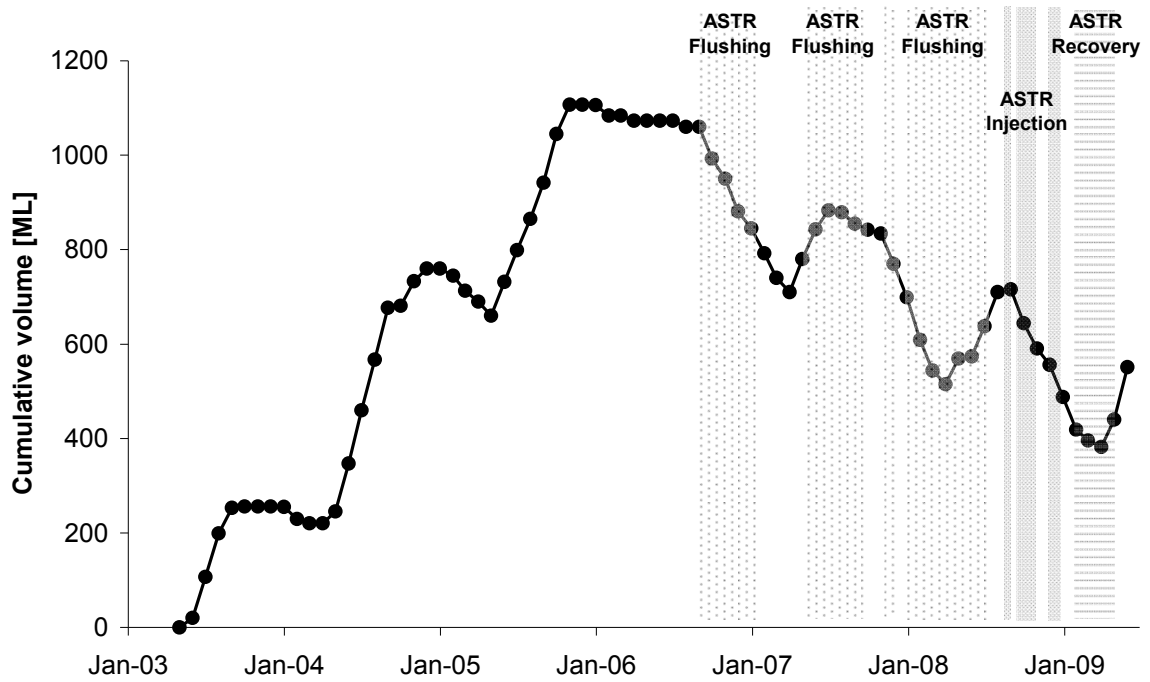


Figure 42 Monthly cumulative volume at the Parafield ASR scheme between June 2003 and June 2009



### Contact Us

Phone: 1300 363 400

+61 3 9545 2176

Email: [enquiries@csiro.au](mailto:enquiries@csiro.au)

Web: [www.csiro.au](http://www.csiro.au)

### Your CSIRO

Australia is founding its future on science and innovation. Its national science agency, CSIRO, is a powerhouse of ideas, technologies and skills for building prosperity, growth, health and sustainability. It serves governments, industries, business and communities across the nation.